Variational Formulation of Charged Curves Confined to a Sphere

A Dissertation

Presented to

the Faculty of the Department of Mechanical Engineering

University of Houston

In Partial Fulfillment

of the Requirements for the Degree

Doctor of Philosophy

in Mechanical Engineering

by

Vikash Chaurasia

August 2018

Variational Formulation of Charged Curves Confined to a Sphere

_____

Vikash Chaurasia

Approved:

_____
Chair of the Committee
Yi-Chao Chen, Professor,
Mechanical Engineering

Committee Members:

_____
Eliot Fried, Professor,
Okinawa Institute of Science and
Technology Graduate University (OIST)

_____
Gemunu Gunaratne, Professor,
Physics

_____
Shailendra Joshi, Assistant Professor,
Mechanical Engineering

_____
Ralph Metcalfe, Professor,
Mechanical Engineering

_____
Kalyana Babu Nakshatrala, Associate
Professor,
Civil and Environmental Engineering

_____
Suresh K. Khator, Associate Dean,
Cullen College of Engineering

_____
Pradeep Sharma, Department Chair,
Mechanical Engineering

Acknowledgements

I am deeply grateful to my advisor Prof. Eliot Fried for his insightful guidance, patience and his kindness. I am thankful to him for teaching me how to develop deep understanding of a research problem, allowing space for me to grow as a researcher and for his strong emphasis on good writing that I will try to emulate with best of my abilities. I sincerely thank my co-advisor Prof. Yi-Chao Chen for inspiring me through his work and the courses he taught me. Discussions with him during the course on Variational mechanics motivated me to pursue this topic further and which eventually led to the foundation of this thesis.

I greatly appreciate Prof. Gemunu Gunaratne for insightful discussions during the course Critical phenomenon and phase transitions and Prof. Kalyana Babu Nakshatrala for the discussions on computational mechanics and for his career advice. I sincerely thank Prof. Shailendra Joshi, Prof. Kalyana Babu Nakshatrala, Prof. Ralph Metcalfe, and Prof. Gemunu Gunaratne for reviewing my dissertation and providing invaluable suggestions to improve the thesis.

I dedicate this thesis to my parents and my dear sisters. Their love, immense support and sacrifices has allowed me to achieve things which at times were beyond my capabilities. I thank my younger sister Shilpi for taking care of Mammi and Papa and bearing the family duties while I have been away from home.

I am immensely thankful to Himani for being a wonderful friend and for her support without which the opportunity to work at OIST was impossible. I thank Nikhil for his help at numerous occasions and for many technical and non-technical discussions.

I had privilege of meeting wonderful friends who made my social life in Okinawa joyful. I am thankful to Hemanta, Tosif, Yoriko, and Shivani for their

Variational Formulation of Charged Curves Confined to a Sphere

An Abstract

of a

Dissertation

Presented to

the Faculty of the Department of Mechanical Engineering

University of Houston

In Partial Fulfillment

of the Requirements for the Degree

Doctor of Philosophy

in Mechanical Engineering

by

Vikash Chaurasia

August 2018

Abstract

In biological structures, charged proteins that are constrained to a surface are ubiquitously encountered. These proteins interact among each other to maintain their shapes and drive the functionality of the overall structure. Among the various such situations, we particularly focus on mature HDL (high density lipoprotein) molecules which are key components of Reverse Cholesterol transport that regulate the cholesterol level in our body. Mature HDL molecules are spheroidal shells with cholesterol encapsulated in their core, the outer shell being constituted of head groups of lipid molecules and charged proteins that are present on the outer surface of it. How these charged proteins arrange themselves on the surface of the sphere could be of key importance in the functionality of HDL molecules.

In our study, we model charged curves that are restricted to the surface of a rigid sphere. Our model consists of two interacting, inextensible elastic loops (closed curves) that are constrained to lie on a sphere. Each loop is endowed with bending energy, a distance-dependent self-interaction energy, and a distance-dependent energy that accounts for interactions with the other loop. The first and second variation conditions are obtained in coordinate-free form. A trivial equilibrium solution exists for such a problem in form of a pair of parallel circular loops situated in opposite hemispheres. We discuss how the interplay between the electrostatic interactions of the loops and their bending rigidity governs the stability of the trivial solution. Motivated by the understandings developed with this analysis, we solve the equilibrium equations numerically and obtain the post-buckled equilibrium configurations.

Table of Contents

List of Figures

List of Tables

CHAPTER 1 INTRODUCTION

In biology and in polymer sciences, we can find situations where there are charged loops interacting with oppositely charged surfaces and the medium around those surfaces. Peptide adsorption on a lipid membrane is one classic example. In particular, anti-microbial peptides (amps) are one of the important component of the immune system of eukaryotic and prokaryotic cells. The initial step in the action of amps against microbes involves their electrostatic attachment to the oppositely charged microbial membranes (Yang et al. [10]). Hancock and Rozek [11] discuss various aspects of amps activities against microbes. Another example for Eukaryotic cells is a negatively charged DNA strand wrapped around a positively charged surface of a histone octamer (Nelson and Cox [12, Chapter 24]). The complexes that are formed after this interaction of DNA with histone proteins act as fundamental building blocks for the compactification of genetic material in chromatin (Khrapunov et al. [13], Shiessel [14], Luger et al. [15]).

We aim to gain mechanistic insights into the interaction between charged curves that are attached to a surface. We assume that curve-surface interactions are strong enough and hence the curves are always constrained to the surface. We motivate our work through two examples that are discussed in the sections below.

1.1   Reverse Cholesterol Transport

Heart diseases are one of today's primary health concerns. The types of abnormalities which could be referred to as heart disease are blood vessels diseases such as coronary heart disease; arrhythmias that is heart rhythm issues; and by birth heart defects such as congenital heart defects.
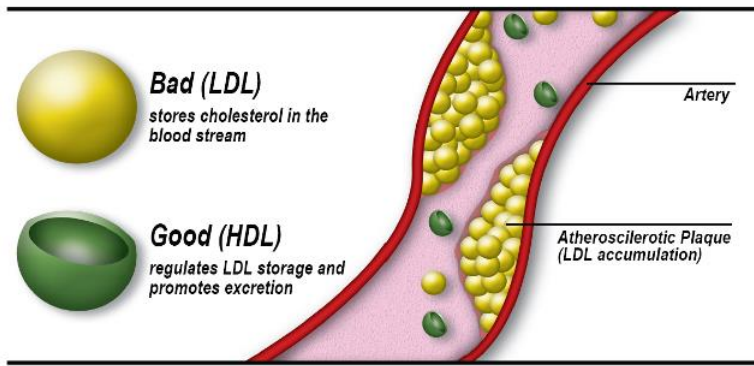
Figure 1.1: Schematic of cholesterol deposition in the arteries (from Rsocial) .

The most prominently studied heart disease is Atherosclerosis which refers to as narrowing of blood vessels and under advanced stages, blocking of the blood vessels. The narrowing of the blood vessels happens through deposition of cholesterol and its derivatives in the arteries and is depicted in the schematic 1.1. The two key components shown are; HDL - High density lipoprotein and LDL - Low density lipoprotein. The HDL is also called good cholesterol and LDL is called bad cholesterol. While the HDL molecules are carriers of cholesterol to the liver where it is decomposed, LDL molecules which are relatively larger in size, deposit in the artery walls and reduces the opening of arteries.

Reverse Cholesterol Transport (RCT) is the intrinsic mechanism in our body that regulates the cholesterol level in the blood stream and reduce the chances of cardiovascular diseases. It involves multiple steps and is mediated by various enzymes. Review article by Remaly, Norata, and Catapano detail the key steps involved in RCT in the Figure 1.2 and their description of RCT pathways is as follows. The first step begins with the formation of nascent Preb-HDL, which largely occurs in the liver and to a lesser degree in the intestine, when apoA-I lipoproteins acquires phospholipid and a small amount of cholesterol by the ABCA1 transporter. Preb-HDL is then transformed into a larger discoidal species

of HDL called a4 HDL when it acquires additional lipid by ABCA1 transporters in the periphery. HDL is then transformed into spherical a1-3 forms of HDL after acquiring additional lipid by other transporters and proteins on cell membranes, such as ABCG1 or SR-BI, or by a passive diffusion process. LCAT is involved in this process by converting cholesterol to cholesteryl esters, which migrate into the core of HDL. Cholesterol on HDL can be delivered directly to the liver after uptake by SR-BI, which then regenerates Preb-HDL. Alternatively, cholesteryl ester is transferred in exchange for triglycerides to VLDL and LDL by CETP and LDL is eventually delivered to the liver by the LDL-receptor. Cholesterol is then excreted by the liver either as free cholesterol or is converted to a bile salt.
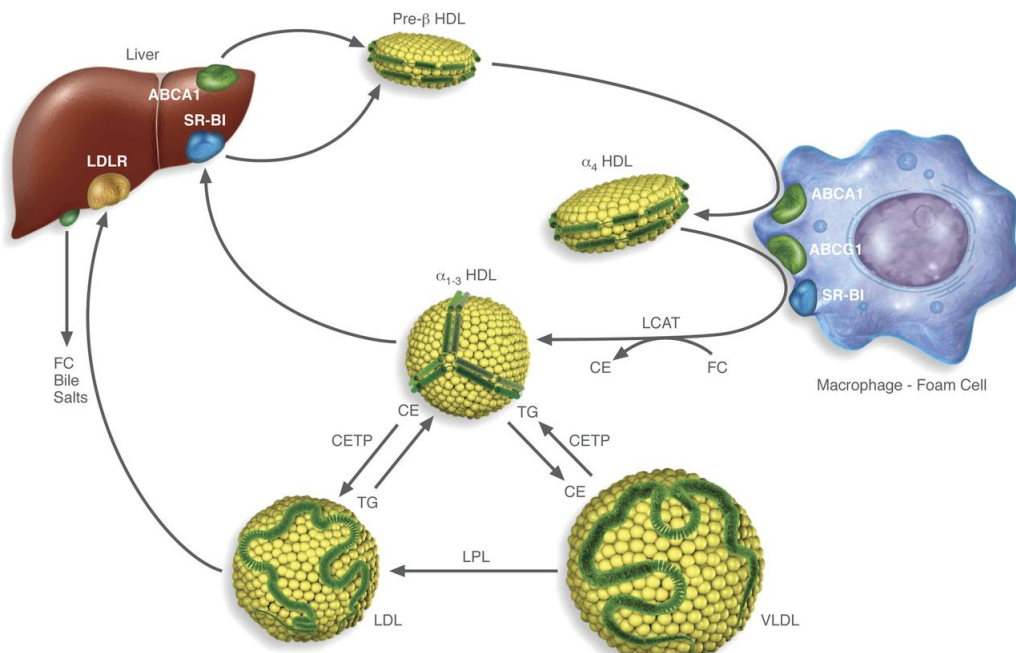
Figure 1.2: Diagram of the Reverse Cholesterol Transport(RCT) pathway. The description and the figure are obtained from Remaly, Norata and Catapano [1] .
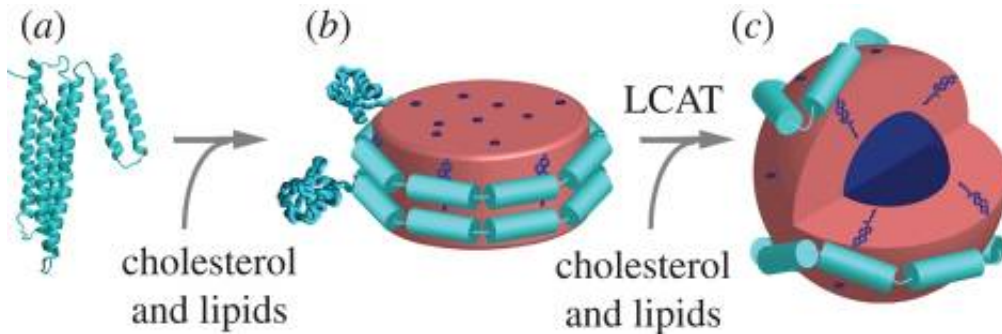
Figure 1.3: Simplified steps of the Reverse Cholesterol Transport (RCT) due to Shih, Sligar and Schulten [2].

In brevity, the RCT cycle can be summarized in three key steps, shown in the Figure 1.3 as

(a) A thread like protein called apoA-I lipoprotein which has cholesterol binding properties, is secreted from liver in the blood stream,

(b) Formation of a disc like unit which is made up of a lipid bilayer with cholesterol embedded in it. The red component shown in the figure is made up of phospholipids and the blue dots signify the embedded cholesterol molecules. The edge of the layer is constituted by the apoA-I lipoprotein. This unit is also called discoidal HDL,

(c) Esterification of the cholesterol molecule through lecithin cholesterol acyltransferase (LCAT) drives it to move into the lipid bilayer. This results in the structural transition from discoidal HDL particle to the spherical HDL which is also known as mature HDL particle. The spherical HDL then floats back into the liver where it is decomposed.

Mature stage of HDL (stage (c)) consists of a spherical core of entangled esterified cholesterol and Trigycerides (TG). This core is encapsulated by a spherical shell made up from phospholipids aligned in a fashion such that the outer surface is formed by the headgroups and the tails are pointing toward the core.

4
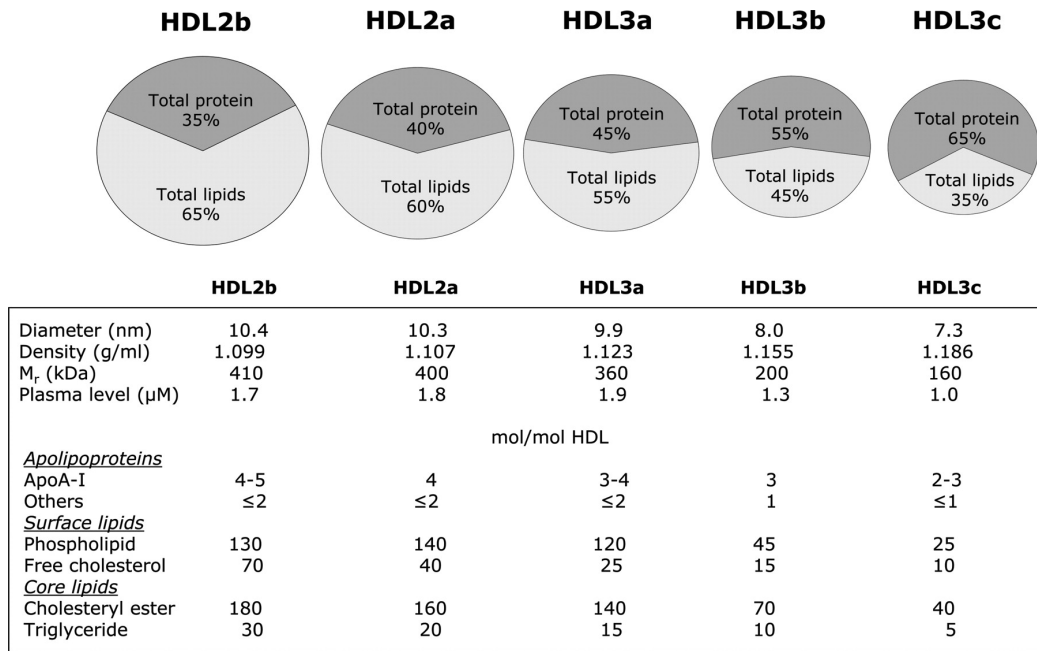
Figure 1.4: Heterogeneity in the physicochemical properties of normal functional HDL due to John et al. [3], Blanche et al.[4], Barter et al. [5], Kontush et al. [6].

On the outer surface of this shell are the apoA-I lipoprotein which supposedly acts as a scaffold for the interaction of mature HDL with the enzymes (Mishra et al. [16]) and providing stability to the overall structure. The size and content of the spherical HDL varies largely as shown in the figure 1.4 .

One crucial difference between the discoidal HDL (stage b) and spherical HDL (stage c), apart from differences in the structure is the role of apoA-I lipoprotein in the two entities. In discoidal HDL, the apoA-I lipoproteins forms the edge of the bilayer to protect the hydrophobic tails of lipids forming the bilayer.

In mature HDL, the outer surface of mature HDL is formed by hydrophilic headgroups of the lipid molecules. This structure provides the shield to hydrophobic entities like tail of the lipids, and the core consisting of esterified cholesterol molecules, tryglycericeds (TG) etc. Therefore, apoA-I lipoproteins that lay on the surface of mature HDL are free from the role of providing the hydrophobic shield. Hence, they can be assumed to float on the spherical surface.

Silva and coworkers [17–19], Mei and Atkinson [20], and Gursky [21] studied the crystal structure of apo-lipoprotein on the surface of HDL particles. Their work shows that multiple peptides wrap around the surfaces of HDL particles in various configurations. Vattulainen et al. [7] performed coarse-grained molecular dynamics simulations to study the structure and dynamics of spherical high density lipoprotein (HDL). They studied both, a lipid droplet without the apolipoprotein A-I (apoA-I lipoproteins) and the full HDL particle including two apoA-I lipoproteins molecules surrounding the lipid compartment as shown in the figure 1.5. . Dark gray stands for POPC headgroup and dark brown for PPC headgroups, light gray for POPC hydrocarbon chains, light brown for PPC chains, light orange for CHOL OH-groups, bright yellow for cholesterol body, dark orange for esterified cholesterol (CE) ester bond, orange for CE ester body and chain, dark green for TG ester bonds, and bright green for TG chain. In HDL, proline residues in apoA-I lipoprotein sequences are in green. They inferred that the hydrophobic residues of apoA-I lipoproteins interact with the lipid tail groups and the cholesterol molecule present in the HDL. These specific bindings restrict the apoA-I lipoproteins to the outer surface of HDL.

Our work is a first step toward modeling the configuration of the charged apoA-I lipoproteins on the surface of mature HDL. We consider charged loops that are inextensible and are endowed with bending stiffness. The loops are restricted to stay on the sphere but they are allowed to float along the surface. These assumptions capture the essential features exhibited by the apoA-I lipoproteins in the mature HDL.
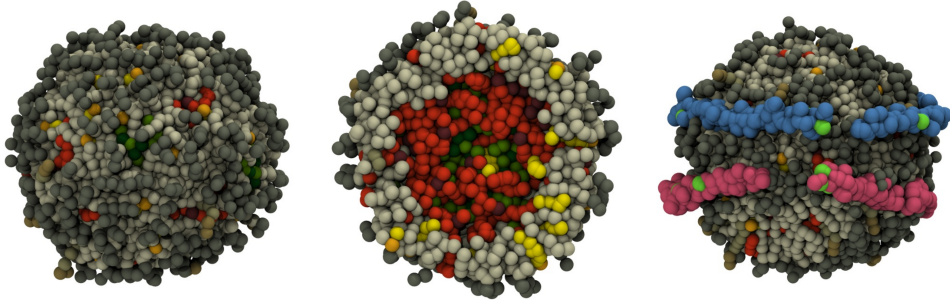
Figure 1.5: Example of a protein-free lipid droplet (left), its molecular distribution shown through a slice across the particle (middle), and HDL including two apoA-I lipoproteins (right) due to Vattulainen et al. [7].

1.2 Polyelectrolyte Nano Containers

The adsorption of polyelectrolytes on oppositely charged surfaces is of central importance in colloidal science. There is a growing interest in methods for fabricating coated nanoparticles and polyelectrolyte shells by the sequential deposition of polyelectrolyte chains on tailored surfaces. Decher [22–25] devised techniques of depositing alternate layers of opposite charged polyelectrolytes on flat support. Caruso et al. [26] and Gittins and Caruso [27] fabricated polyelectrolyte shells by depositing the polyelectrolytes on dissolvable spherical core.

Sukhorukov et al. [8] synthesized thin organic films by the stepwise deposition of polyelectrolyte chains on dissolvable spherical cores as shown in the figure 1.6. Shells that remain after core dissolution have been used as containers for macromolecules, microcarriers, and microreactors.

Processes of adsorption of single charged polymers onto a surface occur in a wide variety of applications and have been studied extensively. Goeler and Muthukumar [28] combined a variational procedure to probe the adsorption of single polyelectrolytes on cylindrical and spherical surfaces. In their unified description for adsorption of polyelectrolyte chains onto planar and curved surfaces, Cherstvy and Winkler [29] highlighted the role of surface curvature on scaling laws for adsorption. A comprehensive list of the theoretical work on this topic
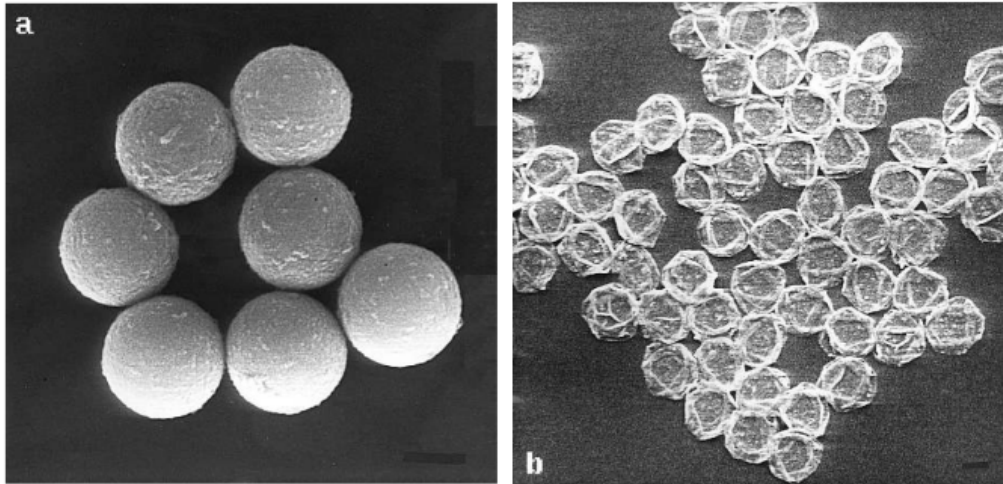
Figure 1.6: Scanning electron microscope (SEM) micrographs of melamine formaldehyde (MF) particles coated with nine layers (Sodium poly(styrene sulfonate) and poly(allylamine hydrochloride)) prior to the dissolution of the core (a) and of the remaining polyelectrolyte shell after removal of the core at pH 1.3 (b). The scale bar corresponds to 1 nm. This figure is taken from work of Sukhorukov et al. [8].

appears in the review articles by Netz and Andelman [30], Dobrynin and Rubinstein [31], and Messina [32]. Monte-Carlo simulations conducted by Kong and Muthukumar [33] confirm the theoretical predictions of scaling laws of adsorption. Results from other simulations are summarized in the review article by Messina, Holm and Kremer [34].

Stoll and Chodanowski [9] used Monte–Carlo simulations to study the adsorption of a semi-flexible polyelectrolyte onto a oppositely charged rigid sphere. They investigated the adsorption/desorption limit and conformation of the adsorbed polyelectrolyte while including the effect of charge density of the polyelectrolyte, its bending rigidity, and the ionic concentration of the solution. The interplay between these effects govern the adsorption limit and the confirmation of adsorbed chain on the sphere. In the figure 1.7, configurations of the adsorbed polyelectrolyte chain for different values of the stiffness of the chain and ionic strength of the solution are shown. The ionic strength of the solution, via
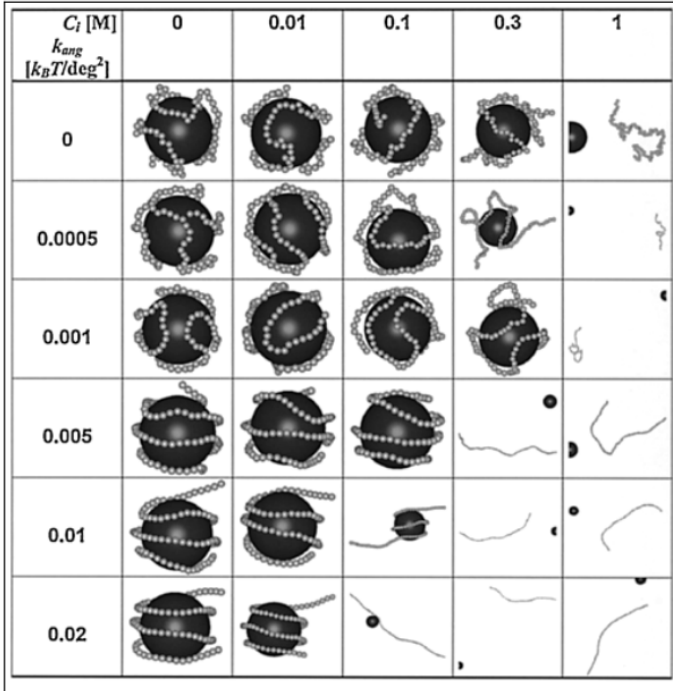
Figure 1.7: Effect of ionic concentration of the solution and bending stiffness of the polyelectrolyte on its adsorption onto the sphere. The ionic strength of the solution and the bending rigidity of the chain are respectively denoted by C_l and κ_{ang}. This figure is due to Stoll and Chodanowski [9].

the screening effect, governs the electrostatic interaction of the chain with itself, with the solution and with the sphere. The bending stiffness and the electrostatic self repulsions among the monomers of the polyelectrolyte drives it to adopt extended conformations and limit the number of monomers that may be attached to the sphere. In contrast, the attractive interaction between the polyelectrolyte monomers and the sphere induces the chain to undergo a structural transition and attach to the sphere. The effect of curvature energy is demonstrated by increasing the intrinsic rigidity, in which case a transition from a disordered and strongly bound complex to a situation where the polymer touches the particle over a finite length, while passing by the formation of a more ordered, solenoid conformation.

The majority of the existing literature on polyelectrolyte adsorption focuses

on single chains because intrachain interactions dominate interchain interactions in most systems of importance (Dobrynin and Rubinstein [31]).

Although our model consists of two charged closed curves, our frame work can be easily specialized to yield the equilibrium and stability condition for a single, open, charged curve. However, our model is unable to handle the situation where a portion of the curve is allowed to leave the surface of sphere, as shown in some of the cases in the figure 1.7.

A brief outline of the following chapters is as follows. In chapter 2, we provide brief description of the differential geometry of space curves and the terminologies that are commonly used in the literature. In chapter 3, we describe the main framework of our model. We introduce the necessary geometrical quantities, the notation, and the assumptions. The first and second variation conditions satisfying the energy stability criterion are presented. In chapter 4, we apply the framework developed in chapter 3 to a special case where we characterize the interaction of two uniformly charged loops that have the same length and material parameters. The trivial equilibrium solution to that special problem is presented. Bifurcations from that trivial solution are identified and associated stability criteria are obtained. Explanation of how the geometric and material parameters effect the stability of the trivial solution are provided. In chapter 5, we solve the equilibrium equations derived for the special case in chapter 4 numerically and obtain the non-trivial equilibrium solutions. In chapter 6, we provide the summary of our results and future directions of our work. For completeness, Appendix contains detailed accounts of the calculations that provide the foundations for our analysis.

CHAPTER 2 DIFFERENTIAL GEOMETRY OF

CURVES

In this chapter, we provide some useful tools to describe a curve in 3-dimensional space and key references for comprehensive understanding of the subject. The material presented in this chapter is adopted from the book titled *Differential Geometry of Curves and Surfaces* [39] by Professor MP do Carmo.

A parameterized curve is a differentiable map $r : I \to R^3$ that takes a one dimensional variable $t \in I$ as an input and yields a 3-dimensional output $r(t) \in R^3$, where I is a subset of R. At each point of the curve, an orthonormal basis also called frame of the curve can be associated that describes how the curve evolves in the space. Below are some of the useful frames that are commonly used.

2.1 Frénet Frame

For a space curve parameterized as $r : I \to R^3$, tangent vector, normal vector, and binormal vector defined respectively as

$$T(t) = \frac{r'(t)}{|r'(t)|}, \quad N(t) = \frac{T'(t)}{|T'(t)|}, \quad \text{and} \quad B(t) = T(t) \times N(t), \qquad (2.1)$$

at each point $r(t)$ form an orthogonal basis called Frénet -frame which was given independently by two French mathematicians Jean Frédéric Frénet [35] and Joseph Alfred Serret ([36], [37]).

Two scalar quantities that characterize a curve in space, curvature and torsion of the curve, are given as

$$\kappa(t) = \frac{|T'(t)|}{|r'(t)|} = \frac{|r'(t) \times r''(t)|}{|r'(t)|^3}, \quad \text{and} \quad \tau(t) = \frac{N'(t) \cdot T(t)}{|r'(t)|} = \frac{r''' \cdot (r' \times r'')}{|r'(t) \times r''(t)|^2}, \qquad (2.2)$$

respectively. While curvature κ measures the change in direction of the unit tangent T, torsion τ measures tendency of the curve to deviate out of its current plan which is spanned by vectors T and N. The derivative of T, N, and B can be written in terms of these vectors, curvature κ and torsion τ as

$$T' = \kappa |r'| N, \quad N' = -\kappa |r'| T + \tau |r'| B, \quad \text{and} \quad B' = -\tau |r'| N. \qquad (2.3)$$

These relations are also called as *Frénet -Serret formula* or *structure equations*.

In mechanics, it is a standard practice to use arc-length parameterization of the curve instead of an arbitrary parameter t as used in the above paragraphs. Let a curve of length L be parameterized with arc-length $s \in [0, L]$ in which case,

$$|r'(s)| = 1. \qquad (2.4)$$

which is a common knowledge in the literature and is referred to as unit speed curve. Now, using this parameterization, the relations (2.1), (2.2), and (2.3) simplify as

$$T = r', \quad N = \frac{T'}{|T'|}, \quad \text{and} \quad B = T \times N, \qquad (2.5)$$

$$\kappa = |T'| = |r''|, \quad \text{and} \quad \tau = N' \cdot T = \frac{r''' \cdot (r' \times r'')}{|r''|^2}, \qquad (2.6)$$

and

$$T' = \kappa N, \quad N' = -\kappa T + \tau B, \quad \text{and} \quad B' = -\tau N, \qquad (2.7)$$

respectively, where the derivatives are taken with respect to arc length s. The Frénet -Serrate relation (2.7) is also written in a matrix form as

$$\begin{bmatrix} T \\ N \\ B \end{bmatrix}' = \begin{bmatrix} 0 & \kappa & 0 \\ -\kappa & 0 & \tau \\ 0 & -\tau & 0 \end{bmatrix} \begin{bmatrix} T \\ N \\ B \end{bmatrix}.$$

Frénet frame fails to describe a curve when the tangent t is a constant such that $T' = 0$ in which case, the normal vector N is arbitrary.

2.2 Darboux Frame

Consider a surface $\mathcal{S}$ and an arc-length parameterized curve r on it. At each point of the curve, we find that

- Unit tangent to the curve, $t = r'$,

- Unit normal to the surface, n, and,

- Tangent-normal vector $g = t \times n$ which is tangent to the surface $\mathcal{S}$ and normal to the curve r

form an orthonormal frame $\{t, n, g\}$ known as Darboux frame which was proposed by French mathematician Jean Gaston Darboux [38].

Differentiating the relation $|r'| = 1$ with respect to arc length s yields

$$r' \cdot r'' = 0, \tag{2.8}$$

which implies that the total curvature of the curve, $\kappa = r''$ is in the plane formed by vector n and g and can be written as

$$\kappa = r'' = \kappa_n n + \kappa_g g. \tag{2.9}$$

The quantities κ_n and κ_g are called normal curvature and geodesic curvature of the curve r on $\mathcal{S}$, respectively. A curve on the surface $\mathcal{S}$ is geodesic if $\kappa_g = 0$. Thus, geodesic curvature measures how far away is the curve from being a geodesic.

Derivative of the Darboux frame vectors can be written in similar fashion as the Frénet -Serret formula described in (2.7) as

$$\begin{bmatrix} t \\ n \\ g \end{bmatrix}' = \begin{bmatrix} 0 & \kappa_n & \kappa_g \\ -\kappa_n & 0 & -\tau_g \\ -\kappa_g & -\tau_g & 0 \end{bmatrix} \begin{bmatrix} t \\ n \\ g \end{bmatrix},$$

where τ_g is called geodesic torsion of the curve. Given a Darboux frame $\{t, n, g\}$, the scalar quantities κ_n, κ_g, and τ_g can be derived as

$$\kappa_n = -n' \cdot t, \quad \kappa_g = t' \cdot g, \quad \text{and} \quad \tau_g = -n' \cdot g. \tag{2.10}$$

The normal curvature κ_n depends only on the shape of the surface $\mathcal{S}$ and the direction in which the curve is traveling on it. Following this argument, Darboux frame naturally encodes the information about the shape of the surface. In contrast, the Frénet -Serret frame has no such information. Therefore, for describing a curve that is constrained to a surface, Darboux frame is a more suitable choice over Frénet -Serret frame.

2.3   Description of a curve constrained to a sphere

In this section, we show how the Darboux frame described in the previous section specialize in the case where the surface $\mathcal{S}$ is a sphere. Without loss of generality, consider a sphere of radius R with origin being center of the sphere. Let $\mathcal{C}$ be a curve of length L constrained to $\mathcal{S}$ which can be parameterized as

$$C = \{r : r = Rn(s), 0 \leq s \leq \ell\}, \tag{2.11}$$

where s is the arc length (dimensionless) which is obtained by scaling the arc length with radius R and $\ell = \frac{L}{R}$ is the dimensionless length of the curve, and n is the unit normal to the surface of the sphere $\mathcal{S}$ pointing outwards. So, in the particular situation where surface is a sphere, the position vector of the curve r and the normal to $\mathcal{S}$, Rn coincide. The Darboux frame vectors t and g, respectively are given as

$$t = n' \quad \text{and} \quad g = n' \times n, \tag{2.12}$$

where the derivatives here, and henceforth in this section are with respect to the dimensionless arc length s. The total curvature of the curve $\mathcal{C}$ is given as

$$\kappa = \frac{1}{R^2} \frac{d\mathbf{r}}{ds^2} = \frac{\mathbf{n}''}{R}. \tag{2.13}$$

The normal curvature, geodesic curvature and the geodesic torsion are given as

$$\kappa_n = -\frac{1}{R} \frac{d\mathbf{n}}{ds} \cdot \mathbf{t} = -\frac{\mathbf{n}' \cdot \mathbf{n}'}{R} = -\frac{1}{R}, \tag{2.14}$$

$$\kappa_g = \frac{1}{R} \frac{d\mathbf{t}}{ds} \cdot \mathbf{g} = \frac{\mathbf{n}'' \cdot (\mathbf{n}' \times \mathbf{n})}{R}, \quad \text{and} \tag{2.15}$$

$$\tau_g = -\frac{1}{R} \mathbf{n}' \cdot \mathbf{g} = 0, \tag{2.16}$$

where $\mathbf{n}'$ is derivative of $\mathbf{n}$ with respect to dimensionless arc length s. We conclude from (2.16) that the geodesic torsion of a curve constrained to a sphere is 0.

CHAPTER 3 VARIATIONAL FRAMEWORK FOR CHARGED CURVES ON A SPHERE

3.1 Introduction

In the present work, we consider a system consisting of two semi-flexible, charged loops that are constrained to lie on a sphere. Semiflexibility implies that persistence length of the polymers represented through these charged loops substantially exceeds the length of its constituent monomers. For such polymers, the energetics of bending decouples from the minutiae of the chemical structure and can thus be described to good accuracy by a continuum-level elastic model. The literature contains many relevant theoretical works on elastic loops constrained to spheres. In a pioneering work, Langer and Singer [40] used a variational approach to study the shape of a closed, inextensible loop restricted to a spherical surface. They considered a simple model in which the bending energy per unit length of the loop is proportional to the square of its curvature. Working with a generalization of that energy, Arroyo et al. [41–44] analyzed the existence and stability of loops on a spherical surface and determined the conditions under which an open loop closes into a loop.

In an effort to model a DNA molecule that exhibits non-local, long-range interactions between its base pairs, Biton et al. [45] explored the three-dimensional equilibrium configurations of a electrically charged loop endowed with bending stiffness. They developed a numerical method that deals effectively with the full Jacobian of the equilibrium configuration that stems from the nonlocal self energy of the system. Hoffmann and Manning [46] studied the equilibrium shape and stability of a open loop that is constrained to lie in a plane an is endowed with

bending stiffness and repulsive self energy, focusing on the challenges related to the singularity that is generated by the self energy of the loop.

The simplest mathematical expression for the self energy of a closed loop of length L with distributed charge density ρ and arclength parameterized position vector r is proportional, by Coulomb's constant, to the divergent integral

$$\frac{1}{2} \int_0^L \int_0^L \frac{\rho(s)\rho(\bar{s})\,\mathrm{d}s\,\mathrm{d}\bar{s}}{|r(s) - r(\bar{s})|}. \tag{3.1}$$

Renormalization techniques have been used to circumvent the divergence arising from the interaction potentials. Fukuhara [47] considered a discretized version of (3.1) that is bounded. Birman and Lomonaco [48] replaced the distance $|r(s) - r(\bar{s})|$ in the denominator of the integrand in (3.1) by $|r(s) - r(\bar{s})| + \epsilon$, with $\epsilon > 0$, to obtain a finite self energy. Other regularization approaches include subtracting from (3.1) an equally divergent term or multiplying the integrand of (3.1) by a factor that decays sufficiently rapidly as $\bar{s} \to s$. In a series of papers, O'Hara [49–51] used the subtractive approach to calculate the self energy of charged knots. Kushner and Sullivan [52] used a multiplicative factor to regularize the inverse power-law that governs the self energy of a charged Möbius band. Hoffmann and Manning [46] used a mollifier with decay such that the self energy of a charged rod is mollified up the second variation of the energy functional.

Building on the works mentioned above, we present a variational framework for studying the interaction between two charged loops that are constrained to a sphere (Figure 3.1). We restrict attention to inextensible loops. Moreover, for simplicity, we follow Langer and Singer [40] by endowing each loop with bending energy with density proportional to the square of its curvature. We limit our study to situations in which the self and interaction energies of the loops are repulsive. Moreover, we use multiplicative approach to regularize the self energy of the curves for uniformly charged loops in chapter 4. On the basis of these simplifying assumptions, we explore the competition between bending resistance

and repulsive interactions, in conjunction with the geometric constraints, to determine energetically preferred equilibrium configurations, the goal being to to explain how these various effects influence the stability of equilibrium configurations and thereby provide insight on the equilibrium phenomena that occur subsequent to adsorption of polyelectrolyte on the curved surface. Although we do not study the equilibrium shape of a single charged polyelectrolyte deposited on a sphere, our framework can also be applied to such problems.

The remainder of this chapter is organized as follows. The necessary geometrical quantities, notation, and assumptions are introduced in §3.2. The first and second variation conditions satisfying the energy stability criterion are presented in §3.3. Summary of this chapter is provided in §3.5.

3.2 Preliminaries

Consider (closed) inextensible loops $\mathcal{C}_1$ and $\mathcal{C}_2$ of respective lengths $L_1 = R\ell_1$ and $L_2 = R\ell_2$ confined to a sphere $\mathcal{S}$ of radius R, as illustrated in Figure 3.1. We suppose that each loop is endowed with a bending energy with density proportional to the square of its curvature and with a self energy with density dependent on the distance between pairs of its points. Additionally, we assume that interactions between the loops are characterized by an energy with density dependent on the distance between pairs of their points.

3.2.1 Kinematics

Without loss of generality, we place the origin at the center of the sphere $\mathcal{S}$ and parameterize each loop $\mathcal{C}_i$ by

$$C_i = \{\boldsymbol{r} : \boldsymbol{r} = R\boldsymbol{n}_i(s), 0 \leq s \leq \ell_i\}, \tag{3.2}$$
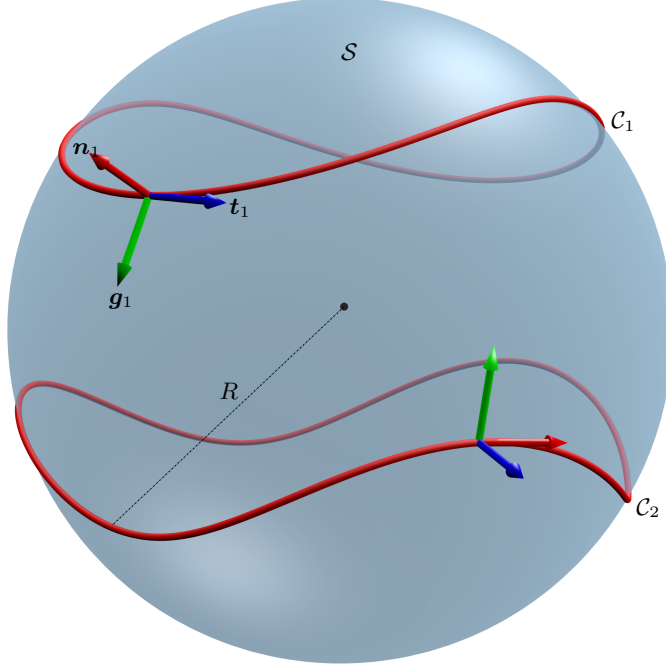
Figure 3.1: Schematic of two inextensible closed loops C_1 and C_2 of length $L_1 = R\ell_1$ and $L_2 = R\ell_2$ confined to a sphere S of radius R. The Darboux frames $\{t, n, g\}$ of C_1 and C_2 are also depicted.

where s represents (dimensionless) arclength on C_i, $i = 1, 2$, and n_i is normal to S, directed away from the origin, and three-times continuously differentiable. As consequences of this smoothness assumption, we have the closure conditions

$$n_i(0) = n_i(\ell_i), \ n_i'(0) = n_i'(\ell_i), \ n_i''(0) = n_i''(\ell_i), \quad \text{and} \quad n_i'''(0) = n_i'''(\ell_i), \quad i = 1, 2,$$

(3.3)

where a prime denote differentiation with respect to s on C_i, $i = 1, 2$. To ensure that each loop C_i, $i = 1, 2$, conforms to S and is inextensible, we stipulate that

$$|n_i| = 1 \quad \text{and} \quad |n_i'| = 1.$$

(3.4)

From (3.2), the vector curvature κ_i of each loop C_i, $i = 1, 2$, is given by

$$\kappa_i = \frac{1}{R} n_i''.$$

(3.5)

It is convenient to decompose the vector curvatures into geodesic and normal components. To achieve this, we adopt the convention that the curvature of S is

19

negative, in which case each loop $\mathcal{C}_i$, $i = 1, 2$, has normal curvature $-1/R$ and its vector curvature κ_i can be expressed as

$$\kappa_i = \frac{1}{R}(\mathbf{1} - \mathbf{n}_i \otimes \mathbf{n}_i)\mathbf{n}_i'' - \frac{\mathbf{n}_i}{R}. \tag{3.6}$$

Differentiating $(3.4)_1$ with respect to arclength, we see that on $\mathcal{C}_i$, $i = 1, 2$,

$$\mathbf{n}_i' \cdot \mathbf{n}_i = 0. \tag{3.7}$$

By (3.4) and (3.7), the triad $\{\mathbf{n}_i', \mathbf{n}_i, \mathbf{n}_i' \times \mathbf{n}_i\}$ provides an orthonormal basis — its Darboux frame — on $\mathcal{C}_i$, $i = 1, 2$. Defining $\mathbf{t}_i$ and $\mathbf{g}_i$ on $\mathcal{C}_i$, $i = 1, 2$, by

$$\mathbf{t}_i = \mathbf{n}_i' \quad \text{and} \quad \mathbf{g}_i = \mathbf{t}_i \times \mathbf{n}_i, \tag{3.8}$$

we thus recognize from (3.6) that $\mathbf{t}_i'$ can be expressed as

$$\mathbf{t}_i' = \mathbf{n}_i'' = -\mathbf{n}_i - k_i \mathbf{g}_i, \tag{3.9}$$

where k_i determined according to

$$k_i = -\mathbf{n}_i'' \cdot \mathbf{g}_i = -\mathbf{t}_i' \cdot \mathbf{g}_i = \mathbf{g}_i' \cdot \mathbf{t}_i \tag{3.10}$$

is the dimensionless geodesic curvature of $\mathcal{C}_i$, $i = 1, 2$. Since $\mathbf{g}_i \cdot \mathbf{t}_i = 0$ on $\mathcal{C}_i$, $i = 1, 2$, we see from (3.10) that

$$\mathbf{g}_i' = k_i \mathbf{t}_i. \tag{3.11}$$

Since $\mathbf{g}_i' \cdot \mathbf{n}_i = (\mathbf{g}_i \cdot \mathbf{n}_i)' - \mathbf{g}_i \cdot \mathbf{n}_i' = \mathbf{g}_i \cdot \mathbf{t}_i = 0$ and the geodesic torsion of $\mathcal{C}_i$, $i = 1, 2$, is $\mathbf{g}_i' \cdot \mathbf{n}_i/R$, (3.11) is consistent with the established fact that the geodesic torsion of a curve on a sphere must vanish. When augmented by given choices $\mathbf{t}_i(0)$, $\mathbf{n}_i(0)$, and $\mathbf{g}_i(0)$ of $\mathbf{t}_i$, $\mathbf{n}_i$, and $\mathbf{g}_i$, we may integrate the system

$$\mathbf{t}_i' = -k_i \mathbf{g}_i - \mathbf{n}_i, \quad \mathbf{n}_i' = \mathbf{t}_i, \quad \mathbf{g}_i' = k_i \mathbf{t}_i, \tag{3.12}$$

to uniquely determine the shape of $\mathcal{C}_i$, $i = 1, 2$, on $\mathcal{S}$.

3.2.2 Energetics

We assume that the total energy $\mathcal{E}$ of the system consisting of the loops $\mathcal{C}_1$ and $\mathcal{C}_2$ can be expressed as a sum,

$$\mathcal{E} = \mathcal{E}_{\mathrm{B}} + \mathcal{E}_{\mathrm{S}} + \mathcal{E}_{\mathrm{I}}, \tag{3.13}$$

of contributions $\mathcal{E}_{\mathrm{B}}$, $\mathcal{E}_{\mathrm{S}}$, and $\mathcal{E}_{\mathrm{I}}$ that account respectively for bending energy, self energy, and interaction energy. For simplicity, we stipulate that the extent to which $\mathcal{C}_i$, $i = 1, 2$, resists bending is characterized by a single constant bending modulus μ_i, so that $\mathcal{E}_{\mathrm{B}}$ has the particular form

$$\mathcal{E}_{\mathrm{B}}[\boldsymbol{n}_1, \boldsymbol{n}_2] = \frac{\mu_1}{2} \int_0^{\ell_1} |\boldsymbol{\kappa}_1(s)|^2 \, \mathrm{d}s + \frac{\mu_2}{2} \int_0^{\ell_2} |\boldsymbol{\kappa}_2(s)|^2 \, \mathrm{d}s. \tag{3.14}$$

It is natural to decompose $\mathcal{E}_{\mathrm{B}}$ into terms associated with the geodesic and normal components of the vector curvature $\boldsymbol{\kappa}_i$ of each loop $\mathcal{C}_i$, $i = 1, 2$. With reference to (3.6) and (3.9), this leads to the representation

$$\begin{aligned}
\mathcal{E}_{\mathrm{B}}[\boldsymbol{n}_1, \boldsymbol{n}_2] &= \frac{\mu_1}{2} \int_0^{\ell_1} \left| \boldsymbol{\kappa}_1(s) + \frac{1}{R} \boldsymbol{n}_1(s) \right|^2 \mathrm{d}s + \frac{\mu_2}{2} \int_0^{\ell_2} \left| \boldsymbol{\kappa}_2(s) + \frac{1}{R} \boldsymbol{n}_2(s) \right|^2 \mathrm{d}s \\
&\quad - \frac{\mu_1 \ell_1 + \mu_2 \ell_2}{2R} \\
&= \frac{\mu_1}{2R} \int_0^{\ell_1} k_1^2(s) \, \mathrm{d}s + \frac{\mu_2}{2R} \int_0^{\ell_2} k_2^2(s) \, \mathrm{d}s - \frac{\mu_1 \ell_1 + \mu_2 \ell_2}{2R},
\end{aligned} \tag{3.15}$$

where the term $-(\mu_1 \ell_1 + \mu_2 \ell_2)/2R$, being a constant, is of no consequence. Furthermore, we stipulate that $\mathcal{E}_{\mathrm{S}}$ has the form

$$\begin{aligned}
&\mathcal{E}_{\mathrm{S}}[\boldsymbol{n}_1, \boldsymbol{n}_2] \\
&= \frac{A_{11}}{2} \int_0^{\ell_1} \int_0^{\ell_1} f(|\boldsymbol{n}_1(s) - \boldsymbol{n}_1(\bar{s})|) \, \mathrm{d}\bar{s} \, \mathrm{d}s + \frac{A_{22}}{2} \int_0^{\ell_2} \int_0^{\ell_2} f(|\boldsymbol{n}_2(s) - \boldsymbol{n}_2(\bar{s})|) \, \mathrm{d}\bar{s} \, \mathrm{d}s,
\end{aligned} \tag{3.16}$$

and that $\mathcal{E}_{\mathrm{I}}$ has the form

$$\mathcal{E}_{\mathrm{I}}[\boldsymbol{n}_1, \boldsymbol{n}_2] = \frac{A_{12}}{2} \int_0^{\ell_1} \int_0^{\ell_2} h(|\boldsymbol{n}_1(s) - \boldsymbol{n}_2(\bar{s})|) \, \mathrm{d}\bar{s} \, \mathrm{d}s, \tag{3.17}$$

21

where A_{11}, A_{22}, and A_{12} are constants with dimensions of energy per unit area, f is the dimensionless self interaction energy density and h is the dimensionless interaction energy density between the two loop. In general, the function f and h may depend explicitly on s and $\bar{s}$ (through, for instance, the difference $|s - \bar{s}|$). This would be the case, for example, if the loops were non uniformly charged. However, we suppress such dependence until further notice.

Our focus is on situations where all interaction energies are repulsive. Consistent with this, we restrict attention to configurations of the system in which contact between the points of a single loop or between points of the two loops cannot occur. This obviates any need to introduce unilateral constraints that would otherwise be necessary to eliminate the passage of either loop through itself or of one loop through another.

3.2.3   Dimensionless parameters

We choose a scaling in which lengths are measured relative to the radius R of the sphere $\mathcal{S}$ to which the loops $\mathcal{C}_1$ and $\mathcal{C}_2$ are confined and energies are measured relative to the bending energy μ_1/R that would be stored in $\mathcal{C}_1$ if it were of length $2\pi R$ and coincident with a great circle of $\mathcal{S}$. On this basis, we identify two dimensionless measures,

$$\ell_1 = \frac{L_1}{R} \quad \text{and} \quad \ell_2 = \frac{L_2}{R}, \tag{3.18}$$

of the length and four dimensionless measures,

$$\nu = \frac{\mu_2}{\mu_1}, \quad \zeta_1 = \frac{R^3 A_{11}}{\mu_1}, \quad \zeta_2 = \frac{R^3 A_{22}}{\mu_1}, \quad \text{and} \quad \chi = \frac{R^3 A_{12}}{\mu_1}, \tag{3.19}$$

of energy. Moreover, we define the dimensionless total energy $\mathcal{F}$ of the system of two loops $\mathcal{C}_1$ and $\mathcal{C}_2$ by

$$\mathcal{F} = \frac{R\mathcal{E}}{\mu_1} = \mathcal{F}_{\mathrm{B}} + \mathcal{F}_{\mathrm{S}} + \mathcal{F}_{\mathrm{I}}, \tag{3.20}$$

where the dimensionless counterparts, $\mathcal{F}_\mathrm{B}$, $\mathcal{F}_\mathrm{S}$, and $\mathcal{F}_\mathrm{I}$, of the bending energy, self energy, and interaction energy are given by

$$\mathcal{F}_\mathrm{B}[n_1, n_2] = \frac{1}{2} \int_0^{\ell_1} k_1^2 \, \mathrm{d}s + \frac{\nu}{2} \int_0^{\ell_2} k_2^2 \, \mathrm{d}s, \tag{3.21a}$$

$$\mathcal{F}_\mathrm{S}[n_1, n_2] = \frac{\zeta_1}{2} \int_0^{\ell_1}\!\!\int_0^{\ell_1} f(|n_1(s) - n_1(\bar{s})|) \, \mathrm{d}\bar{s} \, \mathrm{d}s + \frac{\zeta_2}{2} \int_0^{\ell_2}\!\!\int_0^{\ell_2} f(|n_2(s) - n_2(\bar{s})|) \, \mathrm{d}\bar{s} \, \mathrm{d}s, \tag{3.21b}$$

and

$$\mathcal{F}_\mathrm{I}[n_1, n_2] = \frac{\chi}{2} \int_0^{\ell_1}\!\!\int_0^{\ell_2} h(|n_1(s) - n_2(\bar{s})|) \, \mathrm{d}\bar{s} \, \mathrm{d}s. \tag{3.21c}$$

3.3 First and second variation conditions

Following Ericksen's [53] treatment of elastic stability theory, we focus on obtaining equilibrium configurations of $\mathcal{C}_1$ and $\mathcal{C}_2$, as characterized by n_1 and n_2, that are stable in the sense that the first variation condition

$$\delta \mathcal{F}[n_1, n_2](v_1, v_2) = 0 \tag{3.22}$$

and the second variation condition

$$\delta^2 \mathcal{F}[n_1, n_2](v_1, v_2) \geq 0, \tag{3.23}$$

must both hold for all variations $v_1 = \delta n_1$ and $v_2 = \delta n_2$ of n_1 and n_2 that, consistent with the constraints (3.4), satisfy

$$n_i \cdot v_i = 0 \quad \text{and} \quad n_i' \cdot v_i' = 0, \quad i = 1, 2. \tag{3.24}$$

In so doing, we assume that the variations v_i depends periodically on arclength on $\mathcal{C}_i$, $i = 1, 2$. Moreover, we emphasize that n_1 and n_2 in (3.23) must satisfy (3.22).

23

In appendix A, we derive the first variation condition (3.22) for $\mathcal{F}$ defined by (3.20) and find that it takes the form

$$\delta\mathcal{F}[n_1,n_2](v_1,v_2) = \int_0^{\ell_1} ((n_1''' + \lambda_1 n_1')' + \Lambda_1 n_1 - \zeta_1 \varphi[n_1,n_1] - \chi\varphi[n_1,n_2]) \cdot v_1 \, ds$$

$$+ \int_0^{\ell_2} (\nu(n_2''' + \lambda_2 n_2')' + \Lambda_2 n_2 - \zeta_2 \varphi[n_2,n_2] - \chi\varphi[n_2,n_1]) \cdot v_2 \, ds$$

$$+ n_1'' \cdot v_1'\big|_0^{\ell_1} - (n_1''' + \lambda_1 n_1') \cdot v_1\big|_0^{\ell_1} + \nu n_2'' \cdot v_2'\big|_0^{\ell_2} - \nu(n_2''' + \lambda_2 n_2') \cdot v_2\big|_0^{\ell_2}, \quad (3.25)$$

where Λ_i and λ_i are Lagrange multipliers that are needed to ensure satisfaction of $(3.4)_1$ and $(3.4)_2$, respectively, and φ is defined according to

$$\varphi[n_i,n_j] = \left\{ \begin{array}{ll} -\int_0^{\ell_j} f(n_i - n_j(\bar{s})) \, d\bar{s}, & i = j, \\[2mm] -\int_0^{\ell_j} h(n_i - n_j(\bar{s})) \, d\bar{s}, & i \neq j, \end{array} \right\}, \quad i,j = 1,2, \qquad (3.26)$$

with the integral kernels f and h being given by

$$f(\varrho) = \frac{df(\varrho)}{d\varrho}\bigg|_{\varrho=|\varrho|} \frac{\varrho}{|\varrho|} \quad \text{and} \quad h(\varrho) = \frac{dh(\varrho)}{d\varrho}\bigg|_{\varrho=|\varrho|} \frac{\varrho}{|\varrho|}. \qquad (3.27)$$

Applying the fundamental theorem of the calculus of variations to the first variation condition (3.22), we obtain equilibrium conditions in terms of a coupled pair of Euler–Lagrange equations,

$$\left. \begin{array}{l} (n_1''' + \lambda_1 n_1')' + \Lambda_1 n_1 = \zeta_1 \varphi[n_1,n_1] + \chi\varphi[n_1,n_2], \\[2mm] \nu(n_2''' + \lambda_2 n_2')' + \Lambda_2 n_2 = \zeta_2 \varphi[n_2,n_2] + \chi\varphi[n_2,n_1], \end{array} \right\}, \qquad (3.28)$$

and the boundary conditions

$$\left. \begin{array}{l} n_1'' \cdot v_1'\big|_0^{\ell_1} - (n_1''' + \lambda_1 n_1') \cdot v_1\big|_0^{\ell_1} = 0, \\[2mm] n_2'' \cdot v_2'\big|_0^{\ell_2} - (n_2''' + \lambda_2 n_2') \cdot v_2\big|_0^{\ell_2} = 0, \end{array} \right\}. \qquad (3.29)$$

Crucially, $(3.28)_1$ and $(3.29)_1$ hold on $\mathcal{C}_1$ but $(3.28)_2$ and $(3.29)_2$ hold on $\mathcal{C}_2$. Physical meaning of each of the terms involved in the Euler-Lagrange equations (3.28) is summarized in the table 3.1.

3.3.1 Boundary conditions

For smooth, closed curves, the boundary conditions (3.29) are trivially satisfied. However, for open curves, the terms in (3.29) are simplified depending on the type of boundary condition. For Dirichilet (first-type) boundary condition for curve $\mathcal{C}_i$, where the value of $\boldsymbol{n}_i$ is specified at the end points, the variation in $\boldsymbol{n}_i$ at the end points is zero which yields $\boldsymbol{v}_i(0) = \boldsymbol{v}_i(\ell_i) = 0$. Therefore, the requirement that all the admissible perturbations $\boldsymbol{v}_i$ satisfy (3.29) yields

$$\boldsymbol{n}_i''(0) = \boldsymbol{n}_i''(\ell_i) = 0. \tag{3.30}$$

In other words, the curve $\mathcal{C}_i$ parameterized by $\boldsymbol{n}_i$ that extremizes the dimensionless energy (3.20), when imposed with Dirichilet boundary condition yields zero curvature at the end points. This conclusion hold true even in the case where no interaction is present, i.e., $\mathcal{F}_S = \mathcal{F}_I = 0$. Essentially, a bending energy minimizing curve that satisfies Dirichilet boundary condition, has zero curvature at the end points.

For Neumann (second-type) boundary condition for curve $\mathcal{C}_i$, where the value of the derivative $\boldsymbol{n}_i'$ is specified at the end points, the variation in $\boldsymbol{n}_i'$ at the end points is zero which yields $\boldsymbol{v}_i'(0) = \boldsymbol{v}_i'(\ell_i) = 0$. Therefore, the requirement that all the admissible perturbations $\boldsymbol{v}_i$ satisfy (3.29) yields

$$\boldsymbol{n}_i'''(0) = -\lambda_i(0)\boldsymbol{n}_i'(0) \quad \text{and} \quad \boldsymbol{n}_i'''(\ell_i) = -\lambda_i(\ell_i)\boldsymbol{n}_i'(\ell_i) \tag{3.31}$$

which is a force balance at the end points between the bending resistance and the reactive tension developed in the curve to maintain inextensibility.

Henceforth, our work only involves smooth, closed curves referred to as loops which trivially satisfy the boundary condtions (3.29). In appendix A, we

Table 3.1: Terms in the equilibrium equation (3.28) and their significance.

Term	Dimensionless force
$\Lambda_i \boldsymbol{n}_i$	Adhesive force acting on the curve $\mathcal{C}_i$ to restrict it to $\mathcal{S}$.
$(\lambda_i \boldsymbol{n}_i'' + \lambda_i' \boldsymbol{n}_i')$	Reactive tension in the curve $\mathcal{C}_i$ to ensure inextensibility .
$-\zeta_i \boldsymbol{\varphi}[\boldsymbol{n}_i, \boldsymbol{n}_i]$	Force acting on the element $\mathrm{d}s$ of $\mathcal{C}_i$ at arclength s against repulsion by all the remaining elements of $\mathcal{C}_i$.
$-\chi \boldsymbol{\varphi}[\boldsymbol{n}_i, \boldsymbol{n}_j]$	Force acting on the element $\mathrm{d}s$ of $\mathcal{C}_i$ at arclength s against repulsion by all the remaining elements of C_j, $i, j = 1, 2, i \neq j$.

also derive the second variation condition (3.23) and find that it takes the form

$$
\int_0^{\ell_1} \left(|v_1''|^2 - \lambda_1 |v_1'|^2 + (\lambda_1' v_1' + \Lambda_1 v_1 - \zeta_1 \boldsymbol{\vartheta}[\boldsymbol{n}_1, \boldsymbol{n}_1](v_1, v_1) \right.
$$
$$
\left. - \chi \boldsymbol{\vartheta}[\boldsymbol{n}_1, \boldsymbol{n}_2](v_1, v_2)) \cdot v_1 \right) \mathrm{d}s
$$
$$
+ \int_0^{\ell_2} \left(\nu(|v_2''|^2 - \lambda_2 |v_2'|^2) + (\nu \lambda_2' v_2' + \Lambda_2 v_2 - \zeta_2 \boldsymbol{\vartheta}[\boldsymbol{n}_2, \boldsymbol{n}_2](v_2, v_2) \right.
$$
$$
\left. - \chi \boldsymbol{\vartheta}[\boldsymbol{n}_2, \boldsymbol{n}_1](v_2, v_1)) \cdot v_2 \right) \mathrm{d}s \geq 0, \quad (3.32)
$$

where $\boldsymbol{\vartheta}$ is defined according to

$$
\boldsymbol{\vartheta}[\boldsymbol{n}_i, \boldsymbol{n}_j](v_i, v_j) = \left\{ \begin{array}{ll} -\int_0^{\ell_j} \boldsymbol{F}(\boldsymbol{n}_i - \boldsymbol{n}_j(\bar{s}))(v_i - v_j(\bar{s})) \, \mathrm{d}\bar{s}, & i = j, \\[2mm] -\int_0^{\ell_j} \boldsymbol{H}(\boldsymbol{n}_i - \boldsymbol{n}_j(\bar{s}))(v_i - v_j(\bar{s})) \, \mathrm{d}\bar{s}, & i \neq j, \end{array} \right\}, \quad i, j = 1, 2,
$$
$$
(3.33)
$$

with the integral kernels $\boldsymbol{F}$ and $\boldsymbol{h}$ being given by

$$
\boldsymbol{F}[\varrho] = \frac{1}{\varrho} \left(\frac{\mathrm{d}f(\varrho)}{\mathrm{d}\varrho} \mathbf{1} + \frac{\mathrm{d}}{\mathrm{d}\varrho} \left(\frac{1}{\varrho} \frac{\mathrm{d}f(\varrho)}{\mathrm{d}\varrho} \right) \varrho \otimes \varrho \right) \Big|_{\varrho = |\varrho|} \qquad (3.34\mathrm{a})
$$

and

$$
\boldsymbol{H}[\varrho] = \frac{1}{\varrho} \left(\frac{\mathrm{d}h(\varrho)}{\mathrm{d}\varrho} \mathbf{1} + \frac{\mathrm{d}}{\mathrm{d}\varrho} \left(\frac{1}{\varrho} \frac{\mathrm{d}h(\varrho)}{\mathrm{d}\varrho} \right) \varrho \otimes \varrho \right) \Big|_{\varrho = |\varrho|}. \qquad (3.34\mathrm{b})
$$

3.4 Limitations of our model

One of the major limitation of our framework is that it can not account for thickness of the polyelectrolytes and bio molecules such as peptides, proteins and DNA. A more realistic model for such entities will involve rods that consist of a space curve representing its centerline and a material frame at each point on the centerline that contains information about the cross-section of the rod. Additionally, twist in the rod can describe the effect of helicity of the molecules which our space curve based model is unable to incorporate.

Moreover, since a rod has finite thickness, overlap between two elements of the rod will have finite interaction energy, assuming that the charges are concentrated along the centerline of the rod. Therefore, a model consisting of rods can capture intersections in the molecules. In contrast, our model that involves space curve for which intra-loop or intra-loop overlap of the elements will result in blow up of the interaction energy. Hence, our model is not equipped to capture any kind of self-intersection or the intersection between two molecules.

Flexibility of elongated molecules are usually described in the terms of persistence length. Short range atomic and molecular level interactions lead to the bending rigidity and the notion of persistence length [56]. In the case of charged polymers, the long range nature of the electrostatic interactions modifies the value of the persistence length and effective bending rigidity as described in the seminal work of Odijk, Skolnick, and Fixman (OSF) [57]. In our model, the bending energy is characterized through a single, constant bending modulus which means that the length of the curves we consider are smaller than their persistence length. We do not consider any thermal fluctuation in our model. Moreover, we consider bending energy and intra-loop interaction energy as two independent effects. We do not derive effective bending rigidity due to intra-loop repulsion between elements of a curve.

3.5 Conclusion

We have used a variational model to study the equilibrium configuration and stability behavior of two charged loops constrained to a sphere. Our model involves five material parameters: the bending rigidity of the two loops μ_1 and μ_2, the self energy coefficient of the two loops A_{11} and A_{22} and the interaction energy parameter A_{12} between the two loops. In combination with the length of the two loops L_1 and L_2 and radius of the sphere R, these quantities give rise to six dimensionless parameters: the ratio of the bending modulus $\mu = \mu_2/\mu_1$, the ratio of self energy coefficient and the bending modulus scaled with the radius of the sphere $\zeta_1 = A_{11}R^3/\mu_1, \zeta_2 = A_{22}R^3/\mu_1$, the ratio of the interaction energy coefficient and the bending modulus scaled with the radius of the sphere $\chi = A_{12}R^3/\mu_1$ and the ratio of the length of the loop to the radius of the sphere $l_1 = L_1/R$ and $l_2 = L_2/R$.

CHAPTER 4 SPECIALIZED APPLICATION

4.1 Introduction

In this chapter, we apply the framework developed in developed in chapter 3 to a simplified problem to gain more insight into how the competition between various energy drive the equilibrium configuration and its stability. In §4.2 we characterize the interaction of two uniformly charged loops that have the same length and material parameters. The trivial equilibrium solution to this special problem is presented in §4.2.3. Stability criteria for the trivial solution is identified in §4.3 and the associated bifurcation analysis is obtained in §4.4. Explanation of how the geometric and material parameters effect the stability of the trivial solution are provided in §4.3.

4.2 Model

To acquire a partial understanding of how the effects of bending energy, self energy, and interaction energy combine to influence equilibrium configurations of the system of two loops, we consider the particular situation where the $\mathcal{C}_1$ and $\mathcal{C}_2$ have the same length, bending moduli, and interaction parameters, so that

$$L_1 = L_2 = L, \quad \mu_1 = \mu_2 = \mu, \quad \text{and} \quad A_{11} = A_{22} = A, \tag{4.1}$$

and, thus are both geometrically and physically indistinguishable. With this simplification, the general problem formulated in the previous chapter reduces to one involving only a single dimensionless measure of length, namely

$$a = \frac{L}{2\pi R} \tag{4.2}$$

and two dimensionless measures of energy, namely

$$\zeta = \frac{R^3 A}{\mu} \quad \text{and} \quad \chi = \frac{R^3 A_{12}}{\mu}. \tag{4.3}$$

To ensure the existence of a trivial equilibrium solution in which $\mathcal{C}_1$ and $\mathcal{C}_2$ are circular and lie in parallel planes, we assume that

$$0 < a < 1. \tag{4.4}$$

In view of the stated assumptions, the Euler–Lagrange equations (3.28) specialize to

$$\left. \begin{aligned} (\boldsymbol{n}_1''' + \lambda_1 \boldsymbol{n}_1')' + \Lambda_1 \boldsymbol{n}_1 &= \zeta \boldsymbol{\varphi}[\boldsymbol{n}_1, \boldsymbol{n}_1] + \chi \boldsymbol{\varphi}[\boldsymbol{n}_1, \boldsymbol{n}_2], \\ (\boldsymbol{n}_2''' + \lambda_2 \boldsymbol{n}_2')' + \Lambda_2 \boldsymbol{n}_2 &= \zeta \boldsymbol{\varphi}[\boldsymbol{n}_2, \boldsymbol{n}_2] + \chi \boldsymbol{\varphi}[\boldsymbol{n}_2, \boldsymbol{n}_1], \end{aligned} \right\} . \tag{4.5}$$

Similarly, the second variation condition (3.32) specializes to

$$\int_0^{2\pi a} \left(|\boldsymbol{v}_1''|^2 - \lambda_1 |\boldsymbol{v}_1'|^2 + (\lambda_1' \boldsymbol{v}_1' + \Lambda_1 \boldsymbol{v}_1 - \zeta \boldsymbol{\vartheta}[\boldsymbol{n}_1, \boldsymbol{n}_1](\boldsymbol{v}_1, \boldsymbol{v}_1) \right.$$

$$\left. - \chi \boldsymbol{\vartheta}[\boldsymbol{n}_1, \boldsymbol{n}_2](\boldsymbol{v}_1, \boldsymbol{v}_2)) \cdot \boldsymbol{v}_1 \right) \mathrm{d}s$$

$$+ \int_0^{2\pi a} \left((|\boldsymbol{v}_2''|^2 - \lambda_2 |\boldsymbol{v}_2'|^2) + (\lambda_2' \boldsymbol{v}_2' + \Lambda_2 \boldsymbol{v}_2 - \zeta \boldsymbol{\vartheta}[\boldsymbol{n}_2, \boldsymbol{n}_2](\boldsymbol{v}_2, \boldsymbol{v}_2) \right.$$

$$\left. - \chi \boldsymbol{\vartheta}[\boldsymbol{n}_2, \boldsymbol{n}_1](\boldsymbol{v}_2, \boldsymbol{v}_1)) \cdot \boldsymbol{v}_2 \right) \mathrm{d}s \geq 0. \tag{4.6}$$

4.2.1 Interaction potentials

In an additional simplifying assumption, we take $\mathcal{C}_1$ and $\mathcal{C}_2$ to be uniformly charged, in which case the general expressions for f and h specialize to

$$f(\varrho) = h(\varrho) = \frac{1}{\varrho}, \tag{4.7}$$

while the allied quantities $\boldsymbol{f}$ and $\boldsymbol{h}$ defined in (3.27) and for $\boldsymbol{F}$ and $\boldsymbol{H}$ defined in (3.34a) and (3.34b) are given by

$$\boldsymbol{f}(\boldsymbol{\varrho}) = \boldsymbol{h}(\boldsymbol{\varrho}) = -\frac{\boldsymbol{\varrho}}{|\boldsymbol{\varrho}|^3} \quad \text{and} \quad \boldsymbol{F}(\boldsymbol{\varrho}) = \boldsymbol{H}(\boldsymbol{\varrho}) = \frac{3}{|\boldsymbol{\varrho}|^3} \left(\frac{\boldsymbol{\varrho} \otimes \boldsymbol{\varrho}}{|\boldsymbol{\varrho}|^2} - \frac{1}{3} \boldsymbol{1} \right). \tag{4.8}$$

30

<center>self intersection   inter-loop intersection</center>

<center>f, $\boldsymbol{f}$, and $\boldsymbol{F}$ diverge h, $\boldsymbol{h}$, and $\boldsymbol{H}$ diverge</center>
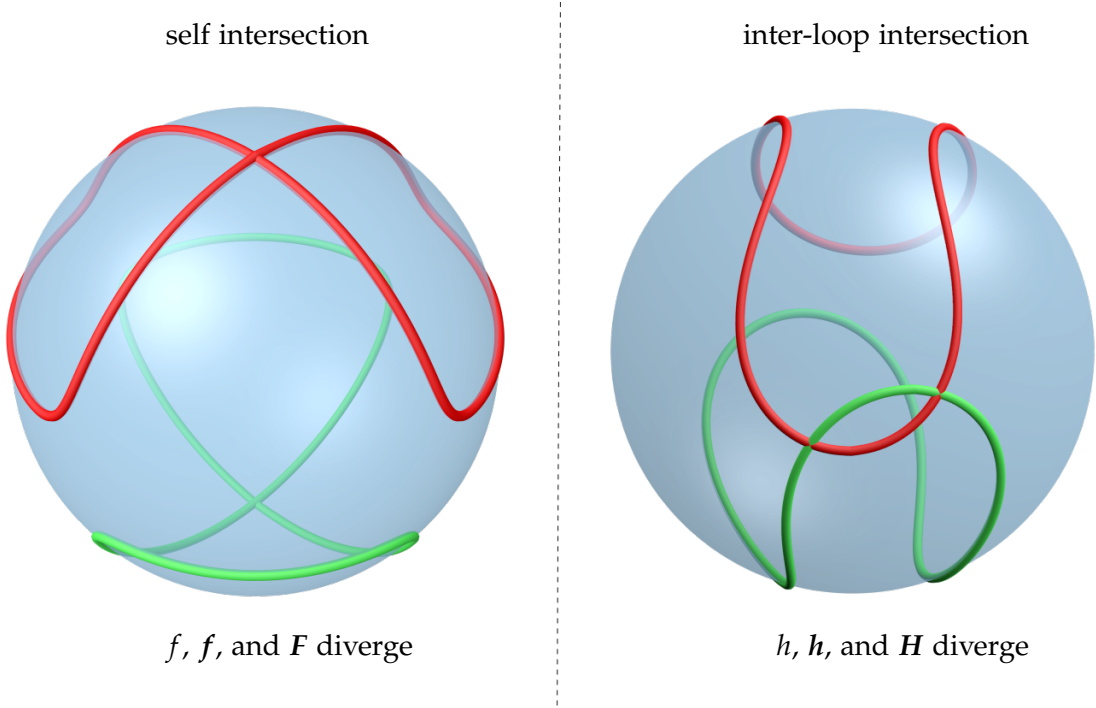
Figure 4.1: Intra-loop and inter-loop intersections and the quantities that diverge in the corresponding situations.

Each of these quantities diverges as $\varrho \to 0$. These divergences stem from the repulsive nature of the potentials f and h and embody our desire to penalize self intersections of $\mathcal{C}_1$ and $\mathcal{C}_2$ and intersections between $\mathcal{C}_1$ and $\mathcal{C}_2$ which are described in the figure 4.1. From this perspective, the functionals $\mathcal{E}_\mathrm{S}$ and $\mathcal{E}_\mathrm{I}$ are analogous to O'Hara's [49] energy functional, which diverges when a curve intersects itself and which O'Hara [50, 51] subsequently interpreted as the potential energy of an electrically charged loop, the Coulomb force of which is proportional to inverse of the cube of the distance between points on the loop. Independent of any divergence of the kind described in the previous paragraph, the situation $\rho = 0$ is encountered in the integrals $(3.26)_1$ and $(3.33)_1$ involving the kernels f and F when the variable of integration coincides with the arclength at which $\boldsymbol{\varphi}[\boldsymbol{n}_i, \boldsymbol{n}_i]$ and $\boldsymbol{\vartheta}[\boldsymbol{n}_i, \boldsymbol{n}_i](v_i, v_i)$ are evaluated, respectively. This kind of divergence is unphysical and therefore warrants regularization. As $\bar{s} \to s$, $\boldsymbol{n}_i(\bar{s}) - \boldsymbol{n}_i(s) \sim (\bar{s} - s)\boldsymbol{n}_i'(s) +$

<center>31</center>
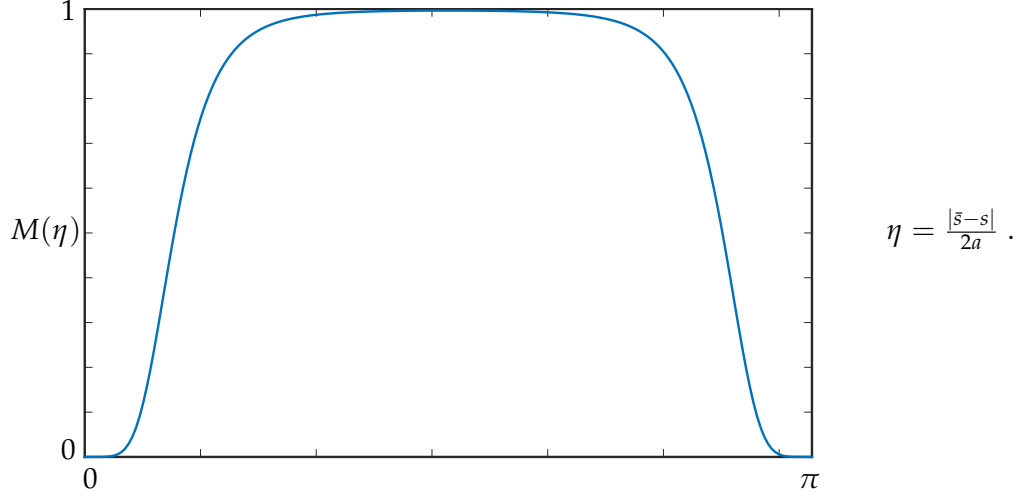
$$\eta = \frac{|\bar{s}-s|}{2a}\ .$$

Figure 4.2: Example of a mollifying function M with compact support.

$\mathcal{O}[(\bar{s}-s)^2]$ and consequently,

$$f(\boldsymbol{n}_i(s) - \boldsymbol{n}_i(\bar{s})) \sim |\bar{s} - s|^{-2} \quad \text{and} \quad F(\boldsymbol{n}_i(s) - \boldsymbol{n}_i(\bar{s})) \sim |\bar{s} - s|^{-3} \qquad (4.9)$$

for $\bar{s}$ in neighborhood of s. To be effective, any regularization strategy must be designed to account for the third-order singularity in the magnitude of its argument that is evident from (4.8) and (4.9). In this regard, it suffices to introduce a mollifier M with compact support and with properties

$$M(|\eta|) > 0 \quad \text{and} \quad M(|\eta|) \sim \eta^4 \quad \text{as} \quad \eta \to 0, \qquad (4.10)$$

and replace the potential f by a regularized potential $\tilde{f}$ of the form

$$\tilde{f}\left(|\boldsymbol{n}_i(s) - \boldsymbol{n}_i(\bar{s})|, \frac{|\bar{s}-s|}{2a}\right) = M\left(\frac{|\bar{s}-s|}{2a}\right) \frac{1}{|\boldsymbol{n}_i(s) - \boldsymbol{n}_i(\bar{s})|}, \quad i = 1, 2. \qquad (4.11)$$

Because $|\bar{s} - s| \in [0, 2\pi a]$, we have normalized this quantity in the argument of M with the factor $2a$ such that domain of the function M is $[0, \pi]$. A typical mollifier M is shown in the figure 4.2.

Since the variable of integration coincides with the arclength at which $\boldsymbol{\varphi}[\boldsymbol{n}_i, \boldsymbol{n}_j]$ and $\boldsymbol{\vartheta}[\boldsymbol{n}_i, \boldsymbol{n}_j](\boldsymbol{v}_i, \boldsymbol{v}_j)$, $i, j = 1, 2, i \neq j$, is evaluated only if $\mathcal{C}_1$ and $\mathcal{C}_2$ intersect and such intersections are penalized as described above, there is no analogous need to regularize interaction potential h and the allied kernels $\boldsymbol{h}$ and $\boldsymbol{H}$.

4.2.2 Regularized equilibrium equations

Granted that the potential f in (4.7) is replaced by $\tilde{f}$ defined in (4.11), the Euler–Lagrange equations (4.5) and the second variation condition (4.6) change to

$$
\left.\begin{aligned}
(n_1''' + \lambda_1 n_1')' + \Lambda_1 n_1 &= \zeta\tilde{\varphi}[n_1, n_1] + \chi\varphi[n_1, n_2], \\
(n_2''' + \lambda_2 n_2')' + \Lambda_2 n_2 &= \zeta\tilde{\varphi}[n_2, n_2] + \chi\varphi[n_2, n_1],
\end{aligned}\right\}, \tag{4.12}
$$

where $\tilde{\varphi}$ is defined by

$$
\tilde{\varphi}[n_i, n_i](s) = -\int_0^{2\pi a} M\left(\frac{|\bar{s} - s|}{2a}\right) f(n_i(s) - n_i(\bar{s}))\, d\bar{s}, \quad i = 1, 2. \tag{4.13}
$$

Similarly, the second variation condition (4.6) changes to

$$
\int_0^{2\pi a} \big(|v_1''|^2 - \lambda_1|v_1'|^2 + (\lambda_1' v_1' + \Lambda_1 v_1 - \zeta\tilde{\vartheta}[n_1, n_1](v_1, v_1)
$$

$$
- \chi\vartheta[n_1, n_2](v_1, v_2)) \cdot v_1\big)\, ds
$$

$$
+ \int_0^{2\pi a} \big((|v_2''|^2 - \lambda_2|v_2'|^2) + (\lambda_2' v_2' + \Lambda_2 v_2 - \zeta\tilde{\vartheta}[n_2, n_2](v_2, v_2)
$$

$$
- \chi\vartheta[n_2, n_1](v_2, v_1)) \cdot v_2\big)\, ds \geq 0, \tag{4.14}
$$

where $\tilde{\vartheta}$ is defined by

$$
\tilde{\vartheta}[n_i, n_i](v_i, v_i) = -\int_0^{2\pi a} M\left(\frac{|\bar{s} - s|}{2a}\right) F(n_i - n_i(\bar{s}))(v_i - v_i(\bar{s}))\, d\bar{s}, \quad i = 1, 2. \tag{4.15}
$$

Whereas $(4.12)_1$ and $(4.12)_2$ are obtained by substituting $\varphi(n_1, n_1)$ in $(4.5)_1$ with $\tilde{\varphi}(n_1, n_1)$ and $\varphi(n_2, n_2)$ in $(4.5)_2$ with $\tilde{\varphi}(n_2, n_2)$, (4.14) is obtained by substituting $\vartheta[n_i, n_i](v_i, v_i)$ in (4.6) with $\tilde{\vartheta}[n_i, n_i](v_i, v_i)$, $i = 1, 2$. The mollified quantities are obtained by multiplying the integral kernels f and F of the $(3.26)_1$ and $(3.33)_1$ by M. As noted in the previous subsection, these modifications eliminate non-physical divergences that arise due to definition of the self interaction potential f.
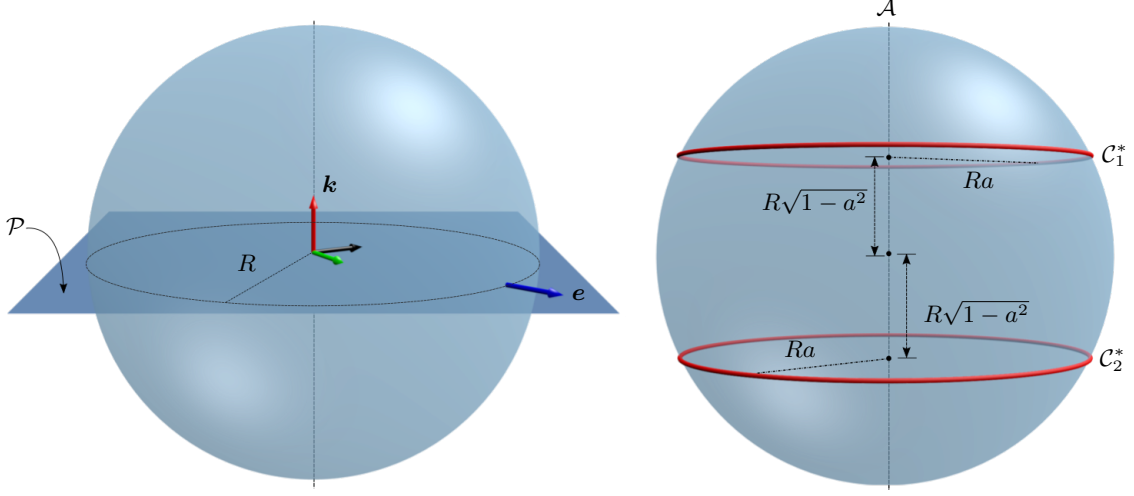
Figure 4.3: Circular loops $\mathcal{C}_1$ and $\mathcal{C}_2$ of dimensionless length $2\pi a$, with $0 < a < 1$, situated on opposing planes parallel to an equatorial plane of a sphere $\mathcal{S}$, of radius R, at respective altitudes $R\sqrt{1-a^2}$ and $-R\sqrt{1-a^2}$. The vector field e describes the restriction to the equatorial great circle of the outward unit normal to $\mathcal{S}$.

4.2.3   Trivial equilibrium solution

Consider an equatorial plane $\mathcal{P}$ of the sphere $\mathcal{S}$ upon which the loops $\mathcal{C}_1$ and $\mathcal{C}_2$ are confined, as shown in Figure 4.3. Let $\{\imath, \jmath, k\}$ be a positively-oriented orthonormal basis with k directed upward along the polar axis $\mathcal{A}$ of $\mathcal{S}$. Then, e defined by

$$e(s) = \left(\cos \frac{s}{a} \right) \imath + \left(\sin \frac{s}{a} \right) \jmath, \quad 0 \leq s \leq 2\pi a, \tag{4.16}$$

represents the restriction to the equatorial great circle of the outward unit normal to $\mathcal{S}$. We suppose that the loops are circles — denoted by $\mathcal{C}_1^*$ and $\mathcal{C}_2^*$ — of radius Ra that reside in planes parallel to and separated from $\mathcal{P}$ by the distance $R\sqrt{1-a^2}$. The total energy of this configuration does not change on fixing one loop and rotating the other loop by an arbitrary angle about $\mathcal{A}$. We may therefore choose the quantities n_1^* and n_2^* that parametrize $\mathcal{C}_1^*$ and $\mathcal{C}_2^*$ to be of the form

$$n_1^* = n \quad \text{and} \quad n_2^* = Qn, \tag{4.17}$$

where n is defined such that

$$n(s) = ae(s) + \sqrt{1 - a^2}k, \quad 0 \le s \le 2\pi a, \tag{4.18}$$

and, Q defined by

$$Q(\phi) = \cos\phi(\imath \otimes \imath + \jmath \otimes \jmath) - \sin\phi(\imath \otimes \jmath - \jmath \otimes \imath) - 2k \otimes k, \quad 0 \le \psi \le 2\pi \tag{4.19}$$

is the orthogonal tensor that transforms any vector by simultaneously reflecting it across $\mathcal{A}$ and rotating it counterclockwise by ϕ about $\mathcal{A}$. The elementary properties of Q that are useful for further calculations are

$$|Qm| = |m| \quad \text{and} \quad Q^\top Q = \mathbf{1}. \tag{4.20}$$

We substitute the particular choices (4.17) of n_1 and n_2 in the equilibrium equations (4.12) and make simplifications by applying $Q^\top$ to second of the equations obtained by using (4.20), leading to

$$\left. \begin{aligned} (n''' + \lambda_1^* n')' + \Lambda_1^* n &= \zeta \int_0^{2\pi a} M\left(\frac{|\bar{s} - s|}{2a}\right) \frac{n - n(\bar{s})}{|n - n(\bar{s})|} \, d\bar{s} \\ &\quad + \chi \int_0^{2\pi a} \frac{n - Qn(\bar{s})}{|n - Qn(\bar{s})|} \, d\bar{s}, \\ (n''' + \lambda_2^* n')' + \Lambda_2^* n &= \zeta \int_0^{2\pi a} M\left(\frac{|\bar{s} - s|}{2a}\right) \frac{n - n(\bar{s})}{|n - n(\bar{s})|} \, d\bar{s} \\ &\quad + \chi \int_0^{2\pi a} \frac{n - Q^\top n(\bar{s})}{|n - Q^\top n(\bar{s})|} \, d\bar{s}, \end{aligned} \right\},$$

where Λ_i^* and λ_i^* are the Lagrange multipliers, as yet undetermined, needed to ensure the circular loop $\mathcal{C}_i^*$, $i = 1, 2$, is configured in consistency with the constraints $(3.4)_1$ and $(3.4)_2$, respectively. Next, since

$$Q^\top(\phi)n(s + 2a\phi) = Q(\phi)n(s), \quad 0 \le s \le 2\pi a, \tag{4.21}$$

we may use the change of variables $\bar{s} \to \bar{s} + 2a\phi$ in the second integral on the right-hand side of $(4.21)_2$ to find that, since n is periodic on the interval from 0 to $2\pi a$,

$$\int_0^{2\pi a} \frac{n - Q^\top n(\bar{s})}{|n - Q^\top n(\bar{s})|} \, d\bar{s} = \int_{2\phi a}^{2(\pi + \phi)a} \frac{n - Qn(\bar{s})}{|n - Qn(\bar{s})|} \, d\bar{s} = \int_0^{2\pi a} \frac{n - Qn(\bar{s})}{|n - Qn(\bar{s})|} \, d\bar{s}. \tag{4.22}$$

Using (4.22) in (4.21)$_2$ and subtracting the resulting equation from (4.21)$_1$, we obtain the condition

$$\lambda_1^* \boldsymbol{n}'' + (\lambda_1^*)' \boldsymbol{n}' + \Lambda_1^* \boldsymbol{n} = \lambda_1^* \boldsymbol{n}'' + (\lambda_2^*)' \boldsymbol{n}' + \Lambda_2^* \boldsymbol{n}. \tag{4.23}$$

Computing the dot product with $\boldsymbol{k}$ on both sides of (4.23) while noting from (4.18) that $\boldsymbol{k} \cdot \boldsymbol{n}' = 0$ and $\boldsymbol{k} \cdot \boldsymbol{n}'' = 0$, we find that

$$\Lambda_1^* = \Lambda_2^* = \Lambda. \tag{4.24}$$

Similarly, computing the dot product with $\boldsymbol{n}''$ on both sides of (4.23), noting that differentiating (3.4)$_1$ twice and using (3.4)$_2$ yields $\boldsymbol{n} \cdot \boldsymbol{n}'' = -1$ and differentiating (3.4)$_2$ yields $\boldsymbol{n}' \cdot \boldsymbol{n}'' = 0$, we find that $\lambda_1^* |\boldsymbol{n}''|^2 - \Lambda_1^* = \lambda_2^* |\boldsymbol{n}''|^2 - \Lambda_2^*$ and, thus, by (4.24), that

$$\lambda_1^* = \lambda_2^* = \lambda. \tag{4.25}$$

In view of (4.22), (4.24), and (4.25), the equilibrium conditions (4.21)$_1$ and (4.21)$_2$ are equivalent. We may thus use either of these conditions to determine Λ and λ. Using (4.24) and (4.25) in the left-hand side of (4.21)$_1$, we get

$$(\boldsymbol{n}''' + \lambda \boldsymbol{n}')' + \Lambda \boldsymbol{n} - \zeta \int_0^{2\pi a} M\left(\frac{|\bar{s} - s|}{2a}\right) \frac{\boldsymbol{n} - \boldsymbol{n}(\bar{s})}{|\boldsymbol{n} - \boldsymbol{n}(\bar{s})|} \, d\bar{s} - \chi \int_0^{2\pi a} \frac{\boldsymbol{n} - Q\boldsymbol{n}(\bar{s})}{|\boldsymbol{n} - Q\boldsymbol{n}(\bar{s})|} \, d\bar{s} = \boldsymbol{0}. \tag{4.26}$$

Bearing in mind that the dimensionless geodesic curvature of $\mathcal{C}_1^*$ is given by

$$k = \frac{\sqrt{1 - a^2}}{a}, \tag{4.27}$$

we obtain the identity

$$(\boldsymbol{n}''' + \lambda \boldsymbol{n}')' + \Lambda \boldsymbol{n} = \lambda' \boldsymbol{t} + \left(\Lambda - \lambda + \frac{1}{a^2}\right) \boldsymbol{n} - \frac{\sqrt{1 - a^2}}{a}\left(\lambda - \frac{1}{a^2}\right) \boldsymbol{g}, \tag{4.28}$$

where $\boldsymbol{t}$ and $\boldsymbol{g}$ given by

$$\boldsymbol{t}(s) = -\left(\sin\frac{s}{a}\right)\boldsymbol{\imath} + \left(\cos\frac{s}{a}\right)\boldsymbol{\jmath}, \quad \boldsymbol{g}(s) = \sqrt{1 - a^2}\boldsymbol{e}(s) - a\boldsymbol{k}, \quad 0 \le s \le 2\pi a, \tag{4.29}$$

36

denote the tangential and geodesic elements of the Darboux frame for $\mathcal{C}_1^*$. With the change of variables $\eta = |\bar{s} - s|/2a$, we next find that the integrals in $(4.26)_1$ can be expressed as

$$\zeta \int_0^{2\pi a} M\!\left(\frac{|\bar{s} - s|}{2a}\right) \frac{\boldsymbol{n} - \boldsymbol{n}(\bar{s})}{|\boldsymbol{n} - \boldsymbol{n}(\bar{s})|}\, d\bar{s} + \chi \int_0^{2\pi a} \frac{\boldsymbol{n} - Q\boldsymbol{n}(\bar{s})}{|\boldsymbol{n} - Q\boldsymbol{n}(\bar{s})|}\, d\bar{s}$$

$$= \left(\frac{\zeta}{2} \int_0^\pi M(\eta)\csc\eta\, d\eta + \frac{\chi a}{2}\int_0^\pi \frac{d\eta}{\sqrt{1 - a^2\cos^2\eta}}\right)\boldsymbol{n}$$

$$+ \left(\frac{\zeta}{2} \int_0^\pi M(\eta)\csc\eta\, d\eta - \frac{\chi a^3}{2}\int_0^\pi \frac{\cos^2\eta\, d\eta}{\sqrt[3]{1 - a^2\cos^2\eta}}\right)\boldsymbol{g}. \quad (4.30)$$

Using (4.28) and (4.30) in $(4.21)_1$, we thus obtain a reduced system

$$\left.\begin{aligned}
&\lambda' = 0, \\[4pt]
&\Lambda - \lambda + \frac{1}{a^2} - \frac{\zeta}{2}\int_0^\pi M(\eta)\csc\eta\, d\eta - \frac{\chi a}{2}\int_0^\pi \frac{d\eta}{\sqrt{1 - a^2\cos^2\eta}} = 0, \\[4pt]
&\lambda - \frac{1}{a^2} + \frac{\zeta}{2}\int_0^\pi M(\eta)\csc\eta\, d\eta - \frac{\chi a^3}{2}\int_0^\pi \frac{\cos^2\eta\, d\eta}{\sqrt[3]{1 - a^2\cos^2\eta}} = 0,
\end{aligned}\right\} \quad (4.31)$$

for Λ and λ. By $(4.31)_1$, we see that λ must be uniform. With this being the case, we see from $(4.31)_2$ that Λ must also be uniform. Finally, solving the linear systems $(4.31)_{2,3}$ for Λ and λ, we find that

$$\Lambda = \frac{a\chi}{2}\int_0^\pi \frac{d\eta}{\sqrt[3]{1 - a^2\cos^2\eta}} \quad \text{and}$$

$$\lambda = \frac{1}{a^2} - \frac{\zeta}{2}\int_0^\pi M(\eta)\csc\eta\, d\eta + \frac{\chi a^3}{2}\int_0^\pi \frac{\cos^2\eta\, d\eta}{\sqrt[3]{1 - a^2\cos^2\eta}}. \quad (4.32)$$

The reactions needed to ensure that the loops adhere to $\mathcal{S}$ are therefore equal and given by $\mu\Lambda/R^2$. Similarly, the reactions needed to ensure that the lengths of the loops are preserved pointwise are equal and given by $\mu\lambda/R^2$. From $(4.32)_1$, we see that the adhesive reaction depends only on the common dimensionless radius a of the loops and the dimensionless measure χ of the importance of the repulsive interaction between the loops relative to their bending stiffness. From
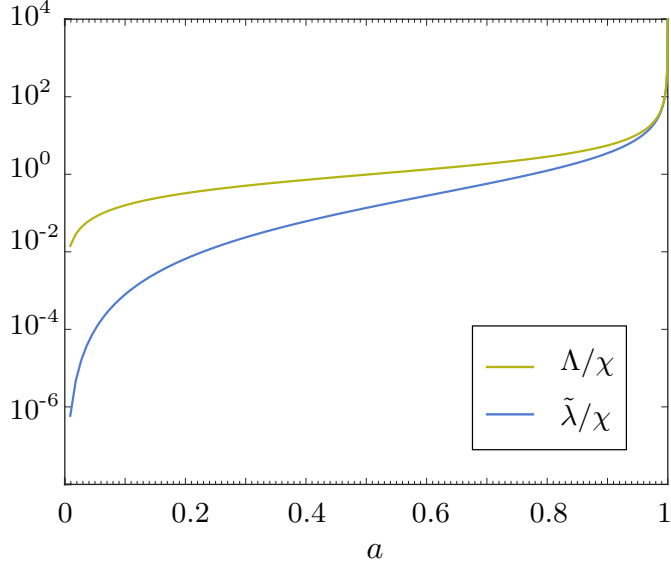
Figure 4.4: Plots of the Lagrange multipliers Λ/χ in $(4.32)_1$ and reduced multiplier $\tilde{\lambda}/\chi$ in (4.34) versus the dimensionless radius a of the circular loops. Λ is the dimensionless adhesive force between the curve and the sphere and $\tilde{\lambda}$ is the dimensionless tension developed in the curves due to repulsion between the two loops. Both the quantities monotonically increase with a.

$(4.32)_1$, we see that the ratio Λ/χ depends only on a and, moreover, that

$$\frac{\Lambda}{\chi} \sim a \quad \text{as} \quad a \downarrow 0, \quad \frac{\Lambda}{\chi} \sim \frac{1}{1-a} \quad \text{as} \quad a \uparrow 1, \quad \text{and} \quad \frac{\mathrm{d}}{\mathrm{d}a}\left(\frac{\Lambda}{\chi}\right) > 0 \quad \text{for} \quad 0 < a < 1.$$

$$(4.33)$$

We thus infer that the magnitude of the adhesive reaction increases monotonically with a for $0 < a < 1$. From $(4.32)_2$, the tensile reaction encompasses several competing effects. The first term, $1/a^2$ on the right-hand side of $(4.32)_2$ is the contribution to the reaction associated with ensuring that the action of bending a straight segments of length $2\pi Ra$ into a circular loop of radius Ra involves neither local elongation nor contraction. Since the integral in the second term on the right-hand side of $(4.32)_2$ is independent of a, that term simply produces a uniform reaction proportional to the dimensionless measure ζ of the repulsive self interactions of the loops relative to their bending stiffness. The final term on

the right-hand side of $(4.32)_2$ depends only on a and χ and, thus, is analogous to the only term on the right-hand side of $(4.32)_1$. To explore the properties of the associated reaction, we therefore consider the reduced multiplier

$$\tilde{\lambda} = \lambda - \frac{1}{a^2} + \frac{\zeta}{2}\int_0^\pi M(\eta)\csc\eta\,\mathrm{d}\eta = \frac{\chi a^3}{2}\int_0^\pi \frac{\cos^2\eta\,\mathrm{d}\eta}{\sqrt[3]{1 - a^2\cos^2\eta}}. \tag{4.34}$$

Emulating the reasoning leading to (4.33), we see that

$$\frac{\tilde{\lambda}}{\chi}\sim a^3 \quad\text{as}\quad a\downarrow 0, \quad \frac{\tilde{\lambda}}{\chi}\sim\frac{1}{1-a} \quad\text{as}\quad a\uparrow 1, \quad\text{and}\quad \frac{\mathrm{d}}{\mathrm{d}a}\left(\frac{\tilde{\lambda}}{\chi}\right) > 0 \quad\text{for}\quad 0 < a < 1. \tag{4.35}$$

We thus infer the magnitude of the reaction needed to ensure that the lengths of the loops are preserved pointwise increases monotonically with a for $0 < a < 1$.

Plots of Λ/χ and $\tilde{\lambda}/\chi$ versus a for $0 < a < 1$ are provided in Figure 4.4. These confirm our qualitative observations. For $a \to 0$, the distance between loops is maximized, meaning that the repulsive interaction between them diminishes. Consequently, Λ and $\tilde{\lambda}$ both vanish as $a \to 0$. Since $\lambda \sim 1/a^2$ in this regime, the tensile reaction is dominated by the bending resistance of the loops. For $a \to 1$, $\Lambda \sim (1-a)^{-1}$ and $\lambda \sim (1-a)^{-1}$, from which we see that the reactions are dominated by the interactions between the loops.

4.3 Stability analysis of the trivial solution

Given a dimensionless radius $0 < a < 1$ of the loops and dimensionless measures $\zeta \geq 0$ and $\chi \geq 0$ of the repulsive intraloop and interloop interactions, n_i^*, Λ_i, and λ_i, $i = 1, 2$, defined by (4.17)–(4.18), (4.24)–(4.25), and (4.32) determine a trivial equilibrium solution to the specialized problem formulated in Section 4.2. We now explore the stability of the resulting family of solutions for different combinations of those parameters.

Let v_1 and v_2 denote variations of the trivial equilibrium configurations $\mathcal{C}_1^*$ and $\mathcal{C}_2^*$ of the loops. Consistent with the symmetry of the trivial configuration,

we stipulate that v_1 and v_2 differ only by a rigid transformation consisting of a reflection across the equatorial plane $\mathcal{P}$ of $\mathcal{S}$ and a rotation, by some angle ϕ, about the polar axis $\mathcal{A}$ of $\mathcal{S}$. It then follows that

$$v_1 = v \quad \text{and} \quad v_2 = Qv_1 = Qv, \tag{4.36}$$

where n is given by (4.18) and, consistent with (3.24) and since, by $(4.20)_2$ $Qn \cdot v_2 = Qn \cdot Qv_1 = Qn \cdot Qv = n \cdot v$ and $Qn' \cdot v_2' = Qn' \cdot Qv_1' = Qn' \cdot Qv' = n' \cdot v'$, the variation v must satisfy

$$n \cdot v = 0 \quad \text{and} \quad n' \cdot v' = 0. \tag{4.37}$$

Using (4.36) and the expressions (4.17) for n_1^* and n_2^* in the stability condition (4.14), recalling from (4.24)–(4.25) and (4.32) that the Lagrange multipliers $\Lambda_1^* = \Lambda_2^* = \Lambda$ and $\lambda_1^* = \lambda_2^* = \lambda$ are constant, we find that the trivial equilibrium solution is stable only if for all admissible v, the inequality

$$\int_0^{2\pi a} \left(|v''|^2 - \lambda |v'|^2 + (\Lambda v - \zeta \tilde{\vartheta}[n,n](v,v) - \chi \vartheta[n,Qn](v,Qv)) \cdot v \right) \mathrm{d}s$$
$$+ \int_0^{2\pi a} \left((|Qv''|^2 - \lambda |Qv'|^2) + (\Lambda Qv - \zeta \tilde{\vartheta}[Qn,Qn](Qv,Qv) \right.$$
$$\left. - \chi \vartheta[Qn,n](Qv,v)) \cdot Qv \right) \mathrm{d}s \geq 0, \tag{4.38}$$

holds, where $\tilde{\vartheta}[n_i,n_i](v_i,v_i)$ and $\vartheta[n_i,n_j](v_i,v_j)$, $i \neq j$, are defined in (4.15) and (3.33), respectively and the kernel F and H of the first and second of these functionals are defined in $(4.8)_2$. We note that these functionals depend linearly on the perturbation v.

Using the elementary properties of Q defined in $(4.20)_1$,

$$|Qv''|^2 = |v''|^2, \quad |Qv'|^2 = |v'|^2, \quad \text{and} \quad |Qv|^2 = |v|^2. \tag{4.39}$$

Also, we show in the (B.8) that

$$\tilde{\vartheta}[Qn,Qn](Qv,Qv) \cdot Qv = \tilde{\vartheta}[n,n](v,v) \cdot v. \tag{4.40}$$

Furthermore, we impose the restriction on the rotation ϕ as follows. Let ϕ_n denote the rotation ϕ for the n-th mode of the perturbation v. Among all the values of ϕ_n, the repulsive interaction energy between the perturbed curves $n + \varepsilon v$ and $Qn + \varepsilon Qv$, where ε is a small number, is minimized for $\phi_n = \frac{\pi}{n}$. Therefore, at $\phi_n = \frac{\pi}{n}$, the equilibrium configuration will first become unstable. Assuming this choice of ϕ_n, we showed in (B.11) that

$$\vartheta[Qn, n](Qv, v) \cdot Qv = \vartheta[n, Qn](v, Qv) \cdot v. \tag{4.41}$$

Equation (4.39), (4.40), and (4.41) imply that the two loops contribute equally to the bending energy terms, the inter-loop interaction terms, and the intra-loop interaction terms, respectively in the left hand side of the stability condition (4.38). Using (4.39), (4.40), and (4.41) in the stability condition (4.38), we obtain a reduced condition as

$$\int_0^{2\pi a} (|v''|^2 - \lambda |v'|^2 + \Lambda |v|^2 - \zeta \tilde{\vartheta}[n, n](v, v) \cdot v - \chi \vartheta[n, Qn](v, Qv) \cdot v) \, ds \geq 0. \tag{4.42}$$

The variation v can be represented by arclength dependent polar and azimuthal angles θ and ψ through

$$v = \sqrt{1 - a^2}\theta e - a\theta k + a\psi k \times e. \tag{4.43}$$

From (4.18) and (4.43), we see that

$$n \cdot v = (ae + \sqrt{1 - a^2}k) \cdot (\sqrt{1 - a^2}\theta e - a\theta k + a\psi k \times e) = 0, \tag{4.44}$$

and thus, that the constraint (4.37) needed to ensure that the variations do not cause the loops to separate from $\mathcal{S}$ is met for all choices of θ and ψ. Next, differentiating (4.18) and (4.43) with respect to arclength and invoking the consequences

$$e \cdot e' = 0, \quad k \cdot e' = 0, \quad k \times e = ae', \quad \text{and} \quad ak \times e' = -e \tag{4.45}$$

41

of (4.16), we see that

$$n' \cdot v' = ae' \cdot (\sqrt{1 - a^2}(\theta'e + \theta e') - a\theta'k + a^2\psi'e' - \psi e) = a(\sqrt{1 - a^2}\theta + a^2\psi')|e'|^2 \tag{4.46}$$

and thus, that constraint $(4.37)_2$ needed to ensure that the variations do not cause local changes in the lengths of the loops is met only if θ and ψ are related by

$$\sqrt{1 - a^2}\theta + a^2\psi' = 0. \tag{4.47}$$

In view of (4.47), we may eliminate θ from the representation (4.43) to yield

$$v = -a^2\psi'\left(e - \frac{a}{\sqrt{1 - a^2}}k\right) + a\psi e \times k. \tag{4.48}$$

Granted that ψ admits the Fourier decomposition

$$\psi = \sum_{n=2}^{\infty}\left(c_n \cos\frac{ns}{a} + d_n \sin\frac{ns}{a}\right), \tag{4.49}$$

we may use the expressions (4.18), $(4.32)_1$, $(4.32)_2$, and (4.48) for n, Λ, λ, and v to convert the stability condition (4.42) into an inequality involving the Fourier coefficients c_n and d_n, $n = 2, \ldots, \infty$, and the dimensionless parameters a, ζ, and χ:

$$\sum_{n=2}^{\infty}(c_n^2 + d_n^2)(\zeta\alpha_n(a) + \beta_n(a) - \chi) \geq 0. \tag{4.50}$$

The steps leading to (4.50) and the definitions of α_n and β_n, $n = 2, \ldots, \infty$, are provided in the appendixB. From (4.50), we see that the trivial equilibrium configuration corresponding to any particular combination of $0 < a < 1$, $\zeta \geq 0$, and $\chi \geq 0$ is stable with respect to all variations v_1 and v_2 of the form (4.36) with v determined by (4.48) only if the condition

$$\chi \leq \alpha_n(a)\zeta + \beta_n(a) \tag{4.51}$$

holds for each mode $n = 2, \ldots, \infty$. For each $\alpha_n > 0$ and $\beta_n > 0$, for $n = 2, \ldots, \infty$, we identify the intra-loop and inter-loop interaction parameters ζ and χ as the

abscissa and ordinate in the first quadrant of a coordinate plane. The trivial equilibrium configuration involving two loops of radius a is unstable with respect to variations of mode n if the ordered combination (ζ, χ) of ζ and χ lies in the portion of the first quadrant of the (ζ, χ)-plane above the straight line

$$\mathcal{L}_n(a) = \{(\zeta, \chi) : \zeta \geq 0, \chi = \alpha_n(a)\zeta + \beta_n(a)\}. \tag{4.52}$$

More generally, the trivial equilibrium configuration involving two loops of radius a is unstable with respect to variations of mode n if the ordered combination (ζ, χ) of ζ and χ lies in the portion of the first quadrant of the (ζ, χ)-plane above the lower envelope

$$\mathcal{L}(a) = \{(\zeta, \chi) : \zeta \geq 0, \chi = \min_{n \leq 2 \leq \infty} (\alpha_n(a)\zeta + \beta_n(a))\} \tag{4.53}$$

of the family $\{\mathcal{L}_n(a) : n = 2, \ldots, \infty\}$ of straight lines of the form (4.52). The curve $\mathcal{L}(a)$ may be polygonal if the lines in the aforementioned family intersect at one or more points.

To obtain more specific information concerning the coefficients $\alpha_n(a)$ and $\beta_n(a)$ entering the stability condition (4.51), we take the mollifier M to be of the particular form

$$M(\eta) = \left(\frac{\sin \eta}{\sin \eta + e^{-7\sin \eta}}\right)^4 \tag{4.54}$$

used previously by Hoffmann and Manning [46] to calculate the self energy of a charged rod. Importantly, the choice (4.54) is consistent with the provision (4.10) that is needed to ensure regularization of the self energy up to its second variation.

We list the α_n and β_n values for two representative values of a, $a = 0.6$ and $a = 0.9$ and mode $n = 2 \ldots 10$ in the table 4.1. We see that for $a = 0.6$, $\alpha_i > \alpha_{i+1}$ and $\beta_i < \beta_{i+1}$, $i \geq 2$. Therefore, the lower envelope $\mathcal{L}(0.6)$ can be constructed by set of points of $P_1, P_2 \ldots P_\infty$ where P_1 is point of intersection of $\mathcal{L}_2$ with χ-axis in the (ζ, χ)-plane, i.e., $(0, \beta_2)$ and P_n is the point of intersection between the

Table 4.1: Coefficient α_n and β_n of the stability condition (4.51) for $a = 0.6$ and $a = 0.9$ and $n = 2 \dots 10$, and for M provided in (4.54).

$a = 0.6$ $a = 0.9$

n	α_n	β_n
2	7.62	62.15
3	6.04	102.60
4	5.92	170.31
5	5.90	259.10
6	5.89	368.20
7	5.87	497.39
8	5.86	646.58
9	5.85	815.73
10	5.84	1004.83

n	α_n	β_n
2	0.4097	1.6300
3	0.4321	3.3835
4	0.4501	5.8718
5	0.4589	9.0618
6	0.4626	12.9517
7	0.4637	17.5435
8	0.4639	22.8390
9	0.4636	28.8394
10	0.4633	35.5454

lines corresponding to consecutive modes, $\mathcal{L}_n$ and $\mathcal{L}_{n+1}$ with $n \geq 2$. For $a = 0.9$, $\alpha_2 < \alpha_i$ and $\beta_2 < \beta_i$, $\forall i > 2$. Therefore, the lower envelope $\mathcal{L}(0.9)$ is constituted only by the line $\mathcal{L}_2(0.9)$. In Figure 4.5, we plot the portion of the lower envelope $\mathcal{L}(a)$ over the interval $0 \leq \zeta \leq 10^6$ for two representative values, $a = 0.6$ and $a = 0.9$, of a and modes $n = 2, \dots, 6$.

We argue that, depending the dimensionless radius a, the stability plot consists of one or more of line segments $\mathcal{L}_n(a)$, $n = 2, \dots, \infty$ and accordingly the dominant mode which determines the stability of the trivial solution changes from $n = 2$ to the higher mode numbers in the corresponding regions. We explain the interchanging behavior for the dominant mode as follows. The bending energy required to displace the configuration from equilibrium solution to a n-th mode perturbation increases with n. However, interaction energy between the two curves could lower as the mode number increases. It requires minimum efforts to move the trivial configuration to the mode with lowest energy. Hence, the dominant mode determining the trivial solution stability changes in different regions.
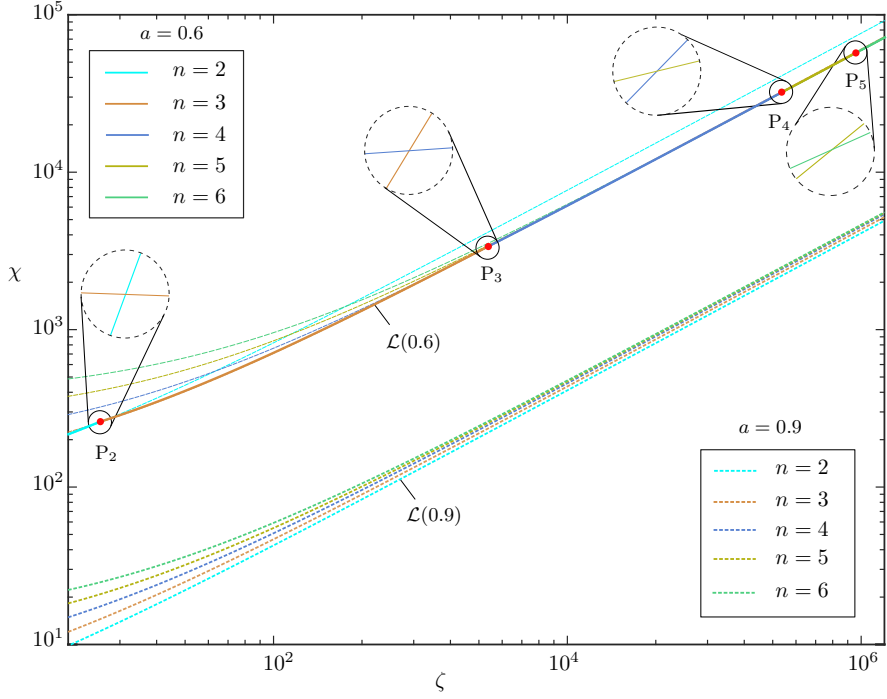
Figure 4.5: Stability plot for $a = 0.6$ and $a = 0.9$. For each a, the stability lines $\mathcal{L}_n$ are shown up to mode $n = 6$. For $a = 0.6$, the point of intersection between $\mathcal{L}_n$ and $\mathcal{L}_{n+1}$ is denoted by P_n. The stability curve $\mathcal{L}(0.6)$ comprises of different line segments between these intersection points. For $a = 0.9$, the stability curve $\mathcal{L}(0.9)$ is constituted only by mode $n = 2$.

We obtain the stability plot for different values of a from 0.02 till 0.98 in the increment of 0.01 to show the effect of the dimensionless radius a on the stability plot in the Figure 4.6. As discussed, the stability line consists of one or more modes depending on the value of a. Below the stability line for the corresponding a, the trivial solution is stable.

Also, we conclude from the Figure 4.6 that (*i*) as the value of a increases, the parameter space in which the trivial solution is stable reduces. This can be attributed to the fact that the loop $\mathcal{C}_1$ and $\mathcal{C}_2$ move closer to each other as the value of a increases and thus repulsion between the loops increases, (*ii*) an increase in the intra-loop interaction parameter ζ stabilizes the trivial solution. For the uniformly
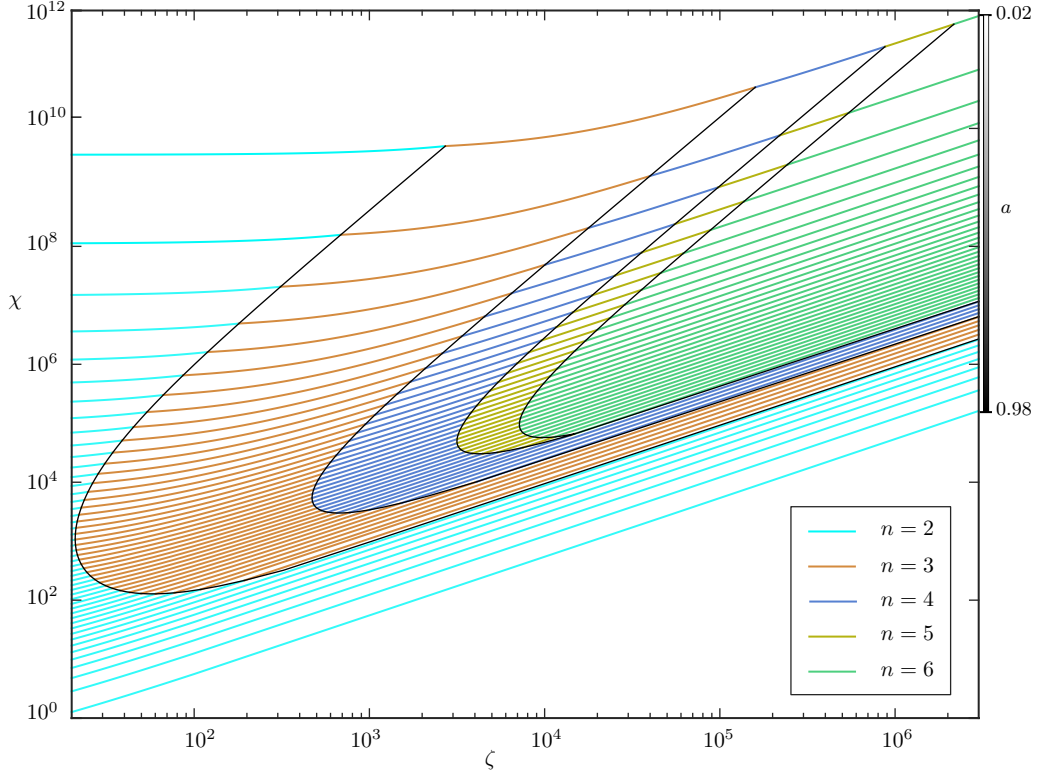
Figure 4.6: ζ versus χ stability plot for different values of a ranging from 0.02 to 0.98. For a given a, the stability curve consists of different colors that correspond to the first mode that makes the trivial configuration unstable in the respective regions. For given a, the trivial solution is stable below the corresponding stability curve.

charged loop, the self interaction energy is minimum for a circular configuration of the loop. Therefore, the increase in ζ favors the circular configuration more, and (*iii*) an increase in the repulsive interaction parameter χ destabilizes the trivial solution. The repulsive interaction between the loops push each other toward the pole. However, the restriction of loop to the sphere in combination with inextensibility of loop implies that trivial circular configuration would tend to adopt a non-trivial shape as χ is increased.

4.4 Bifurcation analysis

In this section, we briefly describe the general concept of bifurcation analysis and non-trivial branches and then specialize the concept to our problem. The explanation provided in the next paragraphs is completely adopted Chen [55] .

Let $\mathcal{X}$ and $\mathcal{Y}$ be Banach spaces (normed linear spaces), $\mathcal{U}$ an open subset of $\mathcal{X}$, and ϑ an open subset of R^n. Consider a smooth mapping $g : \mathcal{U} \times \vartheta \to \mathcal{Y}$. Let

$$g(u, \epsilon) = 0 \tag{4.55}$$

determines the state of a physical system with n parameters. For example, (4.55) can be the equilibrium equation for an elastic body. In this connection, u can be a function that describes the deformation of the body, g a differential operator, and ϵ a set of parameters that specify, for example, the loads, the geometry and the material properties of the body. The variable u is called the state variable, and ϵ the bifurcation parameter.

Suppose that $(u_0, \epsilon_0) \in \mathcal{U} \times \vartheta$ satisfies (4.55). If the number of solutions of (4.55) in an arbitrarily small neighborhood of (u_0, ϵ_0) changes as ϵ varies, the pair (u_0, ϵ_0) is called a bifurcation point. The solutions in this neighborhood are referred to as bifurcation solution branches, and a graphical representation of the bifurcation solution branches is called a bifurcation diagram.

The mapping $g(u, \epsilon)$ is assumed to be smooth in the sense that it has Fréchet derivatives of any order. The first-order Fréchet derivative $\mathcal{D}_u g(u_0, \epsilon_0)$ of $g(u, \epsilon)$ with respect to u at (u_0, ϵ_0) is a linear operator from $\mathcal{X} \to \mathcal{Y}$ such that

$$g(u, \epsilon_0) = g(u_0, \epsilon_0) + \mathcal{D}_u g(u_0, \epsilon_0)(u - u_0) + \mathcal{O}(|u - u_0|) \quad as \quad |u - u_0| \to 0. \tag{4.56}$$

By the implicit function theorem, if $\mathcal{D}_u g(u_0, \epsilon_0)$ is non-invertible, there is no unique way in which we can write u as function of ϵ in neighborhood of the point (u_0, ϵ_0). In other words, there exist multiple solution branches in neighbor-

hood of (u_0, ϵ_0). Therefore, a necessary condition for (u_0, ϵ_0) to be a bifurcation point is that $\mathcal{D}_u g(u_0, \epsilon_0)$ be non-invertible.

For our case, the function g is the Euler-Lagrange equation given by (4.12), $u = (n_1, n_2, \lambda_1, \lambda_2, \Lambda_1, \Lambda_2)$ are the state variables and $\epsilon = (a, \zeta, \chi)$ represents the bifurcation parameters. The Fréchet derivative $\mathcal{D}_u g(u_0, \epsilon_0)$ is obtained by linearizing the equilibrium equation (4.21) about the trivial solution u_0 that is given by $n_1 = n, n_2 = Qn, \lambda_1 = \lambda_2 = \lambda$, and $\Lambda_1 = \Lambda_2 = \Lambda$, where n is defined in (4.17), and λ and Λ are provided in (4.32). The bifurcation parameters $\epsilon_0 = (a, \zeta, \chi)$ are such that $\mathcal{D}_u g(u_0, \epsilon_0)$ is non-invertible.

In other words, the dimensionless boundary-value problem consisting of (3.24) and (4.12) has a nontrivial solution branch that bifurcates from the trivial solution branch characterized by (4.17) and (4.32) only if the boundary-value problem obtained by linearizing (3.24) and (4.5) about (4.17) and (4.32) has a nontrivial solution.

Let v_1 and v_2 denote increments to n and Qn, respectively. Additionally, let σ_i and Σ_i denote increments to λ_i and Λ_i, $i = 1, 2$, respectively. To be consistent with the assumptions made in the linear stability analysis in the previous section, we impose further restrictions on the perturbations v_1 and v_2 according to (4.36).

We substitute the quantities $n_1 = n + v$, $n_2 = Qn + Qv$, $\lambda_i = \lambda + \sigma_i$, and $\Lambda_i = \Lambda + \Sigma_i$, $i = 1, 2$ in the equilibrium equations (4.12) and use the fact that n, Qn, $\lambda_1 = \lambda_2 = \lambda$, and $\Lambda_1 = \Lambda_2 = \Lambda$ defined in (4.32) satisfy (4.12). Ignoring the quadratic and higher order terms in v, σ_i, and Σ_i and applying $Q^\top$ to the second of the equations obtained, we find the linearized equilibrium equations as

$$
\left.
\begin{aligned}
v'''' + \lambda v'' + \Lambda v + \sigma_1' n' + \sigma_1 n'' + \Sigma_1 n &= \zeta \tilde{\vartheta}[n, n](v, v) + \chi \vartheta[n, Qn](v, Qv), \\
v'''' + \lambda v'' + \Lambda v + \sigma_2' n' + \sigma_2 n'' + \Sigma_2 n &= \zeta Q^\top \tilde{\vartheta}[Qn, Qn](Qv, Qv) \\
&\quad + \chi Q^\top \vartheta[Qn,\ n](Qv, v),
\end{aligned}
\right\}
$$

(4.57)

48

where $\tilde{\boldsymbol{\vartheta}}[\boldsymbol{n}_i, \boldsymbol{n}_i](\boldsymbol{v}_i, \boldsymbol{v}_i)$ and $\boldsymbol{\vartheta}[\boldsymbol{n}_i, \boldsymbol{n}_j](\boldsymbol{v}_i, \boldsymbol{v}_j)$, $i \neq j$, are defined in (4.15) and (3.33), respectively and the kernel $\boldsymbol{F}$ and $\boldsymbol{H}$ of the first and second of these functionals are defined in (4.8)$_2$. We also note that these functionals depend linearly on the perturbation $\boldsymbol{v}$. Using the elementary properties of $\boldsymbol{Q}$ in (4.20), we derived in (B.7) that

$$\boldsymbol{Q}^{\top}\tilde{\boldsymbol{\vartheta}}[\boldsymbol{Q}\boldsymbol{n}, \boldsymbol{Q}\boldsymbol{n}](\boldsymbol{Q}\boldsymbol{v}, \boldsymbol{Q}\boldsymbol{v}) = \tilde{\boldsymbol{\vartheta}}[\boldsymbol{n}, \boldsymbol{n}](\boldsymbol{v}, \boldsymbol{v}). \tag{4.58}$$

Consistent with the assumptions followed in the stability analysis, we assume that for n^{th} mode of $\boldsymbol{v}$, the perturbation of the two loops differ by a rotation $\phi_n = \frac{\pi}{n}$. Among all the values of ϕ_n, the repulsive interaction energy between the perturbed curves $\boldsymbol{n} + \varepsilon\boldsymbol{v}$ and $\boldsymbol{Q}\boldsymbol{n} + \varepsilon\boldsymbol{Q}\boldsymbol{v}$, where ε is a small number, is minimized for $\phi_n = \frac{\pi}{n}$. Therefore, at $\phi_n = \frac{\pi}{n}$, the equilibrium configuration will first bifurcate into non trivial shape. Assuming this choice of ϕ_n, we show in (B.10) that

$$\boldsymbol{\vartheta}[\boldsymbol{n}, \boldsymbol{Q}^{\top}\boldsymbol{n}](\boldsymbol{v}, \boldsymbol{Q}^{\top}\boldsymbol{v}) = \boldsymbol{\vartheta}[\boldsymbol{n}, \boldsymbol{Q}\boldsymbol{n}](\boldsymbol{v}, \boldsymbol{Q}\boldsymbol{v}). \tag{4.59}$$

Using (4.58) and (4.59) in (4.57)$_2$ and comparing it with (4.57)$_1$, we arrive at the condition

$$\sigma_1'\boldsymbol{n}' + \sigma_1\boldsymbol{n}'' + \Sigma_1\boldsymbol{n} = \sigma_2'\boldsymbol{n}' + \sigma_2\boldsymbol{n}'' + \Sigma_2\boldsymbol{n}. \tag{4.60}$$

We use the arguments provided to obtain (4.24) and (4.25), respectively and find that the above equation yields

$$\sigma_1 = \sigma_2 = \sigma \quad \text{and} \quad \Sigma_1 = \Sigma_2 = \Sigma. \tag{4.61}$$

In view of (4.58), (4.59), and (4.61), the linearized equilibrium equations (4.57)$_1$ and (4.57)$_2$ are equivalent. We may thus use either of these conditions to determine σ and Σ. Using (4.61) in the left-hand side of (4.57)$_1$, substituting $\boldsymbol{v}$ defined in (4.48) in (4.57)$_1$ and resolving the resulting equation along the vectors $\boldsymbol{e}$, $\boldsymbol{k}$, and $\boldsymbol{k} \times \boldsymbol{e}$, we obtain three equations in terms of three unknowns ψ, σ and Σ.

We use the Fourier representation for the functions ψ defined in (4.49), and σ and Σ defined as

$$
\left.
\begin{aligned}
\sigma &= \sum_{n=0}^{\infty} p \cos \frac{ns}{a} + q \sin \frac{ns}{a}, \\
\Sigma &= \sum_{n=0}^{\infty} u \cos \frac{ns}{a} + v \sin \frac{ns}{a},
\end{aligned}
\right\}
\tag{4.62}
$$

where n is a given mode number. Substituting these quantities in the resolved equations and using the fact that coefficient of $\cos \frac{ns}{a}$ and $\sin \frac{ns}{a}$ independently satisfy resolved equations, for each mode n, we get six equations in six unknowns c_n, d_n, p_n, q_n, u_n and v_n. Detailed derivation of these equations are provided in the appendix C.

Granted that the mollifier M is given, the condition needed to ensure that the homogeneous linear system for c_n, d_n, p_n, q_n, u_n and v_n has a nontrivial solution yields the equality in the stability condition (4.51) , i.e.,

$$
\chi = \alpha_n(a)\zeta + \beta_n(a),
\tag{4.63}
$$

that involves the dimensionless radius a of the loops, the dimensionless parameters ζ and χ dictating the strengths of the repulsive intra- and inter-loop interactions, and the mode number n. The non-invertibility of the Fréchet derivative described earlier is equivalent to the condition (4.63) and is described in the appendix C.

The definition of lower envelope $\mathcal{L}(a)$ and the discussion regarding the intersection between the $\mathcal{L}_n = \alpha_n(a)\zeta + \beta_n(a)$ corresponding to different modes for a given a in the previous section holds true in the bifurcation analysis as well.

In Figure 4.7, we plot bifurcation diagram for two representative values, $a = 0.6$ and $a = 0.9$, of a and modes $n = 2, \ldots, 6$. For $a = 0.9$, the circular configuration will buckle in mode $n = 2$ for any value of ζ. In the case $a = 0.6$, for ζ up to point P_2, the circular configuration buckles in mode $n = 2$ and for ζ in the range P_{n-1} and P_n, with $n \geq 3$, the circular configuration will buckle in n-th mode.
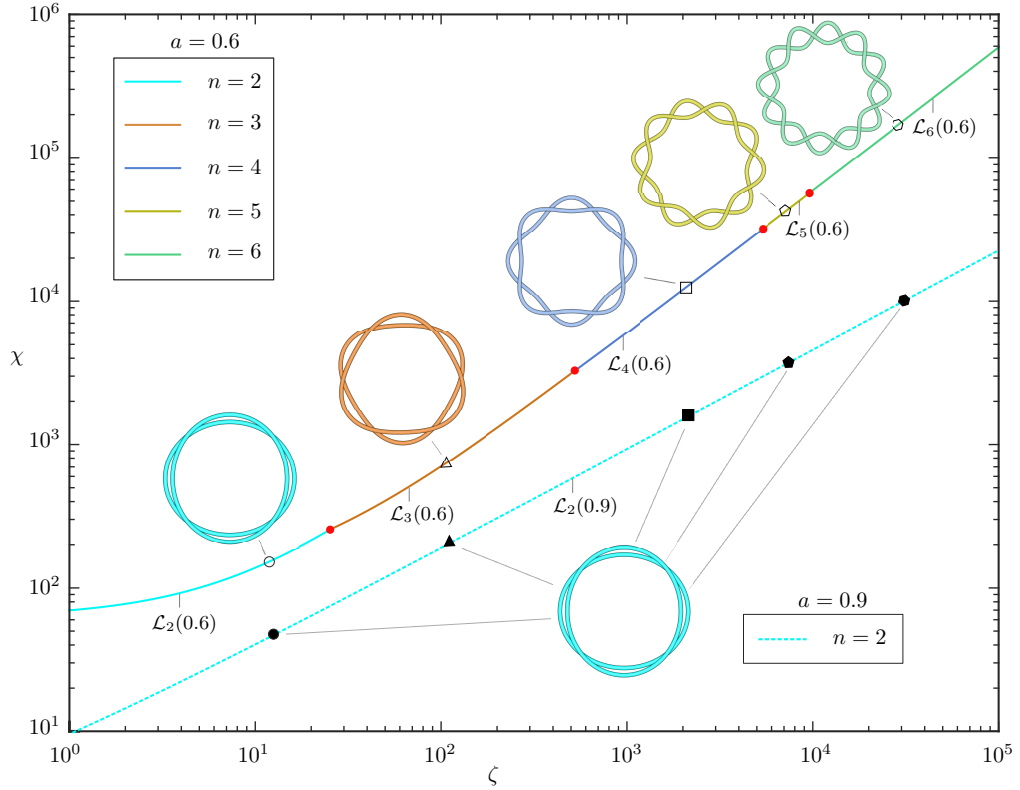
Figure 4.7: ζ versus χ bifurcation plot for $a = 0.6$ and $a = 0.9$. For $a = 0.9$, the lower envelope is constituted by the curve $\mathcal{L}_2(0.9)$. However, for $a = 0.6$, the bifurcation plot consists of segments corresponding to different modes as shown.

4.5 Conclusion

We studied a specialized system in which two loops are identical. For such a specialized system, the number of dimensionless parameters reduces to three: the ratio of the self energy coefficient and the bending modulus scaled with the radius of the sphere $\zeta = A_{11}R^3/\mu_1$, the ratio of the interaction energy coefficient and the bending modulus scaled with the radius of the sphere $\chi = A_{12}R^3/\mu_1$ and the ratio of the length of loop to the radius of the sphere $l = L/R$. We studied the system for repulsive interactions, i.e., $\zeta > 0$ and $\chi > 0$.

For the specialized system, the interplay between the three dimensionless

parameters ζ, χ and a is shown in the stability plot Figure 4.6. The intra-loop interaction parameter ζ stabilizes the trivial solution since the circular configuration has the minimum self energy. The two loops repel each other and therefore increase in χ destabilizes the trivial solution. Also, as the radius (dimensionless) of the trivial solution increases, the loops move closer to each other. Therefore, higher value of a destabilizes the trivial solution. In summary, an increase in ζ stabilizes the trivial solution and an increase in χ and a destabilizes the trivial solution.

CHAPTER 5 NON-TRIVIAL EQUILIBRIUM

SOLUTIONS

5.1   Introduction

In this chapter, we provide the discretized description of the Euler–Lagrange equations derived in chapter 4 for the special case where the two loops $\mathcal{C}_1$ and $\mathcal{C}_2$ are uniformly charged, have the same length, bending moduli, and interaction parameters, so that

$$L_1 = L_2 = L, \quad \mu_1 = \mu_2 = \mu, \quad \text{and} \quad A_{11} = A_{22} = A, \tag{5.1}$$

and, thus are both geometrically and physically indistinguishable. With this simplification, the general problem formulated in the previous chapter reduced to one involving only a single dimensionless measure of length, namely

$$a = \frac{L}{2\pi R} \tag{5.2}$$

and two dimensionless measures of energy, namely

$$\zeta = \frac{R^3 A}{\mu} \quad \text{and} \quad \chi = \frac{R^3 A_{12}}{\mu}. \tag{5.3}$$

We had imposed further restriction $0 < a < 1$ and hence $L < 2\pi R$ on the length of the loops in chapter 4 to ensure the existence of the trivial solution in form of a pair of circular loops. In this chapter, we allow $a > 1$ so that the loops can have length longer that the perimeter $2\pi R$ of the great circle.

5.2   Equilibrium equations

We restrict our study to find equilibrium configurations $\mathcal{C}_1^*$ and $\mathcal{C}_2^*$ of the loops $\mathcal{C}_1$ and $\mathcal{C}_2$, respectively that are *n*-fold symmetric which implies that the
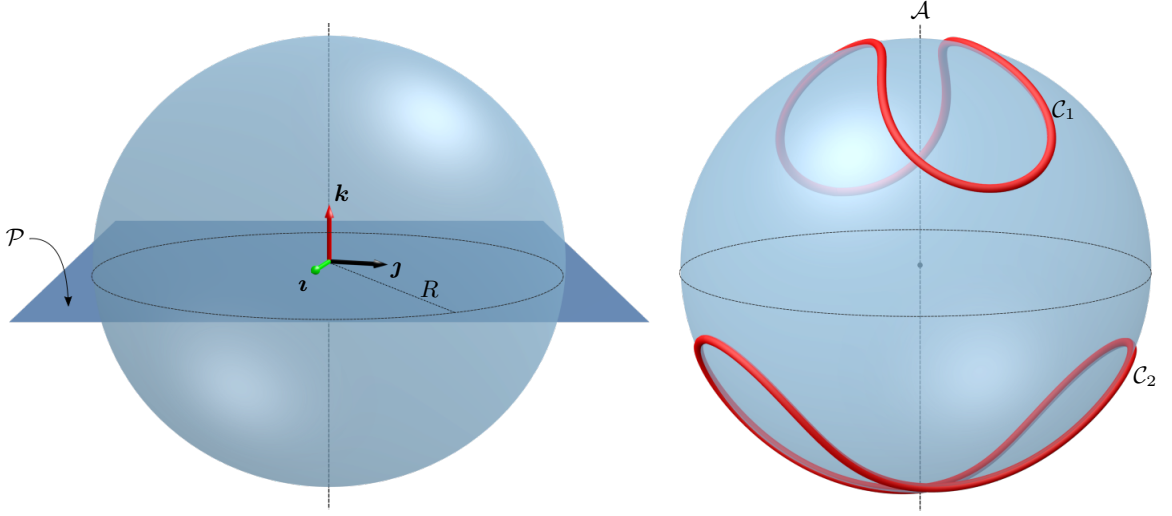
Figure 5.1: Schematic of a 2-fold configuration of $\mathcal{C}_1$ and $\mathcal{C}_2$ situated on opposing sides to an equatorial plane of a sphere $\mathcal{S}$, of radius R. $\mathcal{C}_2$ is rotated with respect to $\mathcal{C}_1$ angle $\phi_2 = \frac{\pi}{2}$ about the polar axis $\mathcal{A}$. The vector field $\imath$ and $\jmath$ are orthogonal unit vectors in the equatorial plane and the vector field k is the unit vector along the polar axis.

curvature of $\mathcal{C}_1^*$ and $\mathcal{C}_2^*$ has period $\frac{\pi}{n}$. Moreover, we assume that $\mathcal{C}_1^*$ and $\mathcal{C}_2^*$ differ only by a rigid transformation consisting of a reflection across the equatorial plane $\mathcal{P}$ of $\mathcal{S}$ and a rotation, by a particular angle $\phi_n = \frac{\pi}{n}$, about the polar axis $\mathcal{A}$ of $\mathcal{S}$ as shown in the schematic 5.1 using 2- fold configuration as an example. We may therefore choose the quantities n_1^* and n_2^* that parametrize $\mathcal{C}_1^*$ and $\mathcal{C}_2^*$ to be of the form

$$n_1^* = n \quad \text{and} \quad n_2^* = Qn, \tag{5.4}$$

where n is a unit normal to the sphere $\mathcal{S}$ and, Q defined by

$$Q(\phi_n) = \cos \phi_n (\imath \otimes \imath + \jmath \otimes \jmath) - \sin \phi_n (\imath \otimes \jmath - \jmath \otimes \imath) - 2k \otimes k, \quad 0 \le \psi \le 2\pi \tag{5.5}$$

is the orthogonal tensor that transforms any vector by simultaneously reflecting it across $\mathcal{A}$ and rotating it counterclockwise by ϕ_n about $\mathcal{A}$. We substitute the particular choices (5.4) of n_1 and n_2 in the equilibrium equations (4.12) and make simplifications by applying $Q^\top$ to second of the equations obtained by using (4.20),

leading to

$$
\left.
\begin{aligned}
(\boldsymbol{n}''' + \lambda_1^*\boldsymbol{n}')' + \Lambda_1^*\boldsymbol{n} &= \zeta \int_0^{2\pi a} M\Big(\frac{|\bar{s}-s|}{2a}\Big) \frac{\boldsymbol{n}-\boldsymbol{n}(\bar{s})}{|\boldsymbol{n}-\boldsymbol{n}(\bar{s})|}\, d\bar{s} \\
&\quad + \chi \int_0^{2\pi a} \frac{\boldsymbol{n}-\boldsymbol{Q}\boldsymbol{n}(\bar{s})}{|\boldsymbol{n}-\boldsymbol{Q}\boldsymbol{n}(\bar{s})|}\, d\bar{s}, \\
(\boldsymbol{n}''' + \lambda_2^*\boldsymbol{n}')' + \Lambda_2^*\boldsymbol{n} &= \zeta \int_0^{2\pi a} M\Big(\frac{|\bar{s}-s|}{2a}\Big) \frac{\boldsymbol{n}-\boldsymbol{n}(\bar{s})}{|\boldsymbol{n}-\boldsymbol{n}(\bar{s})|}\, d\bar{s} \\
&\quad + \chi \int_0^{2\pi a} \frac{\boldsymbol{n}-\boldsymbol{Q}^\top\boldsymbol{n}(\bar{s})}{|\boldsymbol{n}-\boldsymbol{Q}^\top\boldsymbol{n}(\bar{s})|}\, d\bar{s},
\end{aligned}
\right\},
$$

where Λ_i^* and λ_i^* are the Lagrange multipliers, as yet undetermined, needed to ensure the circular loop $\mathcal{C}_i^*$, $i = 1, 2$, is configured in consistency with the constraints $(3.4)_1$ and $(3.4)_2$, respectively. Next, since $\phi_n = \frac{\pi}{n}$,

$$
\boldsymbol{Q}^\top(\phi)\boldsymbol{n}(s + 2a\phi) = \boldsymbol{Q}(\phi)\boldsymbol{n}(s), \quad 0 \le s \le 2\pi a. \tag{5.6}
$$

We remark that while (5.6) is valid on for $\phi_n = \frac{\pi}{n}$ and $\boldsymbol{n}$ being an $n-$ fold symmetric configuration, the analogous relation (4.21) for the trivial configuration $\boldsymbol{n}$ in the chapter 2 is valid for any arbitrary angle ϕ.

Using (5.6) and a change of variables $\bar{s} \to \bar{s} + 2a\phi_n$ in the second integral on the right-hand side of $(5.6)_2$ we find that, since $\boldsymbol{n}$ is periodic on the interval from 0 to $2\pi a$,

$$
\int_0^{2\pi a} \frac{\boldsymbol{n}-\boldsymbol{Q}^\top\boldsymbol{n}(\bar{s})}{|\boldsymbol{n}-\boldsymbol{Q}^\top\boldsymbol{n}(\bar{s})|}\, d\bar{s} = \int_{2\phi_n a}^{2(\pi+\phi_n)a} \frac{\boldsymbol{n}-\boldsymbol{Q}\boldsymbol{n}(\bar{s})}{|\boldsymbol{n}-\boldsymbol{Q}\boldsymbol{n}(\bar{s})|}\, d\bar{s} = \int_0^{2\pi a} \frac{\boldsymbol{n}-\boldsymbol{Q}\boldsymbol{n}(\bar{s})}{|\boldsymbol{n}-\boldsymbol{Q}\boldsymbol{n}(\bar{s})|}\, d\bar{s}. \tag{5.7}
$$

Using (5.7) in $(5.6)_2$ and subtracting the resulting equation from $(5.6)_1$, we obtain the condition

$$
\lambda_1^*\boldsymbol{n}'' + (\lambda_1^*)'\boldsymbol{n}' + \Lambda_1^*\boldsymbol{n} = \lambda_2^*\boldsymbol{n}'' + (\lambda_2^*)'\boldsymbol{n}' + \Lambda_2^*\boldsymbol{n}. \tag{5.8}
$$

Using the restriction that $\boldsymbol{n}$ conforms to $\mathcal{S}$ and is inextensible, we get

$$
\boldsymbol{n} \cdot \boldsymbol{n} = 1 \quad \text{and} \quad \boldsymbol{n}' \cdot \boldsymbol{n}' = 1. \tag{5.9}
$$

Combination of the arc length derivative of $(5.9)_1$ and $(5.9)_2$ yields

$$
\boldsymbol{n} \cdot \boldsymbol{n}' = 0, \quad \boldsymbol{n} \cdot \boldsymbol{n}'' = -1, \quad \text{and} \quad \boldsymbol{n}' \cdot \boldsymbol{n}'' = 0. \tag{5.10}
$$

Computing the dot product on both side of (5.8) with n, n', and n'' respectively and using (5.10), we get

$$\Lambda_1^* - \lambda_1^* = \Lambda_1^* - \lambda_1^*, \tag{5.11}$$

$$(\lambda_1^*)' = (\lambda_2^*)', \quad \text{and} \tag{5.12}$$

$$(n'' \cdot n'')\lambda_1^* - \Lambda_1^* = (n'' \cdot n'')\lambda_2^* - \Lambda_2^*. \tag{5.13}$$

Combination of (5.11) and (5.13) yield

$$(n'' \cdot n'' - 1)(\lambda_1^* - \lambda_2^*) = 0. \tag{5.14}$$

For the case $n'' \cdot n'' = 1$ at each point on a curve n which represents the great circle of the unit circle, λ_1^* and λ_2^* and with (5.11), Λ_1^* and Λ_2^* differ by a constant. For any other curve n, (5.14) and (5.11) yield

$$\lambda_1^* = \lambda_2^* = \lambda \quad \text{and} \quad \Lambda_1^* = \Lambda_2^* = \Lambda. \tag{5.15}$$

In view of (5.15), (5.7) and (5.6), the equilibrium equation $(5.6)_1$ and $(5.6)_2$ are equivalent and we can use either of these equations to determine λ and Λ. Substituting $\lambda_1^* = \lambda$ and $\Lambda_1^* = \Lambda$ in $(5.6)_1$ and expanding the derivatives on left hand side of the resulting equation, we get

$$n'''' + \lambda n'' + \lambda' n' + \Lambda n = \zeta \int_0^{2\pi a} M\left(\frac{|\bar{s} - s|}{2a}\right) \frac{n - n(\bar{s})}{|n - n(\bar{s})|} \, d\bar{s} + \chi \int_0^{2\pi a} \frac{n - Qn(\bar{s})}{|n - Qn(\bar{s})|} \, d\bar{s}. \tag{5.16}$$

5.3 Discretization

We discretize the dimensionless length $\ell = 2\pi a$ of the loops $\mathcal{C}_1^*$ and $\mathcal{C}_2^*$ parameterized by n and Qn, respectively into N equal intervals. Segments in each interval are of equal arc length $h = \frac{\ell}{N}$. The quantities n, λ and Λ evaluated at the ith nodal point are respectively denoted by $n(i)$, $\lambda(i)$, and $\Lambda(i)$. For a closed

curve $\boldsymbol{n}$, $N+1^{\text{th}}$ point is identical to the first point which leads to

$$\boldsymbol{n}(N+1) = \boldsymbol{n}(1),\ \lambda(N+1) = \lambda(1),\quad \text{and}\quad \lambda(N+1) = \lambda(1). \tag{5.17}$$

Therefore, we only need to solve the equilibrium equation (5.16) for at nodal points $i \in [1, N]$. We use the following finite difference scheme to discretize the derivatives on the left hand side of (5.16)

$$\lambda(i)' = \frac{-\lambda(i+2) + 8\lambda(i+1) - 8\lambda(i-1) + \lambda(i-2)}{12h} + \mathcal{O}[h^4], \tag{5.18}$$

$$\boldsymbol{n}(i)' = \frac{-\boldsymbol{n}(i+2) + 8\boldsymbol{n}(i+1) - 8\boldsymbol{n}(i-1) + \boldsymbol{n}(i-2)}{12h} + \mathcal{O}[h^4], \tag{5.19}$$

$$\boldsymbol{n}(i)'' = \frac{-\boldsymbol{n}(i+2) + 16\boldsymbol{n}(i+1) - 30\boldsymbol{n}(i) + 16\boldsymbol{n}(i-1) - \boldsymbol{n}(i-2)}{12h^2} + \mathcal{O}[h^4], \tag{5.20}$$

$$\boldsymbol{n}(i)''' = \frac{\boldsymbol{n}(i+2) - 2\boldsymbol{n}(i+1) + 2\boldsymbol{n}(i-1) - \boldsymbol{n}(i-2)}{2h^3} + \mathcal{O}[h^2],\quad \text{and} \tag{5.21}$$

$$\boldsymbol{n}(i)'''' = \frac{\boldsymbol{n}(i+2) - 4\boldsymbol{n}(i+1) + 6\boldsymbol{n}(i) - 4\boldsymbol{n}(i-1) + \boldsymbol{n}(i-2)}{h^4} + \mathcal{O}[h^2],\quad i \in [1, N]. \tag{5.22}$$

Although the quantities $\boldsymbol{n}(i)$ and $\lambda(i)$ are defined for $i \in [1, N+1]$, we note that the right hand side terms in the above discretization scheme will encounter the additional, yet undefined terms $\boldsymbol{n}(0)$, $\boldsymbol{n}(-1)$, $\lambda(0)$, $\lambda(-1)$, $\boldsymbol{n}(N+2)$, and $\lambda(N+2)$. For a closed curve $\boldsymbol{n}$ it follows that

$$\boldsymbol{n}(0) = \boldsymbol{n}(N),\quad \boldsymbol{n}(-1) = \boldsymbol{n}(N-1),\quad \lambda(0) = \lambda(N),\quad \lambda(-1) = \lambda(N-1), \tag{5.23}$$

and

$$\boldsymbol{n}(N+2) = \boldsymbol{n}(2),\quad \text{and}\quad \lambda(N+2) = \lambda(2). \tag{5.24}$$

In §4.2.1 of chapter 4, we discussed the need for regularization of singularity of the intra-loop interaction potential. In a discretized description, we can avoid the singularity at each nodal point i by replacing the first integral on right hand side of (5.16) with trapezoidal rule of integration

$$h \sum_{\substack{j=1 \\ j \neq i}}^{N} \frac{\boldsymbol{n}(i) - \boldsymbol{n}(j)}{|\boldsymbol{n}(i) - \boldsymbol{n}(j))|}, \tag{5.25}$$

where we have used the fact that $(N+1)^{th}$ point is identical to the 1st point and we have skipped the summation over the element at i^{th} node.

Also, the second integral on the right hand side of (5.16) can be evaluated as

$$\int_0^{2\pi a} \frac{\boldsymbol{n} - \boldsymbol{Qn}(\bar{s})}{|\boldsymbol{n} - \boldsymbol{Qn}(\bar{s})|} \, d\bar{s} = h \sum_{j=1}^{N} \frac{\boldsymbol{n}(i) - \boldsymbol{Qn}(j)}{|\boldsymbol{n}(i) - \boldsymbol{Qn}(j))|}. \tag{5.26}$$

Substituting the first integral in right hand side of (5.16) with (5.25), substituting (5.26) in (5.16), we obtain three equation at each nodal point i,

$$\boldsymbol{n}''''(i) + \lambda(i)\boldsymbol{n}''(i) + \lambda'(i)\boldsymbol{n}'(i) + \Lambda(i)\boldsymbol{n}(i)$$

$$= h\zeta \sum_{\substack{j=1 \\ j\neq i}}^{N} \frac{\boldsymbol{n}(i) - \boldsymbol{n}(j)}{|\boldsymbol{n}(i) - \boldsymbol{n}(j))|} + \chi h \sum_{j=1}^{N} \frac{\boldsymbol{n}(i) - \boldsymbol{Qn}(j)}{|\boldsymbol{n}(i) - \boldsymbol{Qn}(j))|}, \tag{5.27}$$

$$\boldsymbol{n}(i) \cdot \boldsymbol{n}(i) = 1, \tag{5.28}$$

and

$$\boldsymbol{n}'(i) \cdot \boldsymbol{n}'(i) = 1 \tag{5.29}$$

in terms of three unknowns $\boldsymbol{n}(i)$, $\lambda(i)$ and $\Lambda(i)$.

5.4 Re-parameterization using spherical angles

The position vector $\boldsymbol{n}$ restricted to $\mathcal{S}$ can be described in terms of arc length dependent polar and azimuthal angles θ and ϕ as

$$\boldsymbol{n}(s) = \sin\theta(s)\cos\phi(s)\boldsymbol{\imath} + \sin\theta(s)\sin\phi(s)\boldsymbol{\jmath} + \cos\theta(s)\boldsymbol{k}. \tag{5.30}$$

Equivalently, $\boldsymbol{n}$ at i^{th} node can be described in terms of value the functions θ and ϕ at i^{th} node as

$$\boldsymbol{n}(i) = \sin\theta(i)\cos\phi(i)\boldsymbol{\imath} + \sin\theta(i)\sin\phi(i)\boldsymbol{\jmath} + \cos\theta(i)\boldsymbol{k}. \tag{5.31}$$

This parameterization ensures that the restriction of $n(i), i \in [1, N]$ to the sphere $\mathcal{S}$ is naturally satisfied. Defining the vectors

$$e_\theta(i) = \cos\theta(i)\cos\phi(i)\imath + \cos\theta(i)\sin\phi(i)\jmath - \sin\theta(i)k \quad \text{and} \tag{5.32}$$

$$e_\phi(i) = -\sin\phi(i)\imath + \cos\phi(i)\jmath, \tag{5.33}$$

we find that

$$n(i) \cdot e_\theta(i) = 0 \quad \text{and} \quad n(i) \cdot e_\phi(i) = 0. \tag{5.34}$$

Computing the dot product on both side of (5.27) with $e_\theta(i)$ and $e_\phi(i)$ respectively, using (5.34) and noting that (5.28) is trivially satisfied, we find at each nodal point $i \in [1, N]$ three equations

$$[n''''(i) + \lambda(i)n''(i) + \lambda'(i)n'(i)] \cdot e_\theta(i)$$

$$= h\zeta \sum_{\substack{j=1 \\ j \neq i}}^{N} \frac{(n(i) - n(j)) \cdot e_\theta(i)}{|n(i) - n(j))|} + \chi h \sum_{j=1}^{N} \frac{(n(i) - Qn(j)) \cdot e_\theta(i)}{|n(i) - Qn(j))|}, \tag{5.35}$$

$$[n''''(i) + \lambda(i)n''(i) + \lambda'(i)n'(i)] \cdot e_\phi(i)$$

$$= h\zeta \sum_{\substack{j=1 \\ j \neq i}}^{N} \frac{(n(i) - n(j)) \cdot e_\phi(i)}{|n(i) - n(j))|} + \chi h \sum_{j=1}^{N} \frac{(n(i) - Qn(j)) \cdot e_\phi(i)}{|n(i) - Qn(j))|}, \tag{5.36}$$

and

$$n'(i) \cdot n'(i) = 1, \tag{5.37}$$

in terms of three unknowns $\theta(i)$, $\phi(i)$ and $\lambda(i)$ for $i \in [1, N]$. Once we have obtained the equilibrium solution, we can compute the dot product on both sides of (5.27) with $n(i)$ and use (5.10) to make further simplifications and find the Lagrange multiplier $\Lambda(i)$ as

$$\Lambda(i) = \lambda(i) - n''''(i) \cdot n(i) + h\zeta \sum_{\substack{j=1 \\ j \neq i}}^{N} \frac{1 - n(j) \cdot n(i)}{|n(i) - n(j))|} + \chi h \sum_{j=1}^{N} \frac{1 - Qn(j) \cdot n(i)}{|n(i) - Qn(j))|}. \tag{5.38}$$

In the view of bending energy, self energy and the interaction energy defined in (3.21a), (3.21b), and (3.21c), the total dimensionless energy (3.20) can be expressed as function of total dimensionless length of the loop Nh, intra-loop interaction parameter ζ, and the inter-loop interaction parameter χ as

$$\mathcal{F}(Nh, \zeta, \chi) = h \sum_{i=1}^{N} \left(\boldsymbol{n}''(i) \cdot \boldsymbol{n}''(i) + h\zeta \sum_{\substack{j=1 \\ j \neq i}}^{N} \frac{1}{|\boldsymbol{n}(i) - \boldsymbol{n}(j))|} + \frac{\chi}{2} h \sum_{j=1}^{N} \frac{1}{|\boldsymbol{n}(i) - \boldsymbol{Qn}(j))|} \right).$$

(5.39)

5.5   Numerical experiment

We solve the system of equilibrium equations (5.35)-(5.37) for different set of the dimensionless parameters (a, ζ, χ). For all the numerical solutions, we used $N = 100$ and *fsolve* package from *Matlab*.

5.5.1   Effect of χ

To show the effect of the inter-loop repulsion parameter χ, we choose $a = 0.9$, $\zeta = 0$ and $\chi = 6$, 8, and 10. These values of χ are chosen so that the 2-fold, 3-fold, and 4-fold solutions can co-exist. For example, for $\chi > 10$, we could not find a 2-fold equilibrium solution. Similarly, for $\chi < 6$, we could not find any 4-fold solutions and various initial guesses converged to the trivial (circular) equilibrium configuration.

In figure 5.2, we show the equilibrium solution for each set of parameters described above. For 2-fold, 3-fold as well as 4-fold solutions, we find that the equilibrium configuration adopt a more 'squeezed in' configuration as χ increased. We compute the total energy of the equilibrium configuration using (5.39) and list it in 5.1. Within each of the n-fold solution, $n = 2, 3, 4$, the total energy increases monotonically with χ. However, for a given value of χ, there is no such mono-

tonicity among 2-fold, 3-fold, and 4-fold equilibrium solutions. For each value of χ, 2-fold solution has the minimum energy among 2-fold, 3-fold and 4 fold solutions. Also, 3-fold solution has maximum energy for $\chi = 6$ and $\chi = 8$ while 4-fold has the maximum energy for $\chi = 10$.
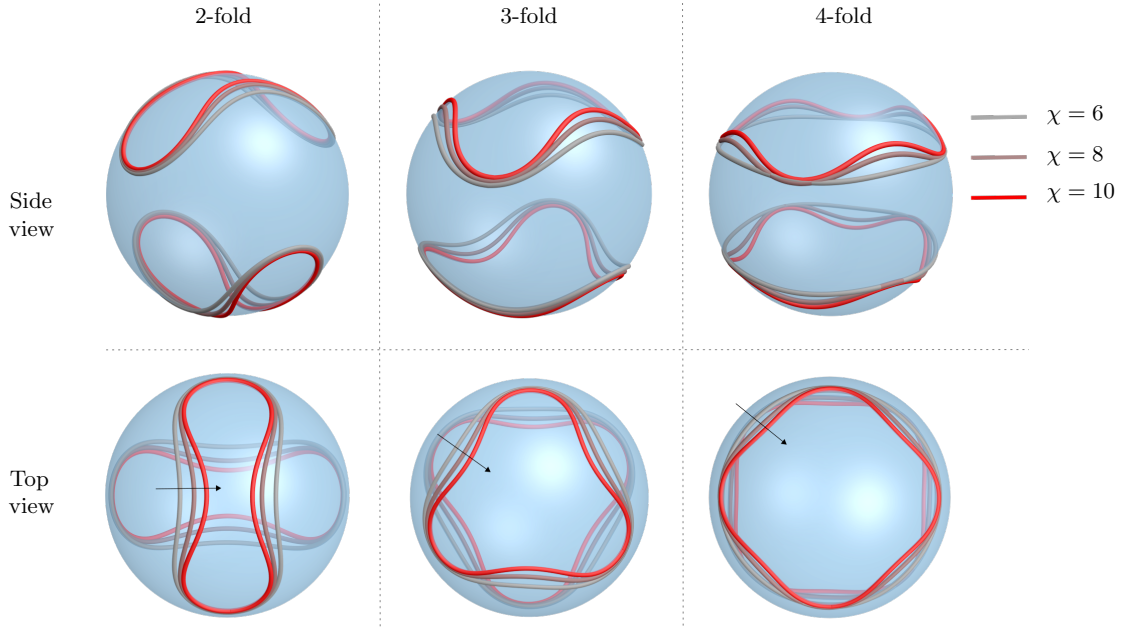

Figure 5.2: 2-fold, 3-fold, and 4-fold equilibrium configuration for $a = 0.9$, $\zeta = 0$ and three representative values, $\chi = 6, 8$, and 10 of χ. For each set (a, ζ, χ), 2-fold, 3-fold, and 4-fold solution co-exist. In the top view for each n-fold solution, we indicate that value of χ is increasing in the direction of arrow.

Table 5.1: Total dimensionless energy for 2-fold, 3-fold and 4-fold equilibrium solution for the set of parameters $a = 0.9$, $\zeta = 0$, and $\chi = 6, 8$, and 10.

χ	2-fold	3-fold	4-fold
6	75.2952	78.1006	75.4863
8	96.0244	101.4535	101.1663
10	116.2028	123.9105	125.8186

5.5.2 Effect of ζ

To demonstrate the effect of the intra-loop interaction parameter ζ, we use $a = 0.9$, $\chi = 10$, and compute 2-fold equilibrium solution for three representative values, $\zeta = 0, 4$, and 8 of ζ. As shown in the figure 5.3, the equilibrium configuration approaches toward the trivial (circular) configuration as ζ is increased which due the fact that the repulsive force among the elements of the loop increase with ζ driving the loops to adopt a more open configuration.
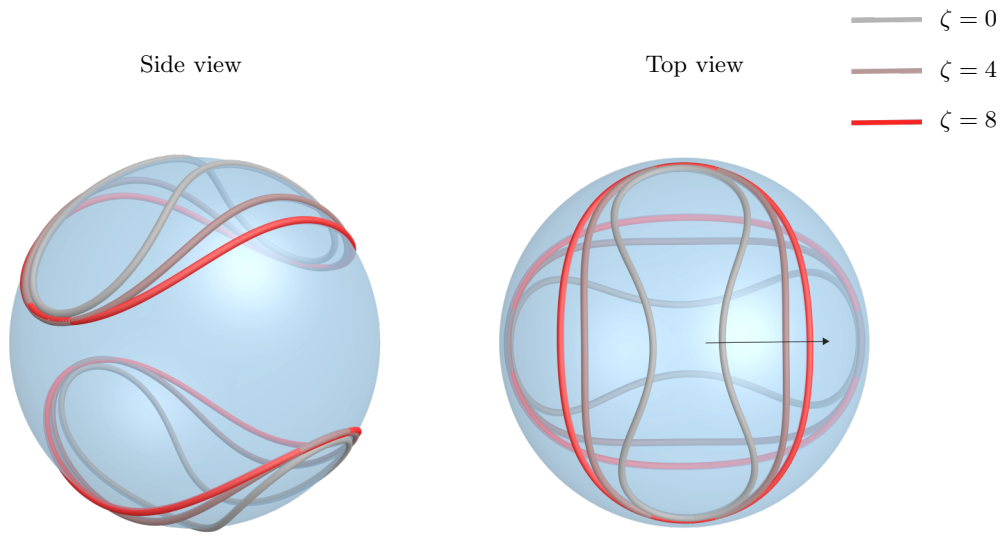
Figure 5.3: 2-fold equilibrium configuration for $a = 0.9$, $\chi = 10$ and three representative values, $\zeta = 0, 4$, and 8 of ζ. In the top view, we indicate that value of ζ is increasing in the direction of arrow.

5.5.3 Loops with parameter $a > 1$

For $a > 1$, the total length of the loop is longer than perimeter of the great circle. Therefore, no trivial equilibrium solution in form of a pair of circular loop is feasible. We first find the equilibrium configuration for pure elastica in which

case $\zeta = 0$ and $\chi = 0$ and thus the equilibrium equations (5.35)-(5.37) reduce to

$$[n''''(i) + \lambda(i)n''(i) + \lambda'(i)n'(i)] \cdot e_\theta(i) = 0, \tag{5.40}$$

$$[n''''(i) + \lambda(i)n''(i) + \lambda'(i)n'(i)] \cdot e_\phi(i) = 0, \quad \text{and} \tag{5.41}$$

$$n'(i) \cdot n'(i) = 1. \tag{5.42}$$

In figure 5.4, we show the 2-fold, 3-fold and 4-fold equilibrium solutions for $a = 1.3$ and $\zeta = \chi = 0$.
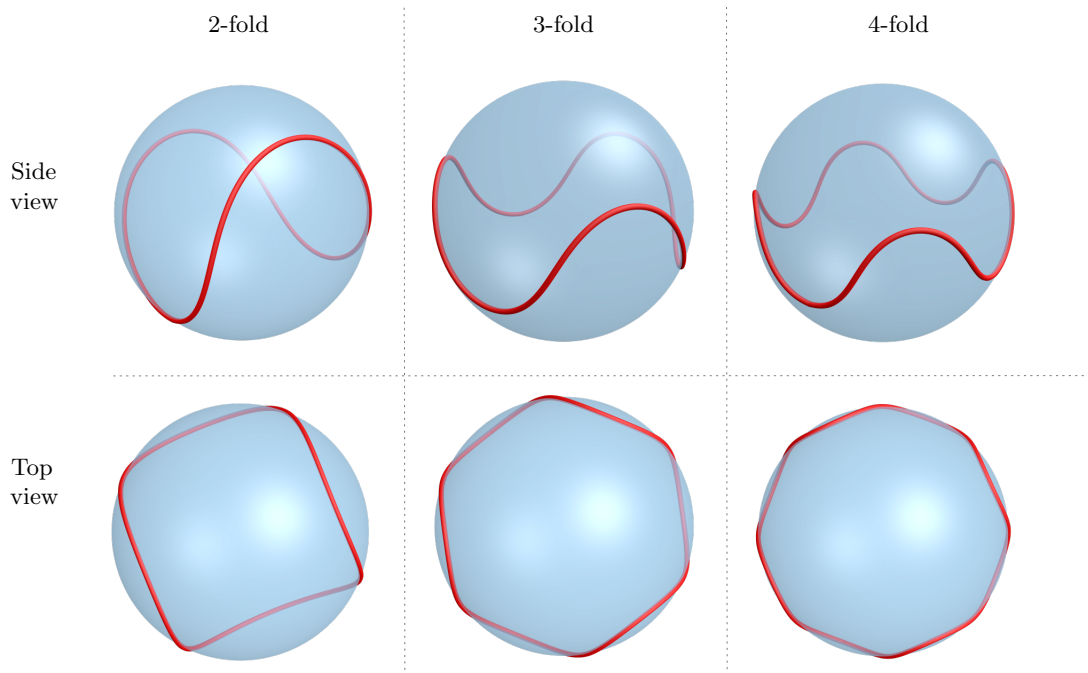

Figure 5.4: 2-fold, 3-fold, and 4-fold equilibrium configuration for $a = 1.3$, $\zeta = 0$, and $\chi = 0$.

To demonstrate the effect of inter-loop interaction parameter χ, we show the 2-fold equilibrium solution for $a = 1.1$, $\zeta = 0$ and two values of χ, $\chi = 0$ and $\chi = 2$ in the figure 5.5. The inter-loop repulsion between the two loops (shown with red color) drives the equilibrium solution toward a squeezed-in configuration compared to the case where $\chi = 0$.
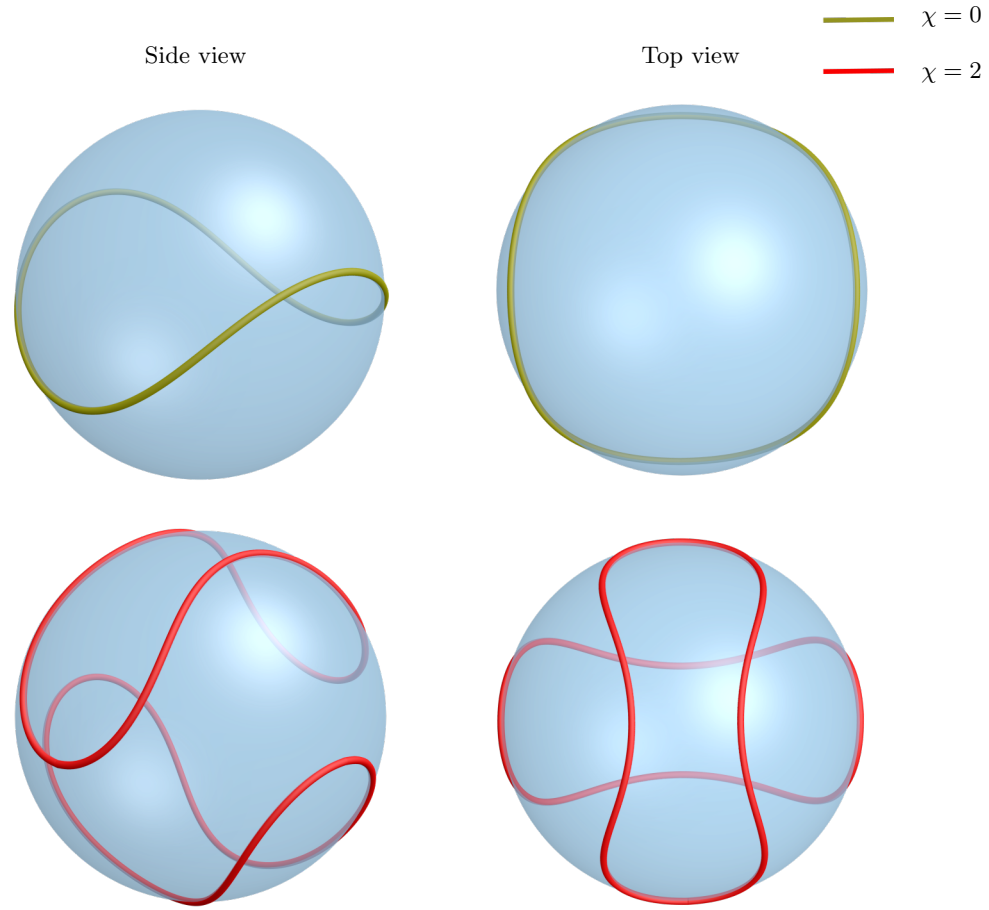

Figure 5.5: 2-fold equilibrium configuration for $a = 1.1$, $\zeta = 0$ and two values of χ, $\chi = 0$ and $\chi = 2$. In the case $\chi = 0$, two loops can orient with respect to each other in arbitrary fashion. Therefore only one of the loop is shown.

5.6 Discussion

In this chapter, we derived the discretized form of the Euler–Lagrange equation for two loops that are uniformly charged, have same bending modulus and same charge density and posses n-fold symmetry. We showed the effect of intra-loop and inter-loop interaction parameters on the equilibrium configurations. Although, we have shown the equilibrium solutions for only a limited set of parameters, this framework provides the basis for computing multiple, co-existing equilibrium solutions for a given set of parameters and thus finding a global minimum energy solution.

It is likely that there is a range of parameters a, ζ, χ outside which a particular n-fold symmetry solution does not exist. For example, we were unable to find a convergent 2-fold solution for $a = 0.9$, $\zeta = 0$, and $\chi > 10$. It is possible that a 2-fold symmetry configuration squeezing further from the equilibrium configuration at $\chi = 10$ may not maintain the point-wise inextensibility constraint. Therefore, for $a = 0.9$, $\zeta = 0$, and $\chi > 10$, a 2-fold equilibrium solution may not exist. Also, we were unable to find a 4-fold equilibrium solution for $a = 0.9$, $\zeta = 0$, and $\chi < 6$. More conclusive arguments can be made by computing the equilibrium solutions over a large set of parameters a, ζ, and χ.

CHAPTER 6 SUMMARY AND FUTURE WORK

6.1 Summary

In this study, we derived a variational framework to model a pair of charged curves that are constrained to a sphere. We showed how the competing factors namely the bending rigidity of the curves, intra-loop interaction, the inter-loop interaction and point-wise inextensibility of the loops govern the equilibrium configuration and its stability. We derived the discretized Euler–Lagrange equations that enabled us to find non-trivial equilibrium shapes. We showed that for a given dimensionless length of the loop, the intra-loop interaction parameter, and the inter-loop interaction parameter, there can exist one or more n-fold equilibrium solutions. Global minimum energy solution can be obtained by comparing the total dimensionless energy of the co-existing equilibrium solutions.

6.2 Future Work

Going forward, a few of the possible directions are as follows. Most of the proteins are made up of segments with alternating positive and negative charge densities. It would be interesting to computing the equilibrium solutions for loops with such charge distribution.

In some cases, helicity of the peptide molecules constrained to a membrane and hence the orientation of the cross section of the peptides can play crucial role in deciding the equilibrium configuration. We can incorporate this effect by working with charged rods instead of charged loops that have been considered in our work.

Another possible direction would be to consider the deformation of the sur-

face to which the charged loops are constrained. In addition to the factors considered in this work, the elasticity of the surface will also govern the over all equilibrium shape and can provide a more realistic model of proteins attached to a flexible membrane.

References

[1] A. T. Remaley, G. D. Norata, and A. L. Catapano. Novel Concepts in Hdl Pharmacology, *Cardiovascular research*, vol. 103, no. 3, pp. 423–428, 2014.

[2] A. Y. Shih, S. G. Sligar, and K. Schulten. Maturation of high-density lipoproteins, *Journal of The Royal Society Interface*, p. rsif20090173, 2009.

[3] A. Kontush and M. J. Chapman. Functionally defective high-density lipoprotein: a new therapeutic target at the crossroads of dyslipidemia, inflammation, and atherosclerosis, *Pharmacological reviews*, vol. 58, no. 3, pp. 342–374, 2006.

[4] P. J. Blanche, E. L. Gong, T. M. Forte, and A. V. Nichols. Characterization of human high-density lipoproteins by gradient gel electrophoresis, *Biochimica et Biophysica Acta (BBA)-Lipids and Lipid Metabolism*, vol. 665, no. 3, pp. 408–419, 1981.

[5] K.-A. Rye, M. A. Clay, and P. J. Barter. High density lipoproteins: The anti-atherogenic fraction, in *Plasma Lipids and Their Role in Disease*. CRC Press, 2014, pp. 120–152.

[6] A. Kontush, S. Chantepie, and M. J. Chapman. Small, dense hdl particles exert potent protection of atherogenic ldl against oxidative stress, *Arteriosclerosis, thrombosis, and vascular biology*, vol. 23, no. 10, pp. 1881–1888, 2003.

[7] T. Vuorela, A. Catte, P. S. Niemelä, A. Hall, M. T. Hyvönen, S.-J. Marrink, M. Karttunen, and I. Vattulainen. Role of lipids in spheroidal high density lipoproteins, *PLoS computational biology*, vol. 6, no. 10, p. e1000964, 2010.

[8] G. B. Sukhorukov, E. Donath, S. Davis, H. Lichtenfeld, F. Caruso, V. I. Popov, and H. Möhwald. Stepwise polyelectrolyte assembly on particle surfaces: a

novel approach to colloid design, *Polymers for Advanced Technologies*, vol. 9, no. 10-11, pp. 759–767, 1998.

[9] S. Stoll and P. Chodanowski. Polyelectrolyte adsorption on an oppositely charged spherical particle. chain rigidity effects, *Macromolecules*, vol. 35, no. 25, pp. 9556–9562, 2002.

[10] L. Ding, L. Yang, T. M. Weiss, A. J. Waring, R. I. Lehrer, and H. W. Huang. Interaction of antimicrobial peptides with lipopolysaccharides, *Biochemistry*, vol. 42, no. 42, pp. 12 251–12 259, 2003.

[11] R. E. Hancock and A. Rozek. Role of membranes in the activities of antimicrobial cationic peptides, *FEMS microbiology letters*, vol. 206, no. 2, pp. 143–149, 2002.

[12] D. L. Nelson, A. L. Lehninger, and M. M. Cox, *Lehninger principles of biochemistry*. Macmillan, 2008.

[13] S. Khrapunov, A. Dragan, A. Sivolob, and A. Zagariya. Mechanisms of stabilizing nucleosome structure. study of dissociation of histone octamer from dna, *Biochimica et Biophysica Acta (BBA)-Gene Structure and Expression*, vol. 1351, no. 1, pp. 213–222, 1997.

[14] H. Schiessel. The physics of chromatin, *Journal of Physics: Condensed Matter*, vol. 15, no. 19, p. R699, 2003.

[15] K. Luger, A. W. Mäder, R. K. Richmond, D. F. Sargent, and T. J. Richmond. Crystal structure of the nucleosome core particle at 2.8 å resolution, *Nature*, vol. 389, no. 6648, pp. 251–260, 1997.

[16] V. Mishra, M. Palgunachari, J. Segrest, and G. Anantharamaiah. Interactions of synthetic peptide analogs of the class a amphipathic helix with lipids. evi-

dence for the snorkel hypothesis. *Journal of Biological Chemistry*, vol. 269, no. 10, pp. 7185–7191, 1994.

[17] R. G. D. Silva, L. A. Schneeweis, S. C. Krishnan, X. Zhang, P. H. Axelsen, and W. S. Davidson. The structure of apolipoprotein A-II in discoidal high density lipoproteins, *Journal of Biological Chemistry*, vol. 282, no. 13, pp. 9713–9721, 2007.

[18] R. G. D. Silva, R. Huang, J. Morris, J. Fang, E. O. Gracheva, G. Ren, A. Kontush, W. G. Jerome, K.-A. Rye, and W. S. Davidson. Structure of apolipoprotein A-I in spherical high density lipoproteins of different sizes, *Proceedings of the National Academy of Sciences*, vol. 105, no. 34, pp. 12 176–12 181, 2008.

[19] R. Huang, R. G. D. Silva, W. G. Jerome, A. Kontush, M. J. Chapman, L. K. Curtiss, T. J. Hodges, and W. S. Davidson. Apolipoprotein A-I structural organization in high-density lipoproteins isolated from human plasma, *Nature structural & molecular biology*, vol. 18, no. 4, pp. 416–422, 2011.

[20] X. Mei and D. Atkinson. Crystal structure of c-terminal truncated apolipoprotein A-I reveals the assembly of high density lipoprotein (HDL) by dimerization, *Journal of Biological Chemistry*, vol. 286, no. 44, pp. 38 570–38 582, 2011.

[21] O. Gursky. Crystal structure of δ (185–243) apoA-I suggests a mechanistic framework for the protein adaptation to the changing lipid load in good cholesterol: from flatland to sphereland via double belt, belt buckle, double hairpin and trefoil/tetrafoil, *Journal of molecular biology*, vol. 425, no. 1, pp. 1–16, 2013.

[22] G. Decher and J. Hong. Buildup of ultrathin multilayer films by a self-assembly process: II consecutive adsorption of anionic and cationic bipolar

amphiphiles and polyelectrolytes on charged surfaces, *Berichte der Bunsenge-sellschaft für physikalische Chemie*, vol. 95, no. 11, pp. 1430–1434, 1991.

[23] G. Decher, J. Hong, and J. Schmitt. Buildup of ultrathin multilayer films by a self-assembly process: III consecutively alternating adsorption of anionic and cationic polyelectrolytes on charged surfaces, *Thin solid films*, vol. 210, pp. 831–835, 1992.

[24] G. Decher, B. Lehr, K. Lowack, Y. Lvov, and J. Schmitt. New nanocomposite films for biosensors: layer-by-layer adsorbed films of polyelectrolytes, proteins or dna, *Biosensors and Bioelectronics*, vol. 9, no. 9-10, pp. 677–684, 1994.

[25] G. Decher. Fuzzy nanoassemblies: toward layered polymeric multicomposites, *science*, vol. 277, no. 5330, pp. 1232–1237, 1997.

[26] F. Caruso, R. A. Caruso, and H. Möhwald. Nanoengineering of inorganic and hybrid hollow spheres by colloidal templating, *Science*, vol. 282, no. 5391, pp. 1111–1114, 1998.

[27] D. I. Gittins and F. Caruso. Tailoring the polyelectrolyte coating of metal nanoparticles, *The Journal of Physical Chemistry B*, vol. 105, no. 29, pp. 6846–6852, 2001.

[28] F. Von Goeler and M. Muthukumar. Adsorption of polyelectrolytes onto curved surfaces, *The Journal of chemical physics*, vol. 100, no. 10, pp. 7796–7803, 1994.

[29] A. Cherstvy and R. Winkler. Polyelectrolyte adsorption onto oppositely charged interfaces: unified approach for plane, cylinder, and sphere, *Physical Chemistry Chemical Physics*, vol. 13, no. 24, pp. 11 686–11 693, 2011.

[30] R. R. Netz and D. Andelman. Neutral and charged polymers at interfaces, *Physics reports*, vol. 380, no. 1, pp. 1–95, 2003.

[31] A. V. Dobrynin and M. Rubinstein. Theory of polyelectrolytes in solutions and at surfaces, *Progress in Polymer Science*, vol. 30, no. 11, pp. 1049–1118, 2005.

[32] R. Messina. Electrostatics in soft matter, *Journal of Physics: Condensed Matter*, vol. 21, no. 11, p. 113102, 2009.

[33] C. Kong and M. Muthukumar. Monte carlo study of adsorption of a polyelectrolyte onto charged surfaces, *The Journal of chemical physics*, vol. 109, no. 4, pp. 1522–1527, 1998.

[34] R. Messina, C. Holm, and K. Kremer. Polyelectrolyte adsorption and multilayering on charged colloidal particles, *Journal of Polymer Science part B: polymer physics*, vol. 42, no. 19, pp. 3557–3570, 2004.

[35] F. Frénet . Sur les courbes a double courbure. *Journal de mathématiques pures et appliquées*, pp. 437–447, 1852.

[36] J.-A. Serret. Sur un théorème relatif aux nombres entiers. *Journal de mathématiques pures et appliquées*, pp. 12–14, 1848.

[37] J.-A. Serret. Sur quelques formules relatives à la théorie des courbes à double courbure. *Journal de mathématiques pures et appliquées*, pp. 193–207, 1851.

[38] G. Darboux. Mémoire sur l'approximation des fonctions de très-grands nombres, et sur une classe étendue de développements en série. *Journal de Mathématiques pures et appliquées*, pp. 5–56, 1878.

[39] M. P. Do Carmo. Differential Geometry of Curves and Surfaces: Revised and Updated Second Edition. Courier Dover Publications, 2016.

[40] J. Langer, D. A. Singer *et al.*. The total squared curvature of closed curves, *Journal of Differential Geometry*, vol. 20, no. 1, pp. 1–22, 1984.

[41] J. Arroyo, O. Garay, and J. Mencía. Elastic circles in 2-spheres, *Journal of Physics A: Mathematical and General*, vol. 39, no. 10, p. 2307, 2006.

[42] J. Arroyo, O. Garay, and J. Mencıa. Extremals of curvature energy actions on spherical closed curves, *Journal of Geometry and Physics*, vol. 51, no. 1, pp. 101–125, 2004.

[43] J. Arroyo, Ó. J. Garay, and J. Mencía. Quadratic curvature energies in the 2-sphere, *Bulletin of the Australian Mathematical Society*, vol. 81, no. 03, pp. 496–506, 2010.

[44] J. Arroyo, O. Garay, and J. Mencıa. Closed generalized elastic curves in s 2 (1), *Journal of Geometry and Physics*, vol. 48, no. 2, pp. 339–353, 2003.

[45] Y. Y. Biton, B. D. Coleman, and D. Swigon. On bifurcations of equilibria of intrinsically curved, electrically charged, rod-like structures that model dna molecules in solution, *Journal of Elasticity*, vol. 87, no. 2-3, pp. 187–210, 2007.

[46] K. A. Hoffman and R. S. Manning. An extended conjugate point theory with application to the stability of planar buckling of an elastic rod subject to a repulsive self-potential, *SIAM Journal on Mathematical Analysis*, vol. 41, no. 2, pp. 465–494, 2009.

[47] S. Fukuhara. Energy of a knot, *A fête of topology*, pp. 443–451, 1988.

[48] B. Joan and J. S.J. Lomonaco. Electrostatic knots, *talk presented at Low Dimensional topology at the joint AMS/CMS meeting held in Vancouver, British Columbia, Canada*, 1983.

[49] J. O'hara. Energy of a knot, *Topology*, vol. 30, no. 2, pp. 241–247, 1991.

[50] J. O'Hara. Family of energy functionals of knots, *Topology and its Applications*, vol. 48, no. 2, pp. 147–161, 1992.

[51] J. O'Hara. Energy functionals of knots II, *Topology and its Applications*, vol. 56, no. 1, pp. 45–61, 1994.

[52] R. B. Kusner and J. M. Sullivan. *Möbius Energies for Knots and Links, Surfaces and Submainfolds*. MSRI, 1994.

[53] J. Ericksen. A thermo-kinetic view of elastic stability theory, *International Journal of Solids and Structures*, vol. 2, no. 4, pp. 573–580, 1966.

[54] M. Golubitsky, I. Stewart, and D. G. Schaeffer. Singularities and groups in bifurcation theory. Springer Science & Business Media, 2012, vol. 2.

[55] Y.C. Chen. Singularity Theory and Nonlinear Bifurcation Analysis . In Y. Fu & R. Ogden (Eds.), *Nonlinear Elasticity: Theory and Applications (London Mathematical Society Lecture Note Series)*, pp. 305-344 . Cambridge: Cambridge University Press. doi:10.1017/CBO9780511526466.010, 2001.

[56] Yamakawa H, Yoshizaki T. Helical wormlike chains in polymer solutions. Berlin: Springer; 1997 Sep.

[57] Skolnick J, Fixman M. Electrostatic persistence length of a wormlike polyelectrolyte. Macromolecules. 1977 Sep;10(5):944-8.

APPENDIX A   DERIVATION OF THE FIRST AND SECOND VARIATION CONDITIONS

A.1   Bending energy

From the identity (3.6) and the constraints (3.24), the first variation of the geodesic curvature squared yields

$$\delta \kappa_i^2 = 2(\boldsymbol{n}_i'' + \boldsymbol{n}_i) \cdot (\boldsymbol{v}_i'' + \boldsymbol{v}_i)$$

$$= 2(\boldsymbol{n}_i'' \cdot \boldsymbol{v}_i'' + \boldsymbol{n}_i \cdot \boldsymbol{v}_i + \boldsymbol{n}_i \cdot \boldsymbol{v}_i'' + \boldsymbol{n}_i'' \cdot \boldsymbol{v}_i)$$

$$= 2\boldsymbol{n}_i'' \cdot \boldsymbol{v}_i'' + \delta(\boldsymbol{n}_i \cdot \boldsymbol{n}_i) + 2\delta(\boldsymbol{n}_i \cdot \boldsymbol{n}_i'')$$

$$= 2\boldsymbol{n}_i'' \cdot \boldsymbol{v}_i''. \tag{A.1}$$

Using above relation, the first variation of $\mathcal{F}_B$ defined in (3.21a) is given as

$$\delta \mathcal{F}_B[\boldsymbol{n}_1, \boldsymbol{n}_2] = \int_0^{\ell_1} \boldsymbol{n}_1'' \cdot \boldsymbol{v}_1'' \, \mathrm{d}s + \nu \int_0^{\ell_2} \boldsymbol{n}_2'' \cdot \boldsymbol{v}_2'' \, \mathrm{d}s$$

$$= \int_0^{\ell_1} -\boldsymbol{n}_1''' \cdot \boldsymbol{v}_1' \, \mathrm{d}s + \nu \int_0^{\ell_2} -\boldsymbol{n}_2''' \cdot \boldsymbol{v}_2' \, \mathrm{d}s + \boldsymbol{n}_1'' \cdot \boldsymbol{v}_1'\big|_0^{\ell_1} + \nu \boldsymbol{n}_2'' \cdot \boldsymbol{v}_2'\big|_0^{\ell_2}. \tag{A.2}$$

Adding the constraints $(3.24)_1$ and $(3.24)_2$ with Langrange multipliers Λ_i and λ_i, respectively yields

$$\delta \mathcal{F}_B[\boldsymbol{n}_1, \boldsymbol{n}_2]$$

$$= \int_0^{\ell_1} ((\boldsymbol{n}_1''' + \lambda_1 \boldsymbol{n}_1)' + \Lambda_1 \boldsymbol{n}_1) \cdot \boldsymbol{v}_1 \, \mathrm{d}s + \nu \int_0^{\ell_2} ((\boldsymbol{n}_2''' + \lambda_2 \boldsymbol{n}_2)' + \Lambda_2 \boldsymbol{n}_2) \cdot \boldsymbol{v}_2 \, \mathrm{d}s$$

$$+ \boldsymbol{n}_1'' \cdot \boldsymbol{v}_1'\big|_0^{\ell_1} - (\boldsymbol{n}_1''' + \lambda_1 \boldsymbol{n}_1) \cdot \boldsymbol{v}_1\big|_0^{\ell_1} + \nu \boldsymbol{n}_2'' \cdot \boldsymbol{v}_2'\big|_0^{\ell_2} - \nu (\boldsymbol{n}_2''' + \lambda_2 \boldsymbol{n}_2) \cdot \boldsymbol{v}_2\big|_0^{\ell_2}.$$

A.2 Intra-loop and Inter-loop interaction energy

The first variation of the intra-loop interaction energy for $\mathcal{C}_i$, $i = 1, 2$ is

$$\delta \int_0^{\ell_i} \int_0^{\ell_i} f(|\boldsymbol{n}_i(s) - \boldsymbol{n}_i(\bar{s})|) \, \mathrm{d}\bar{s} \, \mathrm{d}s$$

$$= \int_0^{\ell_i} \int_0^{\ell_i} \left(\frac{\mathrm{d}f(\varrho)}{\mathrm{d}\varrho} \frac{\boldsymbol{\varrho}}{\varrho} \cdot (\boldsymbol{v}_i(s) - \boldsymbol{v}_i(\bar{s})) \right) \Bigg|_{\substack{\boldsymbol{\varrho} = \boldsymbol{n}_i(s) - \boldsymbol{n}_i(\bar{s}), \\ \varrho = |\boldsymbol{\varrho}|}} \mathrm{d}\bar{s} \, \mathrm{d}s$$

$$= 2 \int_0^{\ell_i} \int_0^{\ell_i} \left(\frac{\mathrm{d}f(\varrho)}{\mathrm{d}\varrho} \frac{\boldsymbol{\varrho}}{\varrho} \cdot \boldsymbol{v}_i(s) \right) \Bigg|_{\substack{\boldsymbol{\varrho} = \boldsymbol{n}_i(s) - \boldsymbol{n}_i(\bar{s}), \\ \varrho = |\boldsymbol{\varrho}|}} \mathrm{d}\bar{s} \, \mathrm{d}s. \quad \text{(A.3)}$$

The first variation of the inter-loop interaction energy is

$$\delta \int_0^{\ell_1} \int_0^{\ell_2} h(|\boldsymbol{n}_1(s) - \boldsymbol{n}_2(\bar{s})|) \, \mathrm{d}\bar{s} \, \mathrm{d}s$$

$$= \int_0^{\ell_1} \int_0^{\ell_2} \left(\frac{\mathrm{d}h(\varrho)}{\mathrm{d}\varrho} \frac{\boldsymbol{\varrho}}{\varrho} \cdot (\boldsymbol{v}_1(s) - \boldsymbol{v}_2(\bar{s})) \right) \Bigg|_{\substack{\boldsymbol{\varrho} = \boldsymbol{n}_1(s) - \boldsymbol{n}_2(\bar{s}), \\ \varrho = |\boldsymbol{\varrho}|}} \mathrm{d}\bar{s} \, \mathrm{d}s$$

$$= \int_0^{\ell_1} \int_0^{\ell_2} \left(\frac{\mathrm{d}h(\varrho)}{\mathrm{d}\varrho} \frac{\boldsymbol{\varrho}}{\varrho} \cdot \boldsymbol{v}_1(s) \right) \Bigg|_{\substack{\boldsymbol{\varrho} = \boldsymbol{n}_1(s) - \boldsymbol{n}_2(\bar{s}), \\ \varrho = |\boldsymbol{\varrho}|}} \mathrm{d}\bar{s} \, \mathrm{d}s$$

$$+ \int_0^{\ell_2} \int_0^{\ell_1} \left(\frac{\mathrm{d}h(\varrho)}{\mathrm{d}\varrho} \frac{\boldsymbol{\varrho}}{\varrho} \cdot \boldsymbol{v}_2(s) \right) \Bigg|_{\substack{\boldsymbol{\varrho} = \boldsymbol{n}_2(s) - \boldsymbol{n}_1(\bar{s}), \\ \varrho = |\boldsymbol{\varrho}|}} \mathrm{d}\bar{s} \, \mathrm{d}s. \quad \text{(A.4)}$$

Defining

$$\boldsymbol{\varphi}[\boldsymbol{n}_i, \boldsymbol{n}_j] = \begin{cases} -\int_0^{\ell_j} \boldsymbol{f}(\boldsymbol{n}_i - \boldsymbol{n}_j(\bar{s})) \, \mathrm{d}\bar{s} & i = j, \\ -\int_0^{\ell_j} \boldsymbol{h}(\boldsymbol{n}_i - \boldsymbol{n}_j(\bar{s})) \, \mathrm{d}\bar{s} & i \neq j, \end{cases} \quad \text{(A.5)}$$

where $i, j = 1, 2$ and $\boldsymbol{f}$ and $\boldsymbol{h}$ are defined such that

$$\boldsymbol{f}(\boldsymbol{\varrho}) = \frac{\mathrm{d}f(\varrho)}{\mathrm{d}\varrho}\Bigg|_{\varrho = |\boldsymbol{\varrho}|} \frac{\boldsymbol{\varrho}}{|\boldsymbol{\varrho}|}, \quad \text{and} \quad \boldsymbol{h}(\boldsymbol{\varrho}) = \frac{\mathrm{d}h(\varrho)}{\mathrm{d}\varrho}\Bigg|_{\varrho = |\boldsymbol{\varrho}|} \frac{\boldsymbol{\varrho}}{|\boldsymbol{\varrho}|}, \quad \text{(A.6)}$$

the first variation of the intra-loop interaction energy (self-energy) (A.3) and the inter-loop interaction energy (A.4) can be written as

$$\delta \mathcal{F}_{\mathrm{S}}[\boldsymbol{n}_1, \boldsymbol{n}_2] = -\zeta_1 \int_0^{\ell_1} \boldsymbol{\varphi}[\boldsymbol{n}_1, \boldsymbol{n}_1] \cdot \boldsymbol{v}_1 \, \mathrm{d}s - \zeta_2 \int_0^{\ell_2} \boldsymbol{\varphi}[\boldsymbol{n}_2, \boldsymbol{n}_2] \cdot \boldsymbol{v}_2 \, \mathrm{d}s, \quad \text{(A.7)}$$

and

$$\delta \mathcal{F}_{\mathrm{I}}[\boldsymbol{n}_1, \boldsymbol{n}_2] = -\chi \int_0^{\ell_1} \boldsymbol{\varphi}[\boldsymbol{n}_1, \boldsymbol{n}_2] \cdot \boldsymbol{v}_1 \, \mathrm{d}s - \chi \int_0^{\ell_2} \boldsymbol{\varphi}[\boldsymbol{n}_2, \boldsymbol{n}_1] \cdot \boldsymbol{v}_2 \, \mathrm{d}s. \quad \text{(A.8)}$$

Combining the $\delta\mathcal{F}_B$, $\delta\mathcal{F}_S$, and $\delta\mathcal{F}_I$, the first variation of the total energy functional is given as

$$\delta\mathcal{F}[n_1, n_2](v_1, v_2) = \int_0^{\ell_1} ((n_1''' + \lambda_1 n_1')' + \Lambda_1 n_1 - \zeta_1\varphi[n_1, n_1] - \chi\varphi[n_1, n_2]) \cdot v_1 \, ds$$

$$+ \int_0^{\ell_2} (\nu(n_2''' + \lambda_2 n_2')' + \Lambda_2 n_2 - \zeta_2\varphi[n_2, n_2] - \chi\varphi[n_2, n_1]) \cdot v_2 \, ds$$

$$+ n_1'' \cdot v_1'|_0^{\ell_1} - (n_1''' + \lambda_1 n_1') \cdot v_1|_0^{\ell_1} + \nu n_2'' \cdot v_2'|_0^{\ell_2} - \nu(n_2''' + \lambda_2 n_2') \cdot v_2|_0^{\ell_2}. \quad \text{(A.9)}$$

For (n_1, n_2) to be the equilibrium configuration, the first variation condition requires that $\delta\mathcal{F}[n_1, n_2](v_1, v_2) = 0$, $\forall v_1, v_2$ that yields the equilibrium equations

$$\left.\begin{aligned}
(n_1''' + \lambda_1 n_1')' + \Lambda_1 n_1 &= \zeta_1\varphi[n_1, n_1] + \chi\varphi[n_1, n_2], \\
\nu(n_2''' + \lambda_2 n_2')' + \Lambda_2 n_2 &= \zeta_2\varphi[n_2, n_2] + \chi\varphi[n_2, n_1],
\end{aligned}\right\}, \quad \text{(A.10)}$$

and the boundary conditions

$$\left.\begin{aligned}
n_1'' \cdot v_1'|_0^{\ell_1} - (n_1''' + \lambda_1 n_1') \cdot v_1|_0^{\ell_1} &= 0, \\
n_2'' \cdot v_2'|_0^{\ell_2} - (n_2''' + \lambda_2 n_2') \cdot v_2|_0^{\ell_2} &= 0,
\end{aligned}\right\}. \quad \text{(A.11)}$$

For smooth, closed curves, the boundary terms are trivially satisfied. The second variation of the energy functional is obtained as

$$\delta^2\mathcal{F}[n_1, n_2](v_1, v_2) = \int_0^{\ell_1} ((n_1''' + \lambda_1 n_1')' + \Lambda_1 n_1 - \zeta_1\varphi[n_1, n_1] - \chi\varphi[n_1, n_2]) \cdot \delta v_1 \, ds$$

$$+ \int_0^{\ell_2} (\nu(n_2''' + \lambda_2 n_2')' + \Lambda_2 n_2 - \zeta_2\varphi[n_2, n_2] - \chi\varphi[n_2, n_1]) \cdot \delta v_2 \, ds$$

$$+ \int_0^{2\pi a} (|v_1''|^2 - \lambda_1|v_1'|^2 + (\lambda_1'v_1' + \Lambda_1 v_1 - \zeta\vartheta[n_1, n_1](v_1, v_1)$$

$$- \chi\vartheta[n_1, n_2](v_1, v_2)) \cdot v_1) \, ds$$

$$+ \int_0^{2\pi a} ((|v_2''|^2 - \lambda_2|v_2'|^2) + (\lambda_2'v_2' + \Lambda_2 v_2 - \zeta\vartheta[n_2, n_2](v_2, v_2)$$

$$- \chi\vartheta[n_2, n_1](v_2, v_1)) \cdot v_2) \, ds, \quad \text{(A.12)}$$

where $\boldsymbol{\vartheta}$ is defined by

$$
\boldsymbol{\vartheta}[\boldsymbol{n}_i, \boldsymbol{n}_j](\boldsymbol{v}_i, \boldsymbol{v}_j) = \begin{cases} -\displaystyle\int_0^{\ell_j} \boldsymbol{F}(\boldsymbol{n}_i - \boldsymbol{n}_j(\bar{s}))(\boldsymbol{v}_i - \boldsymbol{v}(\bar{s})_j)\, d\bar{s} & i = j, \\[4mm] -\displaystyle\int_0^{\ell_j} \boldsymbol{H}(\boldsymbol{n}_i - \boldsymbol{n}_j(\bar{s}))(\boldsymbol{v}_i - \boldsymbol{v}(\bar{s})_j)\, d\bar{s} & i \neq j, \end{cases} \tag{A.13}
$$

where $i, j = 1, 2$, and $\boldsymbol{F}$ and $\boldsymbol{H}$ are defined such that

$$
\boldsymbol{F}[\boldsymbol{\varrho}] = \frac{1}{\varrho}\left(\frac{\mathrm{d}f(\varrho)}{\mathrm{d}\varrho} \mathbf{1} + \frac{\mathrm{d}}{\mathrm{d}\varrho}\left(\frac{1}{\varrho}\frac{\mathrm{d}f(\varrho)}{\mathrm{d}\varrho} \right)\boldsymbol{\varrho}\otimes\boldsymbol{\varrho} \right)\bigg|_{\varrho=|\boldsymbol{\varrho}|}, \tag{A.14}
$$

and

$$
\boldsymbol{H}[\boldsymbol{\varrho}] = \frac{1}{\varrho}\left(\frac{\mathrm{d}h(\varrho)}{\mathrm{d}\varrho} \mathbf{1} + \frac{\mathrm{d}}{\mathrm{d}\varrho}\left(\frac{1}{\varrho}\frac{\mathrm{d}h(\varrho)}{\mathrm{d}\varrho} \right)\boldsymbol{\varrho}\otimes\boldsymbol{\varrho} \right)\bigg|_{\varrho=|\boldsymbol{\varrho}|}. \tag{A.15}
$$

Using (A.10), the second variation (A.12) evaluated at equilibrium simplifies to

$$
\begin{aligned}
\delta^2 \mathcal{F}[\boldsymbol{n}_1, \boldsymbol{n}_2](\boldsymbol{v}_1, \boldsymbol{v}_2) = \\
\int_0^{2\pi a} &\big(|\boldsymbol{v}_1''|^2 - \lambda_1|\boldsymbol{v}_1'|^2 + (\lambda_1'\boldsymbol{v}_1' + \Lambda_1\boldsymbol{v}_1 - \zeta\boldsymbol{\vartheta}[\boldsymbol{n}_1,\boldsymbol{n}_1](\boldsymbol{v}_1,\boldsymbol{v}_1) \\
&\quad - \chi\boldsymbol{\vartheta}[\boldsymbol{n}_1,\boldsymbol{n}_2](\boldsymbol{v}_1,\boldsymbol{v}_2))\cdot\boldsymbol{v}_1\big)\, \mathrm{d}s \\
+ \int_0^{2\pi a} &\big((|\boldsymbol{v}_2''|^2 - \lambda_2|\boldsymbol{v}_2'|^2) + (\lambda_2'\boldsymbol{v}_2' + \Lambda_2\boldsymbol{v}_2 - \zeta\boldsymbol{\vartheta}[\boldsymbol{n}_2,\boldsymbol{n}_2](\boldsymbol{v}_2,\boldsymbol{v}_2) \\
&\quad - \chi\boldsymbol{\vartheta}[\boldsymbol{n}_2,\boldsymbol{n}_1](\boldsymbol{v}_2,\boldsymbol{v}_1))\cdot\boldsymbol{v}_2\big)\, \mathrm{d}s. \tag{A.16}
\end{aligned}
$$

A.3 Open curve

For a single, charged polyelectrolyte, confined to a sphere, the energetics of the system includes bending of the curve and the self energy of the curve. In such situation, the equilibrium equation (A.10), the boundary condition (A.11), and the stability condition (A.12) for chain of length ℓ and intra-loop interaction parameter ζ reduce to be

$$
(\boldsymbol{n}''' + \lambda\boldsymbol{n}')' + \Lambda\boldsymbol{n}_1 = \zeta\boldsymbol{\varphi}[\boldsymbol{n},\boldsymbol{n}], \tag{A.17}
$$

$$
\boldsymbol{n}''\cdot\boldsymbol{v}'\big|_0^\ell - (\boldsymbol{n}''' + \lambda\boldsymbol{n}')\cdot\boldsymbol{v}\big|_0^\ell = 0, \tag{A.18}
$$

78

and

$$\int_0^\ell (|\boldsymbol{v}''|^2 - \lambda |\boldsymbol{v}'|^2 + (\lambda' \boldsymbol{v}' + \Lambda \boldsymbol{v} - \zeta \boldsymbol{\vartheta}[\boldsymbol{n}, \boldsymbol{n}](\boldsymbol{v}, \boldsymbol{v}) \geq 0, \qquad \text{(A.19)}$$

respectively, where the functionals $\boldsymbol{\varphi}$ and $\boldsymbol{\vartheta}$ are defined in (A.5) and (A.13). The Lagrange multipliers λ and Λ ensure the satisfaction of constraints $\boldsymbol{n} \cdot \boldsymbol{v} = 0$ and $\boldsymbol{n}' \cdot \boldsymbol{v}' = 0$ respectively.

Appendix B Second variation condition

for the specialized case

Substituting $n_1 = n$, $n_2 = Qn$, $v_1 = v$, $v_2 = Qv$, $\lambda_1 = \lambda_2 = \lambda$, and $\Lambda_1 = \Lambda_2 = \Lambda$ in (4.14) and noting that the λ and Λ are uniform for the trivial configuration, we find the reduced form of the second variation condition at the equilibrium as

$$\int_0^{2\pi a} (|v''|^2 - \lambda |v'|^2 + (\Lambda v - \zeta \tilde{\vartheta}[n,n](v,v) - \chi \vartheta[n,Qn](v,Qv)) \cdot v) \, \mathrm{d}s$$

$$+ \int_0^{2\pi a} ((|Qv''|^2 - \lambda |Qv'|^2) + (\Lambda Qv - \zeta \tilde{\vartheta}[Qn,Qn](Qv,Qv)$$

$$- \chi \vartheta[Qn,n](Qv,v)) \cdot Qv) \, \mathrm{d}s \geq 0, \quad \text{(B.1)}$$

where

$$\tilde{\vartheta}[n,n](v,v)$$

$$= \int_0^{2\pi a} M\left(\frac{|\bar{s} - s|}{2a}\right) \left(\frac{(v - v(\bar{s}))}{|n - n(\bar{s})|^3} + 3\frac{(n \cdot v(\bar{s}) + n(\bar{s}) \cdot v)}{|n - n(\bar{s})|^5}(n - n(\bar{s}))\right) \, \mathrm{d}\bar{s}, \quad \text{(B.2)}$$

$$\tilde{\vartheta}[Qn,Qn](Qv,Qv) = \int_0^{2\pi a} M\left(\frac{|\bar{s} - s|}{2a}\right) \left(\frac{(Qv - Qv(\bar{s}))}{|Qn - Qn(\bar{s})|^3}\right.$$

$$\left. + 3\frac{(Qn \cdot Qv(\bar{s}) + Qn(\bar{s}) \cdot Qv)}{|Qn - Qn(\bar{s})|^5}(Qn - Qn(\bar{s}))\right) \, \mathrm{d}\bar{s}, \quad \text{(B.3)}$$

$$\vartheta[n,Qn](v,Qv)$$

$$= \int_0^{2\pi a} \left(\frac{(v - Qv(\bar{s}))}{|n - Qn(\bar{s})|^3} + 3\frac{(n \cdot Qv(\bar{s}) + Qn(\bar{s}) \cdot v)}{|n - Qn(\bar{s})|^5}(n - Qn(\bar{s}))\right) \, \mathrm{d}\bar{s}, \quad \text{(B.4)}$$

and

$$\vartheta[Qn,n](Qv,v)$$

$$= \int_0^{2\pi a} \left(\frac{(Qv - v(\bar{s}))}{|Qn - n(\bar{s})|^3} + 3\frac{(Qn \cdot v(\bar{s}) + n(\bar{s}) \cdot Qv)}{|Qn - n(\bar{s})|^5}(Qn - n(\bar{s}))\right) \, \mathrm{d}\bar{s}. \quad \text{(B.5)}$$

Using the elementary properties of Q defined in (4.20)$_1$,

$$|Qv''|^2 = |v''|^2, \quad |Qv'|^2 = |v'|^2, \quad \text{and} \quad |Qv|^2 = |v|^2. \tag{B.6}$$

Furthermore, using (4.20),(4.21) and a change of variable $\bar{s} \to \bar{s} + 2a\phi$, we see that

$$
\begin{aligned}
& Q^\top \tilde{\vartheta}[Qn, Qn](Qv, Qv) \\
&= \int_0^{2\pi a} M\left(\frac{|\bar{s} - s|}{2a}\right) \left(\frac{(v - v(\bar{s}))}{|n - Q^\top n(\bar{s})|^3} + 3\frac{(n \cdot v(\bar{s}) + n(\bar{s}) \cdot v)}{|n - Q^\top n(\bar{s})|^5}(n - n(\bar{s}))\right) d\bar{s} \\
&= \int_{2a\phi}^{2(\pi+\phi)a} M\left(\frac{|\bar{s} - s|}{2a}\right) \left(\frac{(v - v(\bar{s}))}{|n - n(\bar{s})|^3} + 3\frac{(n \cdot v(\bar{s}) + n(\bar{s}) \cdot v)}{|n - n(\bar{s})|^5}(n - n(\bar{s}))\right) d\bar{s} \\
&= \int_0^{2\pi a} M\left(\frac{|\bar{s} - s|}{2a}\right) \left(\frac{(v - v(\bar{s}))}{|n - n(\bar{s})|^3} + 3\frac{(n \cdot v(\bar{s}) + n(\bar{s}) \cdot v)}{|n - n(\bar{s})|^5}(n - n(\bar{s}))\right) d\bar{s} \\
&= \tilde{\vartheta}[n, n](v, v),
\end{aligned}
\tag{B.7}
$$

which implies that

$$\tilde{\vartheta}[Qn, Qn](Qv, Qv) \cdot Qv = Q^\top \tilde{\vartheta}[Qn, Qn](Qv, Qv) \cdot v = \tilde{\vartheta}[n, n](v, v) \cdot v. \tag{B.8}$$

We impose further restriction on the rotation between the perturbation for the two loops as follows. Let ϕ_n denote the rotation ϕ for the n-th mode of the perturbation v. Among all the values of ϕ_n, the repulsive interaction energy between the perturbed curves $n + \varepsilon v$ and $Qn + \varepsilon Qv$, where ε is a small number, is minimized for $\phi_n = \frac{\pi}{n}$. Therefore, at $\phi_n = \frac{\pi}{n}$, the equilibrium configuration will first bifurcate into non trivial shape. Assuming this choice of ϕ_n,

$$Q^\top(\phi_n)v(s + 2a\phi_n) = Q(\phi_n)v(s), \quad 0 \le s \le 2a\pi. \tag{B.9}$$

Using (B.9) and the change of variable $\bar{s} \rightarrow \bar{s} + 2a\phi_n$ in (B.5), using the constraints $\mathbf{n} \cdot \mathbf{v} = 0$, $\mathbf{n}(\bar{s}) \cdot \mathbf{v}(\bar{s}) = 0$, and that $\mathbf{n}$ and $\mathbf{v}$ are periodic functions with period $2\pi a$,

$$
\begin{aligned}
&Q^\top \boldsymbol{\vartheta}[Q\mathbf{n}, \mathbf{n}](Q\mathbf{v}, \mathbf{v}) \\
&= \int_0^{2\pi a} \left(\frac{\mathbf{v} - Q^\top \mathbf{v}(\bar{s})}{|\mathbf{n} - Q^\top \mathbf{n}(\bar{s})|^3} + 3 \frac{(\mathbf{n} \cdot Q^\top \mathbf{v}(\bar{s}) + Q^\top \mathbf{n}(\bar{s}) \cdot \mathbf{v})}{|\mathbf{n} - Q^\top \mathbf{n}(\bar{s})|^5} (\mathbf{n} - Q^\top \mathbf{n}(\bar{s})) \right) \, d\bar{s} \\
&= \int_{2\phi_n a}^{2(\pi + \phi_n)a} \left(\frac{\mathbf{v} - Q\mathbf{v}(\bar{s})}{|\mathbf{n} - Q\mathbf{n}(\bar{s})|^3} + 3 \frac{(\mathbf{n} \cdot Q\mathbf{v}(\bar{s}) + Q\mathbf{n}(\bar{s}) \cdot \mathbf{v})}{|\mathbf{n} - Q\mathbf{n}(\bar{s})|^5} (\mathbf{n} - Q\mathbf{n}(\bar{s})) \right) \, d\bar{s} \\
&= \int_0^{2\pi a} \left(\frac{\mathbf{v} - Q\mathbf{v}(\bar{s})}{|\mathbf{n} - Q\mathbf{n}(\bar{s})|^3} + 3 \frac{(\mathbf{n} \cdot Q\mathbf{v}(\bar{s}) + Q\mathbf{n}(\bar{s}) \cdot \mathbf{v})}{|\mathbf{n} - Q\mathbf{n}(\bar{s})|^5} (\mathbf{n} - Q\mathbf{n}(\bar{s})) \right) \, d\bar{s} \\
&= \boldsymbol{\vartheta}[\mathbf{n}, Q\mathbf{n}](\mathbf{v}, Q\mathbf{v}).
\end{aligned}
\tag{B.10}
$$

Therefore,

$$
\boldsymbol{\vartheta}[Q\mathbf{n}, \mathbf{n}](Q\mathbf{v}, \mathbf{v}) \cdot Q\mathbf{v} = Q^\top \boldsymbol{\vartheta}[Q\mathbf{n}, \mathbf{n}](Q\mathbf{v}, \mathbf{v}) \cdot \mathbf{v} = \boldsymbol{\vartheta}[\mathbf{n}, Q\mathbf{n}](\mathbf{v}, Q\mathbf{v}) \cdot \mathbf{v}. \tag{B.11}
$$

The equations (B.6), (B.8), and (B.11) imply that the contribution to the second variation of the total energy from bending energy, from intra-loop interaction and from the inter-loop interaction, respectively from the two loops are equal. Using these relations in (B.1), we obtain a reduced stability condition as

$$
\int_0^{2\pi a} (|\mathbf{v}''|^2 - \lambda |\mathbf{v}'|^2 + \Lambda |\mathbf{v}|^2 - \zeta \tilde{\boldsymbol{\vartheta}}[\mathbf{n}, \mathbf{n}](\mathbf{v}, \mathbf{v}) \cdot \mathbf{v} - \chi \boldsymbol{\vartheta}[\mathbf{n}, Q\mathbf{n}](\mathbf{v}, Q\mathbf{v}) \cdot \mathbf{v}) \, ds \geq 0.
\tag{B.12}
$$

B.1 Useful relations

Introducing a variable $\eta = \frac{\bar{s} - s}{2a}$, we represent the quantities at arc length $\bar{s}$ in terms of s and η. Below are some of the useful expressions for further calculations

$$
\mathbf{e}(\bar{s}) = \cos 2\eta \, \mathbf{e} + \sin 2\eta \, \mathbf{k} \times \mathbf{e}, \tag{B.13}
$$

$$
\mathbf{n}(\bar{s}) = a \cos 2\eta \, \mathbf{e} + \sqrt{1 - a^2} \mathbf{k} + a \sin 2\eta (\mathbf{k} \times \mathbf{e}), \tag{B.14}
$$

$$
\begin{aligned}
\mathbf{v}(\bar{s}) = &-(a\psi(\bar{s}) \sin 2\eta + a^2 \psi'(\bar{s}) \cos 2\eta) \mathbf{e} + \frac{a^3 \psi'(\bar{s})}{\sqrt{1 - a^2}} \mathbf{k} \\
&+ (a\psi(\bar{s}) \cos 2\eta - a^2 \psi'(\bar{s}) \sin 2\eta) \mathbf{k} \times \mathbf{e}, \tag{B.15}
\end{aligned}
$$

$$Q(\phi_n)n = a\cos\phi_n e + a\sin\phi_n k \times e - \sqrt{1-a^2}k, \tag{B.16}$$

$$Q(\phi_n)n(\bar{s}) = a\cos(2\eta+\phi_n)e - \sqrt{1-a^2}k + a\sin(2\eta+\phi_n)(k\times e), \tag{B.17}$$

$$Q(\phi_n)v(\bar{s}) = -[a\psi(\bar{s})\sin(2\eta+\phi_n) + a^2\psi'(\bar{s})\cos(2\eta+\phi_n)]e$$
$$+ [a\psi(\bar{s})\cos(2\eta+\phi_n) - a^2\psi'(\bar{s})\sin(2\eta+\phi_n)]k\times e - \frac{a^3\psi'(\bar{s})}{\sqrt{1-a^2}}k, \tag{B.18}$$

$$|n - n(\bar{s})| = 2a|\sin\eta|, \quad \text{and} \tag{B.19}$$

$$|n - Qn(\bar{s})| = 2\sqrt{1-a^2\cos^2(\eta+\phi_n/2)}. \tag{B.20}$$

We use the relations defined above to simplify the second variation condition (B.12) as follows.

Bending energy terms : Using the representation of v in terms of ψ and ψ' defined in (4.48) and the identities in (4.45), we find that

$$\left.\begin{aligned}
v &= -a^2\psi'e + \frac{a^3\psi'}{\sqrt{1-a^2}}k + a\psi k \times e, \\
v' &= -(\psi + a^2\psi'')e + \frac{a^3\psi''}{\sqrt{1-a^2}}k, \\
v'' &= -(a^2\psi''' + \psi')e + \frac{a^3\psi'''}{\sqrt{1-a^2}}k - (a\psi'' + \psi/a)k \times e,
\end{aligned}\right\}. \tag{B.21}$$

Intra-loop interaction terms :

Bearing in mind the change of variable $\bar{s} = s + 2a\eta$, using (B.14) and noticing the representation of $\psi(\bar{s})$ in terms of s and η, we find the components of

$\tilde{\boldsymbol{\vartheta}}[\boldsymbol{n},\boldsymbol{n}](v,v)$ defined in (B.2) as

$$\tilde{\boldsymbol{\vartheta}}[\boldsymbol{n},\boldsymbol{n}](v,v)\cdot\boldsymbol{e} = -\frac{\psi'}{4}\int_0^\pi M(\eta)\csc^3\eta\,\mathrm{d}\eta$$
$$+\frac{1}{4a}\int_0^\pi M(\eta)\frac{\psi(s+2a\eta)\sin 2\eta + a\psi'(s+2a\eta)\cos 2\eta}{\sin^3\eta}\,\mathrm{d}\eta$$
$$+\frac{3}{4a}\int_0^\pi M(\eta)\frac{\cos\eta(\psi-\psi(s+2a\eta))+a\sin\eta(\psi'+\psi'(s+2a\eta))}{\sin^2\eta}\,\mathrm{d}\eta,$$

$$\tilde{\boldsymbol{\vartheta}}[\boldsymbol{n},\boldsymbol{n}](v,v)\cdot\boldsymbol{k} = \frac{a\psi'}{4\sqrt{1-a^2}}\int_0^\pi M(\eta)\csc^3\eta\,\mathrm{d}\eta - \frac{a}{4\sqrt{1-a^2}}\int_0^\pi\frac{\psi'(s+2a\eta)}{\sin^3\eta}\,\mathrm{d}\eta,$$

$$\left.\begin{array}{l}\\\\\\\\\\\\\\\\\\\\\\\\\\\end{array}\right\}.$$

$$\tilde{\boldsymbol{\vartheta}}[\boldsymbol{n},\boldsymbol{n}](v,v)\cdot(\boldsymbol{k}\times\boldsymbol{e}) = \frac{\psi}{4a}\int_0^\pi M(\eta)\csc^3\eta\,\mathrm{d}\eta$$
$$-\frac{1}{4a}\int_0^\pi M(\eta)\frac{\psi(s+2a\eta)\cos 2\eta - a\psi'(s+2a\eta)\sin 2\eta}{\sin^3\eta}\,\mathrm{d}\eta,$$
$$-\frac{1}{4a}\int_0^\pi\frac{\cos\eta[\cos\eta(\psi-\psi(s+2a\eta))+a\sin\eta(\psi'+\psi'(s+2a\eta))]}{\sin^3\eta}\,\mathrm{d}\eta$$

(B.22)

Interaction energy terms : Bearing in mind the change of variable $\bar{s} = s + 2a\eta$, using (B.17), (B.18), (B.20) and noticing the representation of $\psi(\bar{s})$ in terms of s and η, and making an additional change of variable $\eta \to \eta - \phi_n/2$, we find the

components of $\boldsymbol{\vartheta}[n, Qn](v, Qv)$ defined in (B.4) as

$$
\left.
\begin{aligned}
\boldsymbol{\vartheta}[n, Qn](v, Qv) \cdot e &= -\frac{a^3}{4}\psi' \int_0^\pi \frac{1}{\sqrt[3]{1 - a^2 \cos^2 \eta}}\, d\eta \\
&+ \frac{a^2}{4}\int_0^\pi \frac{\psi(s + 2a\eta - a\phi_n)\sin 2\eta - a\psi'(s + 2a\eta - a\phi_n)\cos 2\eta}{\sqrt[3]{1 - a^2 \cos^2 \eta}}\, d\eta \\
&+ \frac{3a^4}{4}\int_0^\pi \frac{\sin^2 \eta \cos \eta [\sin \eta (\psi - \psi(s + 2a\eta - a\phi_n))]}{\sqrt[5]{1 - a^2 \cos^2 \eta}}\, d\eta \\
&- \frac{3a^4}{4}\int_0^\pi \frac{\sin^2 \eta \cos \eta [a \cos \eta (\psi' + \psi'(s + 2a\eta - a\phi_n))]}{\sqrt[5]{1 - a^2 \cos^2 \eta}}\, d\eta, \\[4pt]
\boldsymbol{\vartheta}[n, Qn](v, Qv) \cdot k &= \frac{a^4 \psi'}{4\sqrt{1 - a^2}}\int_0^\pi \frac{1}{\sqrt[3]{1 - a^2 \cos^2 \eta}}\, d\eta \\
&- \frac{a^4}{4\sqrt{1 - a^2}}\int_0^\pi \frac{\psi'(s + 2a\eta - a\phi_n)}{\sqrt[3]{1 - a^2 \cos^2 \eta}}\, d\eta \\
&+ \frac{3a^3 \sqrt{1 - a^2}}{4}\int_0^\pi \frac{\cos \eta [\sin \eta (\psi - \psi(s + 2a\eta - a\phi_n))]}{\sqrt[5]{1 - a^2 \cos^2 \eta}}\, d\eta \\
&- \frac{3a^3 \sqrt{1 - a^2}}{4}\int_0^\pi \frac{\cos \eta [a \cos \eta (\psi' + \psi'(s + 2a\eta - a\phi_n))]}{\sqrt[5]{1 - a^2 \cos^2 \eta}}\, d\eta, \\[4pt]
\boldsymbol{\vartheta}[n, Qn](v, Qv) \cdot (k \times e) &= \frac{a^2}{4}\psi \int_0^\pi \frac{1}{\sqrt[3]{1 - a^2 \cos^2 \eta}}\, d\eta \\
&- \frac{a^2}{4}\int_0^\pi \frac{\psi(s + 2a\eta - a\phi_n)\cos 2\eta + a\psi'(s + 2a\eta - a\phi_n)\sin 2\eta}{\sqrt[3]{1 - a^2 \cos^2 \eta}}\, d\eta \\
&- \frac{3a^4}{4}\int_0^\pi \frac{\sin \eta \cos^2 \eta [\sin \eta (\psi - \psi(s + 2a\eta - a\phi_n))]}{\sqrt[5]{1 - a^2 \cos^2 \eta}}\, d\eta \\
&+ \frac{3a^4}{4}\int_0^\pi \frac{\sin \eta \cos^2 \eta [a \cos \eta (\psi' + \psi'(s + 2a\eta - a\phi_n))]}{\sqrt[5]{1 - a^2 \cos^2 \eta}}\, d\eta,
\end{aligned}
\right\} . \tag{B.23}
$$

B.2   Fourier representation

Using the Fourier series representation of the functions ψ as

$$
\psi = \sum_{n=2}^\infty \psi_n, \quad \psi_n(s) = c_n \cos \frac{ns}{a} + d_n \sin \frac{ns}{a}, \tag{B.24}
$$

we simplify the various terms involved in (C.2), (B.22), and (3.33) as follows.

Bending energy terms : Using the periodicity of ψ_n,

$$
\int_0^{2\pi a} \psi_n^2\, ds = \pi a (c_n^2 + d_n^2) \quad \text{and} \quad \int_0^{2\pi a} \psi'^2_n\, ds = \pi a (n/a)^2 (c_n^2 + d_n^2). \tag{B.25}
$$

Substituting (B.24) in (B.21) and using (B.25), we find that

$$\int_0^{2\pi a} |v''|^2 \, ds = \pi a \sum_{n=2}^{\infty} \left[\frac{(n^2-1)^2(n^2+1)}{a^2} + \frac{n^6}{1-a^2} \right] (c_n^2 + d_n^2), \quad (B.26)$$

$$\int_0^{2\pi a} |v'|^2 \, ds = \pi a \sum_{n=2}^{\infty} \left[(n^2-1)^2 + \frac{a^2 n^4}{1-a^2} \right] (c_n^2 + d_n^2), \quad (B.27)$$

$$\int_0^{2\pi a} |v|^2 \, ds = \pi a \sum_{n=2}^{\infty} \left[a^2 + \frac{a^2 n^2}{1-a^2} \right] (c_n^2 + d_n^2), \quad (B.28)$$

and it follows that

$$\int_0^{2\pi a} (|v''|^2 - \lambda |v'|^2 + \Lambda |v|^2) \, ds = \pi a \sum_{n=2}^{\infty} \left[\frac{(n^2-1)^2(n^2+1)}{a^2} + \frac{n^6}{1-a^2} \right.$$
$$\left. - \lambda \left((n^2-1)^2 + \frac{a^2 n^4}{1-a^2} \right) + \Lambda a^2 \left(1 + \frac{n^2}{1-a^2} \right) \right] (c_n^2 + d_n^2). \quad (B.29)$$

Intra-loop interaction terms : Using (B.24), we deduce the following useful relations

$$\psi_n(s + 2a\eta) = \cos 2n\eta \, \psi_n(s) + \sin 2n\eta \frac{a}{n} \psi_n'(s) \quad \text{and} \quad (B.30)$$

$$\psi_n'(s + 2a\eta) = -\sin 2n\eta \frac{n}{a} \psi_n(s) + \cos 2n\eta \, \psi_n'(s). \quad (B.31)$$

Using (B.24), (B.30), and (B.31) in the integrals in the right hand side of the equations in (B.22), we obtain

$$\left. \begin{array}{l} \tilde{\vartheta}[n, n](v, v) \cdot e = \frac{1}{4} \sum_{n=2}^{\infty} [-I_4 + 2I_2/n + I_3 - 2I + 3(I_5 + I_1 - I_2/n)] \psi_n', \\[3mm] \tilde{\vartheta}[n, n](v, v) \cdot k = \frac{a}{4\sqrt{1-a^2}} \sum_{n=2}^{\infty} (I_4 - I_3) \psi_n', \\[3mm] \tilde{\vartheta}[n, n](v, v) \cdot (k \times e) = \frac{1}{4a} \sum_{n=2}^{\infty} [I_4 - 2nI_2 + 2I_1 - I_3 - 3(I_4 - I_5 + I_1 - I_3 - nI_2)] \psi_n, \end{array} \right\}, \quad (B.32)$$

where I_1, I_2, I_3, I_4, and I_5 are defined in (B.47). Using the representation of the perturbation v as

$$v = \sum_{n=0}^{\infty} -a^2 \psi_n' e + \frac{a^3 \psi_n'}{\sqrt{1-a^2}} k + a\psi_n k \times e, \quad (B.33)$$

86

and (B.25),

$$\int_0^{2\pi a} \tilde{\vartheta}[n,n](v,v) \cdot v \, ds = \frac{a^2}{4(1-a^2)} \sum_{n=2}^{\infty} (I_4 - I_3) n^2 (c_n^2 + d_n^2)$$

$$- \frac{1}{4} \sum_{n=2}^{\infty} [-I_4 + 2I_2/n + I_3 - 2I + 3(I_5 + I_1 - I_2/n)] n^2 (c_n^2 + d_n^2)$$

$$+ \frac{1}{4} \sum_{n=2}^{\infty} [I_4 - 2nI_2 + 2I_1 - I_3 - 3(I_4 - I_5 + I_1 - I_3 - nI_2)] (c_n^2 + d_n^2). \qquad (B.34)$$

Inter loop interaction terms : For n^{th} perturbation, choosing the particular value $\phi_n = \frac{\pi}{n}$ of the rotation ϕ,

$$\psi_n(s + 2a\eta - a\phi_n) = -\cos 2n\eta \, \psi_n(s) - \sin 2n\eta \frac{a}{n} \psi_n'(s) \quad \text{and} \qquad (B.35)$$

$$\psi_n'(s + 2a\eta - a\phi_n) = +\sin 2n\eta \frac{n}{a} \psi_n(s) - \cos 2n\eta \, \psi_n'(s). \qquad (B.36)$$

Using (B.24), (B.35), and (B.36) in the integrals in the right hand side of the equations in (3.33), we obtain

$$\left. \begin{array}{l} \vartheta[n, Qn](v, Qv) \cdot e = \dfrac{a^3}{4} \sum_{n=2}^{\infty} [-J_1 - (J_3 + J_4/n) - 6a^2(K_2 + K_3/2n)] \psi_n', \\[2mm] \vartheta[n, Qn](v, Qv) \cdot k = \dfrac{a^4}{4\sqrt{1-a^2}} \sum_{n=2}^{\infty} [J_1 - J_2 - 6(1-a^2)(K_1 + \dfrac{K_3 + K_4}{2n})] \psi_n', \\[2mm] \vartheta[n, Qn](v, Qv) \cdot (k \times e) = \dfrac{a^2}{4} \sum_{n=2}^{\infty} [J_1 + (J_3 + nJ_4) - 6a^2(K_5 - K_2 + nK_4/2)] \psi_n, \end{array} \right\},$$

$$(B.37)$$

where J_1, J_2, J_3, J_4, and J_5 are defined in (B.48) and K_1, K_2, K_3, K_4, and K_5 are defined in (B.49). It follows that

$$\int_0^{2\pi a} \vartheta[n, Qn](v, Qv) \cdot v = \frac{a^3}{4} \sum_{n=2}^{\infty} [J_1 + (J_3 + J_4/n) + 6a^2(K_2 + K_3/2n)] n^2 (c_n^2 + d_n^2)$$

$$+ \frac{a^5}{4(1-a^2)} \sum_{n=2}^{\infty} [J_1 - J_2 - 6(1-a^2)(K_1 + \frac{K_3 + K_4}{2n})] n^2 (c_n^2 + d_n^2)$$

$$\frac{a^3}{4} \sum_{n=2}^{\infty} [J_1 + (J_3 + nJ_4) - 6a^2(K_5 - K_2 + nK_4/2)] (c_n^2 + d_n^2). \qquad (B.38)$$

Substituting (B.29), (B.34), (B.38) and the Lagrange multipliers

$$\Lambda = \frac{a\chi}{2} \int_0^\pi \frac{d\eta}{\sqrt[3]{1 - a^2 \cos^2 \eta}} \quad \text{and}$$

$$\lambda = \frac{1}{a^2} - \frac{\zeta}{2} \int_0^\pi M(\eta) \csc \eta \, d\eta + \frac{\chi a^3}{2} \int_0^\pi \frac{\cos^2 \eta \, d\eta}{\sqrt[3]{1 - a^2 \cos^2 \eta}} \quad \text{(B.39)}$$

in terms of the integrals defined in (B.47) and (B.48) as

$$\Lambda = \frac{a\chi}{2} J_1, \quad \text{and} \quad \lambda = \frac{1}{a^2} - \frac{\zeta}{2} I_5 + \frac{\chi a^3}{2} J_5, \quad \text{(B.40)}$$

in (B.12), we get the second variation condition as

$$\sum_{n=2}^\infty \pi a (Y_B(n,a) + \zeta Y_S(n,a) - Y_I(n,a)\chi)[c_n^2 + d_n^2] \geq 0, \quad \text{(B.41)}$$

or, equivalently,

$$\sum_{n=2}^\infty (\beta_n(a) + \zeta \alpha_n(a) - \chi)[c_n^2 + d_n^2] \geq 0, \quad \text{(B.42)}$$

where,

$$\alpha_n(a) = \frac{Y_S(n,a)}{Y_I(n,a)}, \quad \beta_n(a) = \frac{Y_B(n,a)}{Y_I(n,a)}, \quad \text{(B.43)}$$

$$Y_B(n,a) = \frac{n^2(n^2 - 1)}{1 - a^2}(n^2 - 1 + a^2), \quad \text{(B.44)}$$

$$Y_S(n,a) = \frac{1}{4} \left[3[n^2(I_5 + I_1) - 2nI_2 + I_1 - I_3 + I_4 - I_5] \right.$$

$$- I_4 - \frac{n^2 I_4}{1 - a^2} + (n^2 + 1)(I_3 - 2I_1)$$

$$\left. + 4I_2 n + \frac{a^2 n^2}{1 - a^2} I_3 + 2I_5 \left((n^2 - 1)^2 + \frac{a^2 n^4}{1 - a^2} \right) \right], \quad \text{(B.45)}$$

$$Y_I(n,a) = \frac{1}{2} \left[-3a^5(n^2(K_1 - K_2) + nK_4 + K_5 - K_2) \right.$$

$$+ \frac{a^3}{2} \left[J_1 + \frac{n^2 J_1}{1 - a^2} + (n^2 + 1)J_3 + 2nJ_4 - \frac{a^2 n^2}{1 - a^2} J_2 \right]$$

$$\left. + a^3 \left((n^2 - 1)^2 + \frac{a^2 n^4}{1 - a^2} \right) J_5 - a^3 \left(1 + \frac{n^2}{1 - a^2} \right) J_1 \right], \quad \text{(B.46)}$$

$$I_1 = \int_0^\pi M(\eta) \cos 2n\eta \csc \eta \, d\eta,$$

$$I_2 = \int_0^\pi M(\eta) \sin 2n\eta \cos \eta \csc^2 \eta \, d\eta,$$

$$I_3 = \int_0^\pi M(\eta) \cos 2n\eta \csc^3 \eta \, d\eta,$$

$$I_4 = \int_0^\pi M(\eta) \csc^3 \eta \, d\eta,$$

$$I_5 = \int_0^\pi M(\eta) \csc \eta \, d\eta,$$

(B.47)

$$J_1 = \int_0^\pi \frac{1}{\sqrt[3]{1 - a^2 \cos^2 \eta}} \, d\eta,$$

$$J_2 = \int_0^\pi \frac{\cos 2n\eta}{\sqrt[3]{1 - a^2 \cos^2 \eta}} \, d\eta,$$

$$J_3 = \int_0^\pi \frac{\cos 2\eta \cos 2n\eta}{\sqrt[3]{1 - a^2 \cos^2 \eta}} \, d\eta,$$

$$J_4 = \int_0^\pi \frac{\sin 2\eta \sin 2n\eta}{\sqrt[3]{1 - a^2 \cos^2 \eta}} \, d\eta,$$

$$J_5 = \int_0^\pi \frac{\cos^2 \eta}{\sqrt[3]{1 - a^2 \cos^2 \eta}} \, d\eta,$$

(B.48)

and

$$K_1 = \int_0^\pi \frac{\cos^2 \eta \sin^2 n\eta}{\sqrt[5]{1 - a^2 \cos^2 \eta}} \, d\eta,$$

$$K_2 = \int_0^\pi \frac{\cos^2 \eta \sin^2 \eta \sin^2 n\eta}{\sqrt[5]{1 - a^2 \cos^2 \eta}} \, d\eta,$$

$$K_3 = \int_0^\pi \frac{\cos \eta \sin^3 \eta \sin 2n\eta}{\sqrt[5]{1 - a^2 \cos^2 \eta}} \, d\eta,$$

$$K_4 = \int_0^\pi \frac{\sin \eta \cos^3 \eta \sin 2n\eta}{\sqrt[5]{1 - a^2 \cos^2 \eta}} \, d\eta,$$

$$K_5 = \int_0^\pi \frac{\sin^2 \eta \cos^2 \eta}{\sqrt[5]{1 - a^2 \cos^2 \eta}} \, d\eta.$$

(B.49)

APPENDIX C LINEAR BIFURCATION ANALYSIS

Substituting $\sigma_1 = \sigma$ and $\Sigma_1 = \Sigma$ from (4.61) in (4.57)$_1$, we obtain

$$v'''' + \lambda v'' + \Lambda v + \sigma' n' + \sigma n'' + \Sigma n = \zeta \tilde{\vartheta}[n,n](v,v) + \chi \vartheta[n,Qn](v,Qv). \quad \text{(C.1)}$$

Using the representation of v in (4.48) in terms of ψ and ψ' and the identities in (4.44), we find that

$$\left.\begin{aligned}
v'''' &= (-a^2 \psi'''' + 2\psi''' + 3\psi'/a^2)e + \frac{a^3 \psi''''''}{\sqrt{1-a^2}}k \\
&\quad + (-3a\psi'''' - 2\psi''/a + \psi/a^3)k \times e, \\
v'' &= -(a^2 \psi''' + \psi')e + \frac{a^3 \psi'''}{\sqrt{1-a^2}}k - (a\psi'' + \psi/a)k \times e, \\
v &= -a^2 \psi' e + \frac{a^3 \psi'}{\sqrt{1-a^2}}k + a\psi k \times e,
\end{aligned}\right\} \quad \text{(C.2)}$$

Using the Fourier representation of ψ in (B.24) and the equations in (C.2), components first three terms in the left hand side of the linearized equilibrium equations (C.1) in the direction e, k, and $k \times e$ can be written as

$$\left.\begin{aligned}
[v'''' + \lambda v'' + \Lambda v] \cdot e &= \sum_{n=2}^{\infty} \left(-\frac{(n^2-1)(n^2+3)}{a^2} + \lambda(n^2-1) - \Lambda a^2 \right) \psi_n', \\
[v'''' + \lambda v'' + \Lambda v] \cdot k &= \sum_{n=2}^{\infty} \frac{1}{\sqrt{1-a^2}} \left(\frac{n^4}{a} - \lambda a n^2 + \Lambda a^3 \right) \psi_n', \\
[v'''' + \lambda v'' + \Lambda v] \cdot k \times e &= \sum_{n=2}^{\infty} \left(\frac{-3n^4 + 2n^2 + 1 + \lambda a^2(n^2-1)}{a^3} + a\Lambda \right) \psi_n,
\end{aligned}\right\} \quad \text{(C.3)}$$

Additionally, we assume that the σ and Σ take the form

$$\sigma = \sum_{n=2}^{\infty} \sigma_n, \quad \text{and} \quad \Sigma = \sum_{n=2}^{\infty} \Sigma_n, \quad \text{(C.4)}$$

where

$$\left.\begin{aligned}
\sigma(s) &= p_n \cos \frac{ns}{a} + q_n \sin \frac{ns}{a}, \\
\Sigma(s) &= u_n \cos \frac{ns}{a} + v_n \sin \frac{ns}{a},
\end{aligned}\right\} \quad \text{(C.5)}$$

Substituting (C.3), (B.32), and (B.37) in (C.1), using the Fourier series represen-tation of ψ, σ, Σ, and noting that the coefficient of the Fourier terms $\cos\frac{ns}{a}$ and $\sin\frac{ns}{a}$ independently satisfy (C.1), we obtain for each mode n, a system of six linear equation in six unknowns c_n, d_n, p_n, q_n, u_n, and v_n that can be written as

$$\mathbf{A}\mathbf{x} = \mathbf{0}, \tag{C.6}$$

where

$$
\mathbf{A} = \left[
\begin{array}{c|c|c}
\Theta\Omega & -1/a\mathbb{1} & a\mathbb{1} \\
\hline
\Pi\Omega & & (1-a^2)\mathbb{1} \\
\hline
\Psi\mathbb{1} & n/a\Omega &
\end{array}
\right]
\quad \text{and} \quad
\mathbf{x} = \begin{bmatrix} c \\ d \\ p \\ q \\ u \\ v \end{bmatrix}.
\tag{C.7}
$$

Ω and $\mathbb{1}$ are 2×2 matrices defined as

$$
\Omega = \begin{bmatrix} 0 & 1 \\ -1 & 0 \end{bmatrix}, \quad
\mathbb{1} = \begin{bmatrix} 1 & 0 \\ 0 & 1 \end{bmatrix},
\tag{C.8}
$$

and

$$
\left.
\begin{aligned}
\Theta =\ & -\frac{n(n^2-1)(n^2+3)}{a^3} + \lambda\frac{n(n^2-1)}{a} - \Lambda an \\
& - \frac{\zeta n}{4a}\left[-I_4 + \frac{2I_2}{n} + I_3 - 2I_1 + 3I_5 + 3I_1 - \frac{3I_2}{n} \right] \\
& + \frac{n\chi a^2}{4}\left[J_1 + \left(J_3 + \frac{J_4}{n}\right) + 6a^2 K_2 + \frac{3a^2 K_3}{n} \right], \\
\Pi =\ & \frac{n^5}{a^2} - \lambda n^3 + \Lambda na^2 - \frac{\zeta n}{4}(I_4 - I_3) \\
& + \frac{n\chi a^3}{4}\left[-J_1 + J_2 + 6(1-a^2)\left(K_1 + \frac{K_3+K_4}{2n}\right) \right], \\
\Psi =\ & \frac{-3n^4 + 2n^2 + 1 + \lambda a^2(n^2-1)}{a^3} + a\Lambda \\
& - \frac{\zeta}{4a}(I_4 - 2nI_2 + 2I_1 - I_3 - 3(I_4 - I_5 + I_1 - I_3 - nI_2)) \\
& - \frac{\chi a^2}{4}(J_1 + (J_3 + nJ_4) - 6a^2(K_5 - K_2 + nK_4/2)),
\end{aligned}
\right\}
\tag{C.9}
$$

91

the integrals $(I_1, I_2, I_3, I_4, I_5)$ are defined in (B.47), $(J_1, J_2, J_3, J_4, J_5)$ are defined in (B.48), and $(K_1, K_2, K_3, K_4, K_5)$ are defined in (B.49).

For the system of equations (C.6) to have a non zero solution $\mathbf{x}$, it is required that the matrix $\mathbf{A}$ is non-invertible which yields

$$\det \mathbf{A} = 0. \tag{C.10}$$

This condition is equivalent to the criteria that $D_u g(u_0, \epsilon_0)$ is non-invertible which is a necessary condition for (u_0, ϵ_0) to be a bifurcation point described in section 4.4 of chapter 4

APPENDIX D RIGID ROTATION ABOUT A VECTOR IN EQUATORIAL PLANE

Consider a particular form of perturbation such that the perturbed loops are circular but are no more co-axial. This can be achieved by rotating either of the circular loop about a vector in the equatorial plane. The bending energy and the intra-loop energy remains unchanged by such class of perturbation. However, using symmetry argument, one can say that the repulsive interaction will increase and therefore, the trivial solution is stable with respect to this class of perturbation. In other words, when the trivial configuration is perturbed in this fashion, the perturbed loops with reach the equilibrium where the two circular loops are parallel to each other. We will now use linear stability analysis to show that indeed this is true. Without loss of generality, we assume that the circular configuration $\mathcal{C}_2^*$ remains unperturbed and $\mathcal{C}_1^*$ is rotated by an infinitesimal angle ϕ about the unit vector i as shown in the figure D.1. In such situation, the
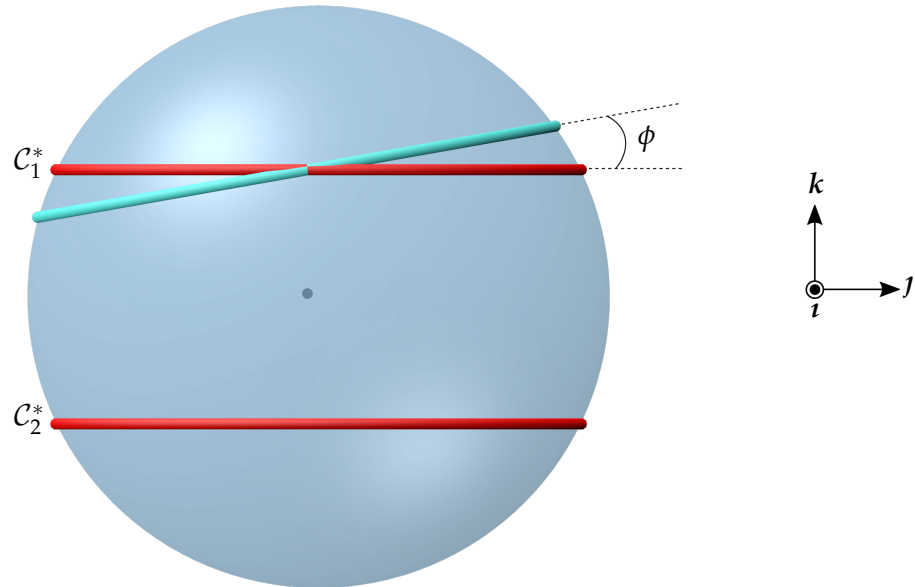

Figure D.1: Schematic of the trivial equilibrium solution and the perturbation of the configuration $\mathcal{C}_1^*$.

perturbations v_1 and v_2 are given as

$$v_1 = v \quad \text{and} \quad v_2 = 0. \tag{D.1}$$

Also, the circular loops $\mathcal{C}_1^*$ and $\mathcal{C}_2^*$ are parameterized as

$$n_1 = n \quad \text{and} \quad n_2 = Rn, \tag{D.2}$$

where

$$n(s) = ae(s) + \sqrt{1-a^2}k, \quad 0 \le s \le 2\pi a, \tag{D.3}$$

$$e(s) = \left(\cos\frac{s}{a}\right)\imath + \left(\sin\frac{s}{a}\right)\jmath, \quad 0 \le s \le 2\pi a, \tag{D.4}$$

and $R = I - 2k \otimes k$ is a reflection tensor that reflects a vector about the equatorial plane in the opposite hemisphere. Using above parameterization of the equilibrium configuration and perturbations, the regularized second variation condition (4.14) reduces to

$$\int_0^{2\pi a} (|v''|^2 - \lambda|v'|^2 + \Lambda|v|^2 - (\zeta\tilde{\vartheta}[n,n](v,v) + \chi\vartheta[n,Rn](v,0)) \cdot v)\, ds \ge 0. \tag{D.5}$$

The function v is given as

$$v = \phi\left(-\sqrt{1-a^2}\jmath + a\left(\sin\frac{s}{a}\right)k\right), \tag{D.6}$$

that trivially satisfies both the constraints $n \cdot v = 0$ and $n' \cdot v'$. Now, we evaluate the integrals in the second variation condition (D.5) as follows :

Bending energy terms :

$$\int_0^{2\pi a} |v|^2\, ds = \phi^2(2-a^2)(\pi a), \quad \int_0^{2\pi a} |v'|^2\, ds = \phi^2(\pi a), \quad \int_0^{2\pi a} |v''|^2\, ds = \frac{\phi^2}{a^2}(\pi a). \tag{D.7}$$

Expressing the Lagrange multipliers λ and Λ in terms of the integrals as defined in (B.40), we get

$$\int_0^{2\pi a} (|v''|^2 - \lambda|v'|^2 + \Lambda|v|^2 = \phi^2(\pi a)\left[\frac{\zeta}{2}I_5 + \chi a J_1 - \frac{\chi a^3}{2}(J_1 + J_5)\right]. \tag{D.8}$$

94

Intra-loop energy terms : Using (4.15),

$$\tilde{\vartheta}[n, n](v, v)$$
$$= \int_0^{2\pi a} M\left(\frac{|\bar{s} - s|}{2a}\right) \left(\frac{(v - v(\bar{s}))}{|n - n(\bar{s})|^3} + 3\frac{(n \cdot v(\bar{s}) + n(\bar{s}) \cdot v)}{|n - n(\bar{s})|^5}(n - n(\bar{s}))\right) d\bar{s}. \quad \text{(D.9)}$$

Therefore,

$$\int_0^{2\pi a} \tilde{\vartheta}[n, n](v, v) \cdot v \, ds$$
$$= \int_0^{2\pi a} \int_0^{2\pi a} M\left(\frac{|\bar{s} - s|}{2a}\right) \left(\frac{(v - v(\bar{s})) \cdot v}{|n - n(\bar{s})|^3} - 3\frac{(n \cdot v(\bar{s}) + n(\bar{s}) \cdot v)}{|n - n(\bar{s})|^5}n(\bar{s}) \cdot v\right) ds \, d\bar{s}.$$
$$\text{(D.10)}$$

Using a change of variable $\bar{s} = s + 2a\eta$, we find that

$$|n - n(\bar{s})| = 2a|\sin \eta|, \quad \text{(D.11)}$$
$$v(\bar{s}) = \phi\left(-\sqrt{1 - a^2}J + a\left(\sin\frac{s}{a}\cos 2\eta + \cos\frac{s}{a}\sin 2\eta\right)k\right), \quad \text{and} \quad \text{(D.12)}$$
$$(v - v(\bar{s})) \cdot v = 2a^2\phi^2 \sin^2\frac{s}{a}\sin^2\eta - a^2\phi^2 \cos 2\eta \sin\frac{s}{a}\cos\frac{s}{a}. \quad \text{(D.13)}$$

The first term on the right hand side in (D.10) simplify as

$$\int_0^{2\pi a} \int_0^{2\pi a} M\left(\frac{|\bar{s} - s|}{2a}\right) \left(\frac{(v - v(\bar{s})) \cdot v}{|n - n(\bar{s})|^3}\right) d\bar{s} \, ds = \phi^2(\pi a)\frac{J_5}{2}. \quad \text{(D.14)}$$

Also,

$$n \cdot v(\bar{s}) = a\phi\sqrt{1 - a^2}\left(-\sin\frac{s}{a} + \sin\frac{\bar{s}}{a}\right), \quad \text{and} \quad \text{(D.15)}$$
$$n(\bar{s}) \cdot v = a\phi\sqrt{1 - a^2}\left(\sin\frac{s}{a} - \sin\frac{\bar{s}}{a}\right), \quad \text{(D.16)}$$

which yields $n \cdot v(\bar{s}) + n(\bar{s}) \cdot v = 0$. Therefore, equation (D.10) simplifies as

$$\int_0^{2\pi a} \tilde{\vartheta}[n, n](v, v) \cdot v \, ds = \phi^2(\pi a)\frac{J_5}{2}. \quad \text{(D.17)}$$

Inter-loop interaction energy : Using (D.2) and (D.1) in (3.33),

$$\vartheta[n, Rn](v, 0) = \int_0^{2\pi a} \left(\frac{v}{|n - Rn(\bar{s})|^3} + 3\frac{(Rn(\bar{s})) \cdot v}{|n - Rn(\bar{s})|^5}(n - Rn(\bar{s}))\right) d\bar{s}, \quad \text{(D.18)}$$

which using the fact that $n \cdot v = 0$, yields

$$\int_0^{2\pi a} \vartheta[n, Rn](v, 0) \cdot v \, ds = \int_0^{2\pi a} \int_0^{2\pi a} \left(\frac{v \cdot v}{|n - Rn(\bar{s})|^3} - 3 \frac{((Rn(\bar{s})) \cdot v)^2}{|n - Rn(\bar{s})|^5} \right) d\bar{s} \, ds.$$

(D.19)

Using (D.2), we find that

$$|n - Rn(\bar{s})| = 2\sqrt{1 - a^2 \cos^2 \eta} \quad \text{and} \quad v \cdot v = \phi^2 \left(1 - a^2 \cos^2 \frac{s}{a} \right).$$

(D.20)

Therefore,

$$\int_0^{2\pi a} \int_0^{2\pi a} \left(\frac{v \cdot v}{|n - Rn(\bar{s})|^3} \right) d\bar{s} \, ds = \phi^2 (\pi a) \left(\frac{a}{2} - \frac{a^3}{4} \right) J_1.$$

(D.21)

Also, using (D.1) and (D.2), a straightforward calculation yields

$$Rn(\bar{s}) \cdot v = a^2 \phi^2 (1 - a^2) 4 \cos^2 \eta \left(\sin^2 \frac{s}{a} \cos^2 \eta + \sin^2 \eta \cos^2 \frac{s}{a} \right).$$

(D.22)

Using the fact that

$$\int_0^{2\pi a} \sin^2 \frac{s}{a} \, ds = \int_0^{2\pi a} \cos^2 \frac{s}{a} \, ds = \pi a,$$

(D.23)

we find that

$$\int_0^{2\pi a} \int_0^{2\pi a} \frac{(Rn(\bar{s}) \cdot v)}{|n - Rn(\bar{s})|^5} \, d\bar{s} \, ds = \frac{a^3}{4} \phi^2 (1 - a^2)(\pi a) K_6,$$

where

$$K_6 = \int_0^\pi \frac{\cos^2 \eta}{\sqrt[5]{1 - a^2 \cos^2 \eta}} \, d\eta.$$

(D.24)

Thus, equation (D.18) simplifies as

$$\int_0^{2\pi a} \vartheta[n, Rn](v, 0) \cdot v \, ds = \frac{\pi a^2 \phi^2}{4} \left((2 - a^2) J_1 - 3a^2 (1 - a^2) K_6 \right).$$

(D.25)

Combining the bending energy terms in (D.8), intra-loop interaction term (D.17),

and inter-loop interaction term , we get

$$\int_0^{2\pi a} (|v''|^2 - \lambda |v'|^2 + \Lambda |v|^2 - (\zeta \tilde{\vartheta}[n, n](v, v) + \chi \vartheta[n, Rn](v, 0)) \cdot v) \, ds =$$

$$\frac{\chi \pi a^2 \phi^2}{4} \left((2 - a^2) J_1 - 2a^2 J_5 + 3a^2 (1 - a^2) K_6 \right). \quad (D.26)$$

We observe that the second variation only consists of terms proportional to the inter-loop repulsion parameter χ which indicates that the second variation is zero with respect to the bending energy and the intra-loop interaction energy as we had proposed in beginning of this appendix. Using the definition of the integrals J_1 and J_5 in (B.48) and K_6 in (D.24), the integrals on the right hand side of the above equation simplifies as

$$\mathscr{I}_1 = \int_0^\pi \frac{(2-a^2)(1-a^2\cos^2\eta) - 2a^2\cos^2\eta(1-a^2\cos^2\eta) + 3a^2(1-a^2)\cos^2\eta}{\sqrt[5]{1-a^2\cos^2\eta}} \, d\eta.$$

(D.27)

Consider another integral

$$\begin{aligned}
\mathscr{I}_2 &= \int_0^\pi \left[(2-a^2)(1-a^2\cos^2\eta) - 2a^2\cos^2\eta(1-a^2\cos^2\eta) + 3a^2(1-a^2)\cos^2\eta \right] d\eta \\
&= \frac{1}{4}(8 - 6a^2 - a^4) \\
&> 0 \quad \forall a \in [0,1].
\end{aligned}$$

(D.28)

Using the fact that $\mathscr{I}_2$ is obtained by replacing $\sqrt[5]{1-a^2\cos^2\eta}$ in the dominator of kernel of $\mathscr{I}_1$ with unity and that $\mathscr{I}_2 > 0$, it can be deduced that $\mathscr{I}_1 > \mathscr{I}_2$ which further implies that $\mathscr{I}_1 > 0$. Therefore, we have shown that

$$\int_0^{2\pi a} \left(|\boldsymbol{v}''|^2 - \lambda |\boldsymbol{v}'|^2 + \Lambda |\boldsymbol{v}|^2 - (\zeta \tilde{\boldsymbol{\vartheta}}[\boldsymbol{n},\boldsymbol{n}](\boldsymbol{v},\boldsymbol{v}) + \chi \boldsymbol{\vartheta}[\boldsymbol{n},\boldsymbol{Rn}](\boldsymbol{v},\boldsymbol{0})) \cdot \boldsymbol{v} \right) ds > 0. \quad \text{(D.29)}$$

Hence, the trivial configuration $\mathcal{C}_1^*$ and $\mathcal{C}_2^*$ described by the parameterization (D.2)-(D.4) are stable with respect to the perturbation given in (D.1) and (D.6).